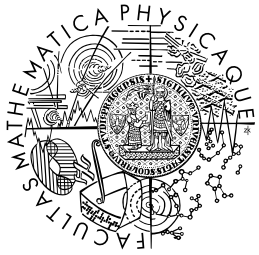

FACULTY
OF MATHEMATICS
AND PHYSICS
Charles University

HABILITATION THESIS

Daniela Korčáková

FS CMa Stars: History, Properties, and Challenges

Astronomical Institute of Charles University

Prague 2022

I declare that I carried out this habilitation thesis independently, and only with the cited sources, literature and other professional sources. It has not been used to obtain another or the same degree.

I understand that my work relates to the rights and obligations under the Act No. 121/2000 Sb., the Copyright Act, as amended, in particular the fact that the Charles University has the right to conclude a license agreement on the use of this work as a school work pursuant to Section 60 subsection 1 of the Copyright Act.

In ..... date ....

Author's signature

To my parents

I could not have gotten far without the support of my parents. I would not be who I am without them. Their love and respect for all living creatures was as the light of a candle in dark times. My great thanks also go to my brothers, who were always there for me.

Let me allow to use this place to thank all the people who never appear in papers, but we could hardly make progress in the research without them. Especially, I thank all the technical staff taking care of the Perek's 2m telescope at the Ondřejov Observatory, namely, J. Fuchs, J. Havelka, K. Kalaš, E. Kortusová, R. Novotný, M. Tlamicha, L. Řezba, L. Šarounová (Kotková), J. Sloup, R. Veselý, and F. Ždárský. They took me in. They were not only my colleagues and teachers, but also very good friends. I do not know people at other observatories but, I hope, they took these words as my thanks also to them. I also would like to thank the people taking care about the service at conferences which I organised. They were the people who prepared a nice time for others.

My thanks also go to all my colleagues who have supported me in difficult times.

Title: FS CMa Stars: History, Properties, and Challenges

Author: Daniela Korčáková

Department: Astronomical Institute of Charles University

Abstract: FS CMa stars are a sub-group of stars showing the B[e] phenomenon, i.e., the presence of the forbidden lines in their spectra and strong infrared excess. While the nature and evolutionary status of other stars showing these spectral properties have been satisfactorily explained, the FS CMa stars remain an open question. Recently, a strong magnetic field was detected in one of these stars, IRAS 17449+2320. The properties of this star indicate that it is a post-merger system. This discovery brought a new scenario of the evolution of FS CMa stars, which finally may link all the observed properties. To identify the mergers among FS CMa stars and remove from their list the other stars with similar spectral properties (e.g., post-AGB objects or symbiotic stars), the need for a review has arisen. Therefore, the style of this thesis is a review of the observed properties, as well as applied models. In the end of this thesis, the contribution of the author to the field of FS CMa stars is summarised.

Keywords: hot stars; emission-line stars; B[e] stars; binaries; mergers; circumstellar matter; spectroscopy; mass-loss; magnetic field; stellar evolution

Contents

Preface

My trip along FS CMa stars started just after the PhD study. During the PhD study, I developed a radiative transfer code for the extended atmospheres, stellar wind, and accretion disks. The code was tested and accelerated and it has become time to use it in real situations.

B[e] stars with lower luminosity caught my attention. No one had any idea what they really were. It was a secret that could not be resisted. But, when I started working, I had to stop just at the beginning. I found that there is so little information that it was not possible to set boundary conditions for the model. Everything would be just modelling for the sake of modelling. At that time, I worked at the Stellar Department at the Ondřejov Observatory. I had access to the 2 m telescope with a very good and stable spectrograph and, what is more important, we were really free. It was possible to start a long-term project at that time. This is exactly what was necessary, because FS CMa stars are completely hidden in the circumstellar material. One spectrum can hardly say which physical processes are there. After three months in 2004 of reading papers about these stars, I selected a small group of stars and started following them.

I did not make a random selection, but I chose the stars whose properties were close to the classical Be stars that were studied at the department for several decades. Later, in 2007, Anatoly Miroshnichenko defined a new group called FS CMa stars, where these selected stars were included. I worked with many colleagues and students over the years. We found expanding decelerating layers, signatures of the material ejecta as well as infall, instabilities in the rotating disk, iron curtain, and we were able to describe the periodical behaviour of the selected objects. Based on our observations, I was able to construct the empirical model (Korčáková et al. 2019). However, the reactions were not positive because of the inconsistency with the α disk model. But, one cannot apply a simple model to something very complex. Unfortunately, there was no proof. And then one spectrum came ...

''If one is to understand the great mystery, one must study all its aspects, not just the dogmatic, narrow view of the pure theoreticians or pure observers. Only a combination of these two approaches will take us further.''

slightly changed speech of senator Palpatine

Chapter 1

FS CMa Stars and their Place Among the B[e] Stars

FS CMa stars are a sub-group of about seventy members of peculiar stars showing the B[e] phenomenon. The term "B[e] phenomenon" refers to B-type stars with emission lines ("e" in the name) of permitted, but especially forbidden (square brackets) transitions. These stars also have very strong infrared excess. The word "phenomenon" is used here to emphasise that such spectral properties show stars of different types and at different evolutionary stages. However, for practical purposes, it is better to use the name "the B[e] stars" introduced by Conti at the IAU Symposium 70 (1975). The presence of forbidden emission lines and strong infrared excess points to the large amount of circumstellar gas and dust. This complicates the study of central stars, because we have no information directly coming from the photosphere for most of these objects.

The first note about such a peculiar star comes from Fleming (Pickering 1898). She noticed the Hβ emission in the spectra of FS CMa. This discovery was followed by findings of nebular or emission lines of novae in other stellar spectra, e.g. at famous η Car (Gill 1901). However, knowledge of quantum physics at that time was not sufficient to identify all emission lines. Merrill (1924) discussed the spectrum of HD 161114 in detail. He correctly guessed that the unknown lines must be formed at low pressure and that the temperature of the central star must be high enough to have sufficiently strong UV radiation. The key point in the study of the astronomical spectra was the explanation of nebulium and other unidentified lines as the forbidden lines Bowen (1927b,a). In the more detailed study of FS CMa, Merrill (1928) presented a list of many forbidden emission lines, especially of Fe II and O I. Some of the individual studies pointed to the variability of the spectra of these objects. Merrill (1931) showed how much in the ten-year study of HD 50138. The good base for the systematic study built Wackerling (1970) creating the extended catalogue of emission-line stars.

IR observations brought another milestone. Geisel (1970) found the correlation between the IR excess and the presence of the low-excitation permitted and forbidden emission lines in the stellar spectra. In the following study, Allen & Swings (1972) searched for forbidden lines of low-ionisation species between stars with a large H-K color index. Ciatti et al. (1974) compared the spectra of MWC 17, MWC 349, HD 45677, and HD 51585 (so-called BQ[] stars at that time) with symbiotic stars and compact planetary nebulae. The review of emis-

sion B-type stars with infrared excess presented Allen & Swings (1976). This became the key paper taken as the beginning of the study of the B[e] stars.

Crucial for the study of the B[e] supergiants were UV spectra that reveal the P Cygni profiles of resonance lines of highly ionised metals, e.g. N V, C IV, ... These observations allowed to study stellar wind in more detail. The first model of a B[e] supergiant sketched Zickgraf et al. (1985). Based on the observations, he found that there must be two different regions; a cold geometrically thick slowly expanding disk surrounded by the dusty ring and hot fast radiatively driven wind at poles. Hydrogen lines are formed in the inner parts of the disk, permitted lines of neutral and singly ionised metals in the central parts of the disk, and the forbidden lines of these species in the outer part of the disk. The lines from higher ionization stages of the metals come from the wind areas. Going through the properties of known B[e] stars, Lamers et al. (1998) noticed that this kind of spectra show stars among supergiants (sgB[e] stars), pre-main sequence Herbig Ae/Be stars (HAeB[e] stars), compact planetary nebulae (cPNB[e]), and symbiotic stars (SymB[e] stars).

Important progress in the study of the B[e] stars always brought the meeting of the community. The first workshop took place in Paris in June 1997. The first conference *"Stars with the B[e] phenomenon"* held on the island of Vlieland, The Netherlands, in July 2005. The second conference *"The B[e] Phenomenon: Forty Years of Studies"* was organised in July 2016 in Prague, Czech Republic, on the anniversary of the paper of Allen & Swings (1976). Next conference *"Hot Stars Life with Circumstellar Matter"* planned in June 2020 in Almaty, Kazakhstan, had to be moved due to the global pandemic.

This short introduction summarises only the key points in the study of the B[e] stars for experts from other fields. I do not go deeper and rather refer to the previous very good reviews of Zickgraf (1998), Zickgraf (2000), Swings (2006), Miroshnichenko (2006), Hillier (2006), and Oudmaijer & Miroshnichenko (2017) to keep more space for FS CMa stars, the main focus of this thesis.

1.1 FS CMa Stars, their Properties, Nature, and Troubles

Not every B[e] star fits into the four original groups defined by Lamers et al. (1998), sgB[e] stars, HAeB[e] stars, cPNB[e], or SymB[e] stars. They were able to classify only about half of the B[e] stars known at that time. Partially because of the lack of data, but there were also stars whose spectral properties did not allow it. They did not fit into any group, or their properties were compatible with more groups. Sheikina et al. (2000) focused on these unclassified objects and found that the IR excess of some of these stars steeply decreases longward of 25 μm. Including more stars, Miroshnichenko et al. (2001) recognised that there must be another group hidden between the unclassified stars and called them the B[e] stars with warm dust (B[e]WD). They constructed the first Hertzsprung-Russell diagram (HRD) of these objects and found that the B[e]WD stars are located near the terminal-age main sequence (TAMS). This excluded the possibility that the B[e]WD stars are pre-main sequence stars. Moreover, the B[e]WD stars are located too far from the star-forming regions and do not have an IR excess cor-

responding to the cold dust. They also excluded the possibility that the B[e]WD stars are classical Be stars. The list of the B[e]WD stars was extended by Miroshnichenko et al. (2002c). The common properties of the B[e]WD stars described in detail Miroshnichenko (2007) and started to call them the FS CMa stars. The group was extended and described in detail several times in Miroshnichenko et al. (2007, 2011, 2017, 2021b).

Miroshnichenko (2007) defined the properties of FS CMa stars. The most remarkable is the strong emission of hydrogen lines and the presence of forbidden emission lines, especially [O I]. Emission lines, from permitted and also forbidden transitions, of other neutral or singly ionised metals are also present. Sometimes weak [O III] lines may also be detected. The large IR excess steeply decreases around 20 μm. The FS CMa stars are located outside the star-forming regions. They have temperatures between 9 000 K and 30 000 K and luminosity $\log L/L_{\odot}$ in the range of 2.5 and 4.5. If they are binaries, the secondary is fainter and cooler, or it is degenerate. After more than a decade, more observations reveal other properties of these objects, which we will see in the following sections.

Even if FS CMa stars played an important role in the study of hot emission line stars and the main representatives, FS CMa and HD 50138, were observed for more than a century, the nature and evolution status of these objects is still not determined. The main reason is the large amount of circumstellar matter. We do not have direct information from the central star for some objects. In this case, one spectrum can hardly reveal the physical processes in the atmosphere and surrounding medium and systematic observations becomming crucial. The first analysis of long-term observations published Merrill (1931). He analysed 76 photographic plates from December 1920 to February 1930. Unfortunately, there is a gap in long-term observations for almost a century (MWC 623, Polster et al. 2012; MWC 342, Kučerová et al. 2013; MWC 728, Miroshnichenko et al. 2015; HD 50138, Jeřábková et al. 2016; HD 85567, Khokhlov et al. 2017; AS 386, Khokhlov et al. 2018; 3 Pup, Miroshnichenko et al. 2020a). Such a large gap in the observational data is not the only problem. The first photographic plates used by Merrill were sensitive in the blue region, allowing to follow almost only the Hβ line, while the most intensive forbidden lines [O I] were often underexposed. CCDs are more sensitive in red, therefore the Hα line was followed in the slit spectra. Nowadays, èchelle spectra allow to link the old observations.

A lot of excellent work was done also based on short-term spectroscopic observational runs. For all of them, let us mention the study of Pogodin (1997), where the line variability of HD 50138 during four nights is visible very well. The stars are variable also photometrically (Sects. 2.12 and 3.4). I would like to point to the observations of MWC 342 (Shevchenko et al. 1993; Mel'Nikov 1997; Chkhikvadze et al. 2002), because they show the multiperiodic, even chaotic behaviour of the object. The data revealed a short period between 14 and 16 days changing from season to season. A longer, also variable, period around 40 days was detected in every season, while the longest one around 120 days was not proven for every season. Reading this, one might note that this is only a matter of wrong data. However, the temporal coverage should be sufficient to describe short, even long-term periods well. Moreover, MWC 342 is north enough to be observed for three-quarters of the year from used observatories. Such kind of behaviour is probably real for FS CMa objects.

Spectra of FS CMa stars mimique the spectra of Herbig Ae/Be stars. Therefore, many of them are included in the list of Herbig Ae/Be stars, which is a great advantage, because sometimes they are in an observing schedule of Herbig Ae/Be stars. One such example is a spectro-astrometrical study of Baines et al. (2006), where four FS CMa stars were measured. The similar situation is with polarimetry. Several stars were also observed in CO maser line. The circumstellar environment of six FS CMa was resolved by Marston & McCollum (2008) using Hα narrow band imaging at the 60-inch telescope at Mt. Palomar. The higher resolution was achieved by interferometry. I would like to emphasise the observations done by Kluska et al. (2016) at this place. They present the first interferometric imaging of a FS CMa star HD 50138, and their findings may play a key role in the revealing of the nature of these objects. They showed that a disk model with a spot fits the data well, while a binary model failed. Moreover, they found that the envelope is variable.

The IR observations of IRAS were crucial. Based on these data, the group was identified. The spectral energy distribution (SED) is used for the determination of the dust temperature, or temperatures, if multiple dust rings are present (Sect. 2.14). The peaks in the extinction curves revealed the dust composition, size of the grains, and even their orientation, if the polarimetry was used (Sect. 3.3). Silicates and also graphite grains were found. IR spectra showed the presence of CO, SiO, TiO, H_3^+, and, in some cases, also more complex polycyclic aromatic hydrocarbons (PAHs) (Sect. 2.13).

Unfortunately, the UV observations were left out, although the UV radiation significantly affects the formation of the visual and IR spectra. The UV spectra of FS CMa itself and HD 50138 show strong absorption of iron group elements, so-called iron curtain, which is observed in classical novae, cataclysmic variables, and B[e] supergiants (Korčáková et al. 2019). The absorbed energy is subsequently reemitted in the visible and IR regions. UV spectra of eleven FS CMa stars obtained the International Ultraviolet Explorer (IUE). Only two stars (HD 50138 and CI Cam) were observed with the HST/STIS camera. Additional spectra were taken during the Astro-1 (FS CMa) and Astro-2 (HD 50138) space shuttle missions. GALEX provided the UV photometrical data for twenty three stars. Unfortunately, if these stars were included in an observation program of classical Be stars, the FUV photometry was not done and only NUV filters were used. There are ground-based observations in the U filter. For example, Bergner et al. (1990) points to the variability in the U filter, which is in anticorrelation with brightness in the K filter. All these UV observations suggest that the answer to the question "what are we dealing with?" may lie in the UV region.

The current data reveal the basic properties of the circumstellar matter and some of the physical processes playing a significant role there. The central object is surrounded by a geometrically and optically thick disk and a dusty ring. The outer regions are very stable, the turbulent velocities do not exceed 40 km s^{-1}. The density in the outer parts is comparable to the nebular conditions in some objects. For example, the absorption lines from triplet transitions are stronger than those of singlets. In contrast to the outer parts, the inner parts are usually very dynamical. The material ejection, but also infall, as well as continuous outflow are observed. However, the velocity of the material is about an order of magnitude smaller than the observed one in supergiants, it does not exceed

200 km s^{-1}, even for the material ejecta. The disk is not homegeous, which is natural because of its size which is about 100 – 150 $R_\star$ (Kříček et al. 2017). The rotating structures (Jeřábková et al. 2016), but also expanding layers (Kučerová et al. 2013) are observed. The expanding layers may even decelerate (Kučerová et al. 2013), which is an important finding for the construction of stellar wind models and calculation of the mass-loss rate ($\dot{M}$, see Sec. 3.7). The photosphere is usually dynamical and the pulsations play a role there, probably also the beating phenomenon, which may be responsible for the material ejecta.

Despite the observed data, the nature and evolution status of FS CMa stars is still not determined. The most accepted scenario is the binarity. The main argument is the presence of the dust and large $\dot{M}$, which is not possible to explain by the evolution of a single star during the main-sequence stage, while the mass transfer between binary companions can easily produce it (Miroshnichenko et al. 2006). However, the HRDs constructed with more stars and more accurate data showed that the FS CMa stars are located at the end of the main-sequence, but there are also more evolved objects. Therefore, one of the explanations coming into consideration are post-AGB stars (see Sect. 4.3). The main argument for the binarity, the large $\dot{M}$, is questioned based on the current observations. The models used for the determination of the $\dot{M}$ were constructed with the assumption of a smoothly accelerated medium. However, the observations of Kučerová et al. (2013) revealed the decelerated layers. In such the case, the $\dot{M}$ is highly overestimated (for details see Sects. 3.7 and 4.1). In favour of the binarity would be the period based on the radial velocity measurements, a companion discovered using astro-spectrometry, or interferometry. However, almost every proof of the binarity may be questioned, the observations do not reach sufficient accuracy, or another explanation exists (for details see Secs. 3.7). The literature is highly biased in this topic. For example, if in the original paper is written "we found slight hints of a binarity", in the introduction of the follow-up paper appeared "they found that this star is a binary", and in the following paper "they proved that this star is a binary". Summarising this, up to now, not a sufficient part of the binaries was really proven among FS CMa stars. Moreover, the best interferometric measurements up to now (Kluska et al. 2016) are not in favour in the presence of the companion in HD 50138.

Latest works show that the merger origin of FS CMa stars is more likely. The first suggestion of the merger scenario supported by observational evidence comes from de la Fuente et al. (2015). They discovered two FS CMa stars in the central parts of two clusters. Based on Gaia DR2, Boubert & Evans (2018) found that IRAS 17449+2320 escaped from the birth cluster. It is an important finding, because binaries that left the cluster, merge soon afterwards. This is the natural consequence of the momentum conservation. During the merger process, the strong magnetic field may be generated (Schneider et al. 2020). Indeed, a strong magnetic field was detected in IRAS 17449+2320 (Korčáková et al. 2021). As stronger the magnetic field is, as faster the stellar rotation slows down, which is in the agreement with the observation because FS CMa stars are slow rotators (Miroshnichenko 2007).

Let us have a look on the properties of FS CMa stars in more detail.

Chapter 2

Observed Properties of FS CMa Stars

The most distinctive feature in the spectra of FS CMa stars is very strong emission of the Hα line and forbidden emission lines of neutral and singly ionised metals. The strongest is [O I] doublet $\lambda\lambda$ 6 300, 6 364 Å. The lines from the permitted transitions of He I and other neutral and singly ionised metals are also present. The Fig. 2.1 shows the part of the spectrum of FS CMa, which was selected for the systematic observation at the Ondřejov Observatory using the slit spectrograph. The chosen spectral region contains He I 6 678 Å, forming in the deeper photosphere, Si II doublet $\lambda\lambda$ 6 347, 6 371 Å, forming in the upper layers of the photosphere, the forbidden [O I] doublet $\lambda\lambda$ 6 300, 6 364 Å, which originates in the outer parts of the circumstellar medium, and the Hα line, which line-forming region is very extended and the physical processes from the photosphere to the outer parts affect its line profile and variability.

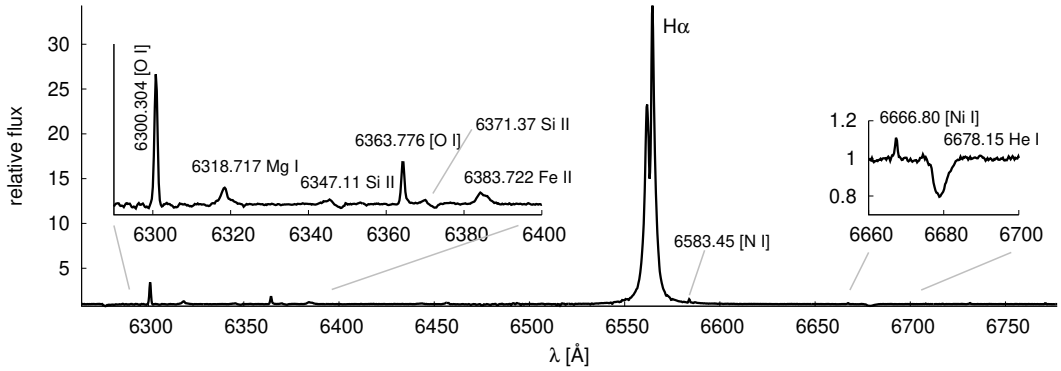

Figure 2.1: Part of FS CMa spectra followed at the Ondřejov Observatory. The shown spectrum was taken on 2007-03-11. (The figure is adopted from Korčáková et al. 2017b and improved.)

The spectral lines are variable on many timescales, usually showing the multiperiodicity, even the chaotic behaviour rather than the regular periodicity. The lines of He I and other neutral and singly ionised metals may show stable emission, but if they are in absorption, they are almost always strongly variable. The line profile may change from night to night from the pure absorption to the P Cygni

profile, inverse P Cygni profile, absorption with emission wings, and to the pure emission. This indicates very dynamical inner parts. However, in contrast to the B[e] supergiants, the velocity does not exceed ~ 200 km s^{-1}. The Hα line shows changes on the time scale of weeks and years, both simultaneously. The forbidden lines vary on the time scale of decades. However, there are strong non-LTE effects due to which the behaviour of these lines must not unambiguously describe the dynamical processes of the outer parts. For example, the Lβ line coincides with the O I resonance line 1 026 Å. The UV radiation pumps efficiently this transition and the following cascade creates the [O I] lines (Fig. 2.6). Therefore, [O I] line variability follows the Hα variability in some objects (Jeřábková et al. 2016).

2.1 UV Radiation

The UV radiation plays a key role in the formation of spectra of the FS CMa stars. Pumping the resonance lines, the multiple scattering starts to play an important role. The coincidence of wavelengths of the resonance lines connects the lines of different elements (Fig. 2.6). This effect is supported by the velocity gradient, which allows the connection of more lines compared to the static case. The cascade from the upper overpopulated levels creates the emission in the visible and IR regions. Very strong absorption of iron group elements (see Fig. 2.2), so-called iron curtain, is created through the disk and observable under high inclination angles. Such strong absorption is observed in classical novae, symbiotic stars, and B[e] supergiants, but not in classical Be stars.

Only two FS CMa stars were observed by HST/STIS camera, namely, HD 50138 and CI Cam. However, it is questionable if CI Cam is a member of this group. Hynes et al. (2002) and Robinson et al. (2002) classified it as a high mass X-ray binary and Bartlett et al. (2019) included it among B[e] supergiants. Spectra of eleven stars (FS CMa, HD 50138, 3 Pup, HD 85567, GG Car, Hen3-847, CPD-52 9243, HDE 327083, MWC 623, MWC 349, and HD 87643) were obtained by the IUE satellite. FS CMa and HD 50138 spectra were also acquired by Wisconsin Ultraviolet Photo-Polarimetr (WUPPE) during the missions Astro-1 and Astro-2. GALEX obtained UV photometry for 23 objects, unfortunately only four are in FUV filter. These data are complemented by several ground-based observations in U photometrical filter.

The UV spectra of HD 50138 (Fig.2.2) and FS CMa show strong absorption of iron-group elements, which reduces the flux by about an order of magnitude compared to the classical Be stars. This strong absorption originates in the circumstellar disk, therefore the size of this effect is angle dependent. Indeed, the GALEX photometry of the pole-on oriented star IRAS 17449+2320 shows the UV excess compared to a classical Be star of the same spectral type (Korčáková et al. 2022). Moreover, there are signatures that UV radiation is variable in this case. The variation in U filter discovered Bergner et al. (1990) in MWC 342. They noticed that there is the anticorrelation between the brightness in U and K filters, which is the consequence of the energy redistribution in the circumstellar matter.

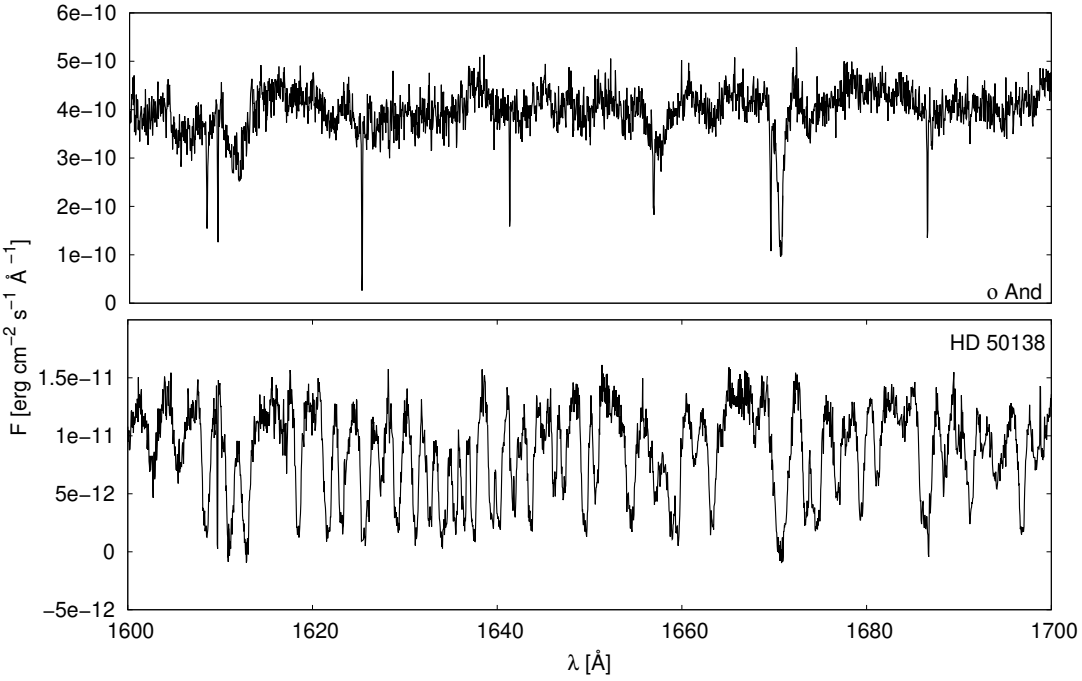

Figure 2.2: Iron curtain of FS CMa stars. IUE spectrum of HD 50138 (SWP camera; 1978-12-21) is compared with the classical Be star *o* And of the similar spectral type (B6; IUE/SWP camera; 1981-11-16). The flux of both stars is corrected to the flux at the distance of 10 pc. (The figure is adopted from Korčáková et al. 2019.)

2.2 Hydrogen Lines

The strongest line in the spectra of FS CMa stars is the Hα line. It may be almost a hundred times more intensive than the surrounding continuum. The higher the member of the series, the weaker the emission is relative to the absorption and the line is narrower (Fig. 2.3). This is the natural effect connected with the line formation, which is also observed in other emission-line stars. The higher members of Paschen series are in emission, while lower members may be in the absorption exhibiting a central emission peak. Both series contain large number of spectral lines. The transitions from about fortieth level are detected (Fig. 2.3).

2.2.1 Hα Line

The Hα line has been observed many times. We do not go into details of all studies and instead focus on its common behaviour in FS CMa stars.

The Hα line is almost always double peaked. Up to now, the violet peak was observed to be stronger than the red one only for IRAS 17449+2320 (Korčáková et al. 2022), at three spectra of AS 386 (Khokhlov et al. 2018), and during one event of HD 50138 (Jeřábková et al. 2016). Once both peaks were comparable also in the spectra of MWC 728 (Miroshnichenko et al. 2015). The ratio of the peak intensities, so called V/R ratio, is very variable. The period was possible to find for MWC 342 ($\sim$4.3 yrs, Kučerová et al. 2013) and IRAS 17449+2320 ($\sim$2.2,

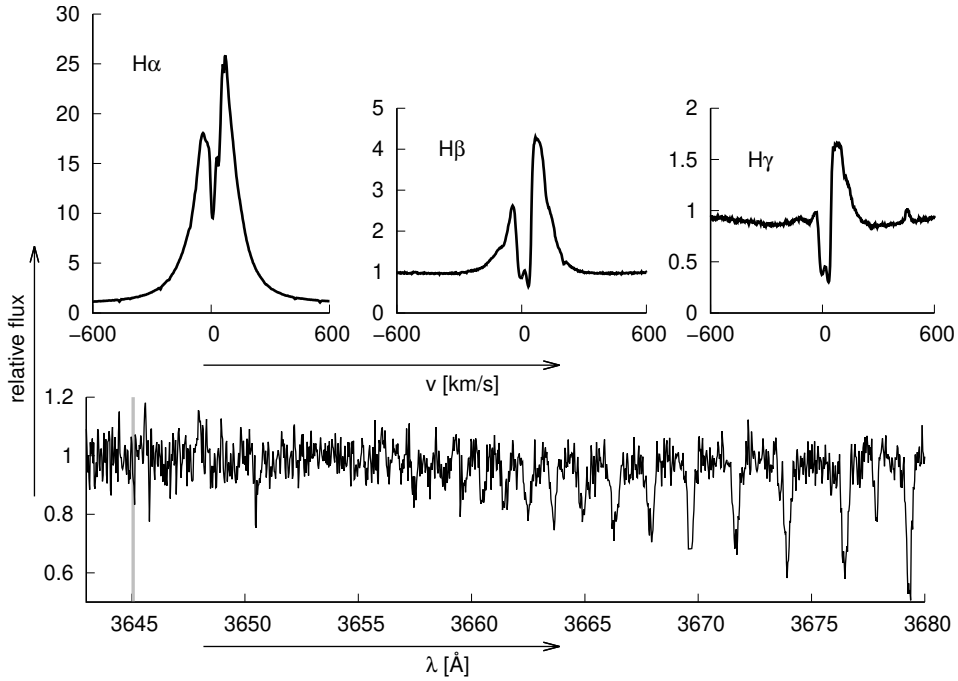

Figure 2.3: Balmer lines of FS CMa on the spectra taken on 2005-12-16 at McDonald Observatory. The central quasi-emission peak is visible on Hα, Hβ, and Hγ lines. The bottom panel shows the higher members of the Balmer series. The grey vertical line denotes the Balmer edge.

Korčáková et al. 2022). The changes on the shorter time-scales show HD 50138 (Jeřábková et al. 2016) and MWC 728 (Miroshnichenko et al. 2015).

The line profiles are deformed by the occasional presence of moving humps (see e.g. Figs.2.3). Behaviour of these features is described very well in Pogodin (1997), Kučerová et al. (2013), and Jeřábková et al. (2016). They reveal either the rotating structures in the disk, or the material ejecta, depending on the object and occasion.

2.2.2 Paschen Lines

Let us focus rather than on the intensity or the number of the Paschen lines on their shape. The detailed profile of the Paδ line is plotted in the Fig. 2.5 together with the Hϵ line. As we can see, the shape of Paδ is the "mirror image" of Hϵ. The reason is that these two lines have the common upper level and therefore the velocity gradient in the line forming region of the Hϵ line affects also Paδ line.

2.2.3 Density and Turbulent Velocity Limit

The number of the Balmer as well as Paschen lines is large, which allows the usage of the Inglis-Teller formula (Inglis & Teller 1939; Nissen 1954) to set the upper limits of the ion density as well as the turbulent velocity. Kříček et al. (2017) found the transitions from the 41th level in the spectra of FS CMa and derived the ion density $\sim 1 \cdot 10^{11}$ cm^{-3} and turbulent velocity $v_{\rm turb} < 40$ km/s. Korčáková et al. (2022) identified the Paschen transition from the 28th level in IRAS 127449+2320, which gives the limit of the ion density to $\sim 2 \cdot 10^{12}$ cm^{-3}

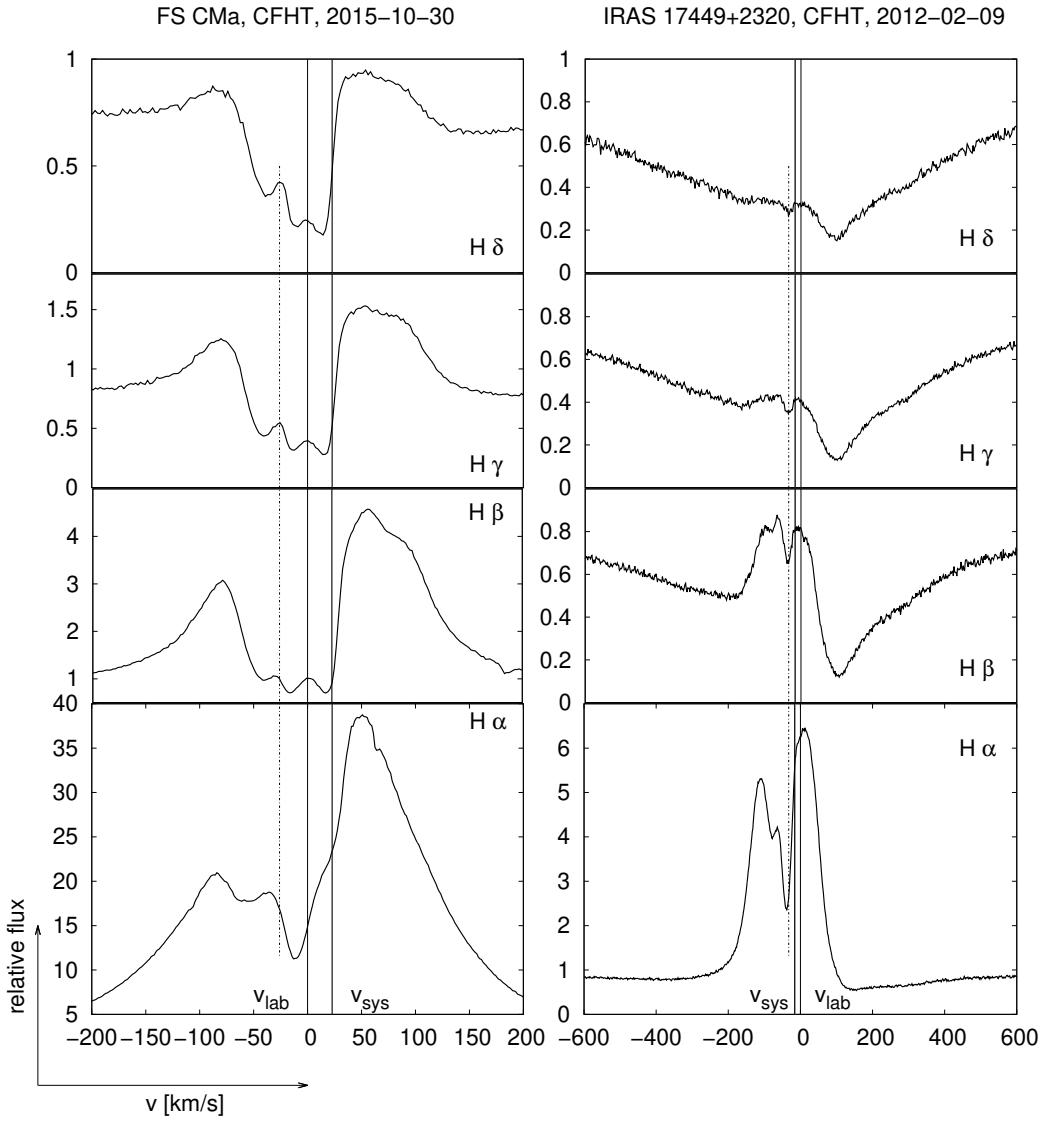

Figure 2.4: Moving structures in Balmer line profiles.

and the turbulent velocity to $\sim$ 130 km s^{-1}. Compared to the dynamical inner part of the disk, the outer regions are extremely quiet.

2.3 He Lines

FS CMa stars, as B-type stars, show only the spectral lines of the neutral He. In the region observable from the ground, singlet 4 009, 4 144, 4 169, 4 388, 4 438, 5 048, 7 281, and 6 678 Å lines and triplet 3 733, 3 820, 3 867, 4 026, 4 471, 4 713, and 5 876 Å lines are detectable. They usually show rapid night-to-night variability with extreme changes of the line-profile shape. Pure absorption may change to pure emission and vice versa through the P-Cygni profile, inverse P-Cygni profile, or absorption with the emission wings. Some stars, e.g. FS CMa or IRAS 17449+2320 (Korčáková et al. 2022) show stable absorption of He I lines. In

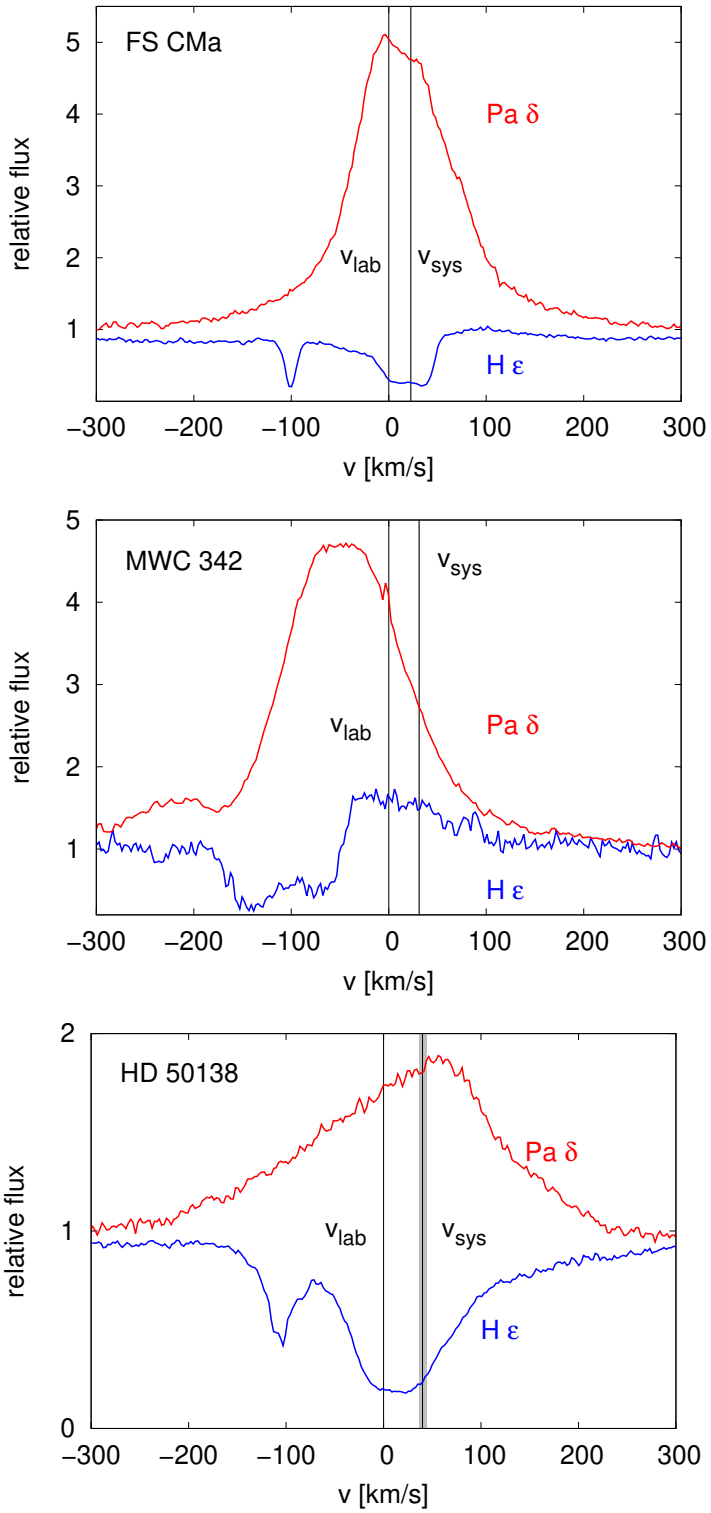

Figure 2.5: Profiles of the Hϵ and Pa δ lines of three FS CMa stars. Non-LTE effects arising from the connection of these two lines through a common upper level are well visible in the spectra of FS CMa and HD 50138. The velocity gradient in the line-forming region of the Hϵ line affects both lines. The absorption feature around -100 km s^{-1} is Ca II 3 968 Å line. Spectra are obtained at McDonald Observatory on 2005-12-19 (MWC 342) and 2005-12-20 (FS CMa and HD 50138) by A. Miroshnichenko.

that case, the lines originated from triplet states may be systematically stronger than singlet lines. This is the effect observed in nebulae, where the collision excitation rate is very small, which allows the overpopulation of lower energy triplet stages. We discuss this effect in detail in the Sec. 3.1.

2.4 Lithium Lines

One should not find the Li lines in the spectra of B-type stars. The ionisation energy of neutral Li ($\sim$ 5.4 eV) is too low that all neutral Li is ionised and the second level of Li II has energy about 59 eV which is too high to be excited by the central star. Despite the theory, the resonance doublet of Li I 6 708 Å is observed in about half of FS CMa stars (Korčáková et al. 2020). The presence of Li I lines is taken as the evidence of the binarity (e.g. Miroshnichenko et al. 2015). However, we are dealing with stars surrounded by extreme amounts of material. This offers another explanation. Li I lines may be formed in the circumstellar disk.

Korčáková et al. (2020) compared high resolution and high S/N spectra of 16 FS CMa stars and found that Li I lines are always in the absorption. And if present, the He I line 5 876 Å shows very sharp central absorption indicating the formation through the disk. Observations and analysis of MWC 623 support the idea of the line formation in the pseudo-atmosphere of the disk. This star has the strongest Li I 6 708 Å doublet, reaching almost 0.6 continuum level. The spectrum of MWC 623 shows the presence of a hot B-type and cold K-type component. This, if it were a standard star, it would have to be the unambiguous evidence of binarity. But not in stars surrounded by an optically thick disk. Indeed, the Hα bisector variability of MWC 623 can not be explained by the companion and modelling points rather to the line-formation in the circumstellar disk (Polster et al. 2018). In support of this hypothesis are polarimetric measurements of Zickgraf & Schulte-Ladbeck (1989).

If it will be proven that Li I lines are really formed in the disk, it may help to resolve one of the long-standing cosmological problems, the lithium problem. The standard Big Bang nucleosynthesis explains the observations of H and He very well, but fails explaining the Li abundance. The calculated Li abundance is three times larger than the observed one derived from the spectral analysis of metal-poor halo stars. A new view on this problem is necessary now, because the theoretical physicists claim that their calculations are correct, while astrophysics do not know how to improve the measurements. FS CMa stars may be helpful in this situation. B-type stars do not burn Li in the atmosphere during the star formation. However, standard main-sequence B-type stars do not allow the appearance of Li lines in its spectrum due to the inappropriate temperature range. However, FS CMa stars have sufficiently low temperature in their disk to allow the formation of the Li I resonance doublet.

2.5 Oxygen

Neutral oxygen has a special place in stellar and nebular spectroscopy. The main reason is that the ionization potential of O I (13.618 eV) is practically the same as

the ionization potential of hydrogen (13.598 eV). This leads not only to the linking of HII regions with the regions of ionized oxygen, but also to the blurring of the HII boundary (e.g. Osterbrock & Ferland 2006). Another important coincidence is that UV O I resonance line 1026 Å is shifted by only about ∼10 km s^{-1} from Lyβ which has consequences for non-LTE line formation, e.g. photo-excitation by accidental resonance can occur there.

The most tracked O I lines are $\lambda\lambda$ 7 772–7 776, 8 446 Å, and [O I] $\lambda\lambda$ 6 300, 6 364 Å. Forbidden emission lines $\lambda\lambda$ 6 300, 6 364 Å are always narrow with FWZI of $\sim$ 60 km s^{-1}, and sometimes double-peaked at high resolution. The line ratio F_{6300}/F_{6364} slightly varies around an optically thin limit value 3 (Jeřábková et al. 2016). At high S/N data, another forbidden oxygen line 5 577 Å may be detected.

The oxygen triplet at 7 772, 7 774, and 7 776 Å shows a complicated structure. Pure emission or pure absorption may be observed, but also broad emission (FWZI from 400 to 600 km s^{-1}) with the triplet lines in absorption, which can be shifted either blueward or redward. Usually all three lines are well separated. The type of the profile can change on a time scale of months or years.

Permitted O I 8 446 Å line is almost always observed in emission, reflecting the shape of the forbidden lines at $\lambda\lambda$ 6300, 6364 Å. However, an exception has been observed in the spectrum of IRAS 07080+0605 (CFHT, 2004-12-21), which shows a complicated structure – inverse P Cygni profile over a wide absorption.

To shed light on the problems of O I line formation, we plot the Grotrian diagram (Fig. 2.6). The kinetic energy of electrons corresponding to their most likely velocity for temperatures of 10 000, 15 000, and 20 000 K is denoted in the lower right corner as grey rectangles. We stress three excitation cycles caused by the resonance transition ^{3}P $\rightarrow^3$ D^0, which creates the absorption line 1 026 Å. This line plays an important role because of its blending with Lyβ. De-excitation of the ^{3}D^0 stage occurs through the 8 446 Å line, from which the electrons can go to the ground stage *i)* directly, *ii)* by creating forbidden lines $\lambda\lambda$ 6 300, 6 364 Å, or *iii)* by creating the line 5 577 Å line followed by the $\lambda\lambda$ 6 300, 6 364 Å lines.

The transition 9 024 Å is highlighted by the red line, because it connects the triplets and singlets with quadruplets. We found that the spectra of FS CMa stars can be sorted by the presence of 9 024 Å line. We plot the examples under the Grotrian diagram. The spectrum of HD 50138 does not show the 9 024 Å line. The 8 446 Å line is in emission, while the triplet at 7 442 Å shows absorption over broad emission wings. This spectrum also has all three forbidden emission lines 5 577, 6 300, and 6 364 Å. A similar case is the spectrum of MWC 342, where the triplets and quadruplet also are radiatively decoupled, showing the same structure of the triplet 7 442 Å and 8 446 Å lines. In contrast to HD 50138, the forbidden line 5 577 Å is not present. The last case is FS CMa itself, whose spectrum shows the 9 024 Å line, and both permitted lines 7 442 and 8 446 Å are purely in emission. Let us note that here we named these three groups following the stars, whose spectra we use here for demonstration in the figure. Because of the spectral variability of FS CMa stars, any star can show any of these three types in another observing season.

In the Fig. 2.6 are also marked resonance transitions which do not occur so frequently in the ordinary main-sequence B-type stars because of the low intensity of the stellar flux at shorter UV wavelengths. However, these transitions may play

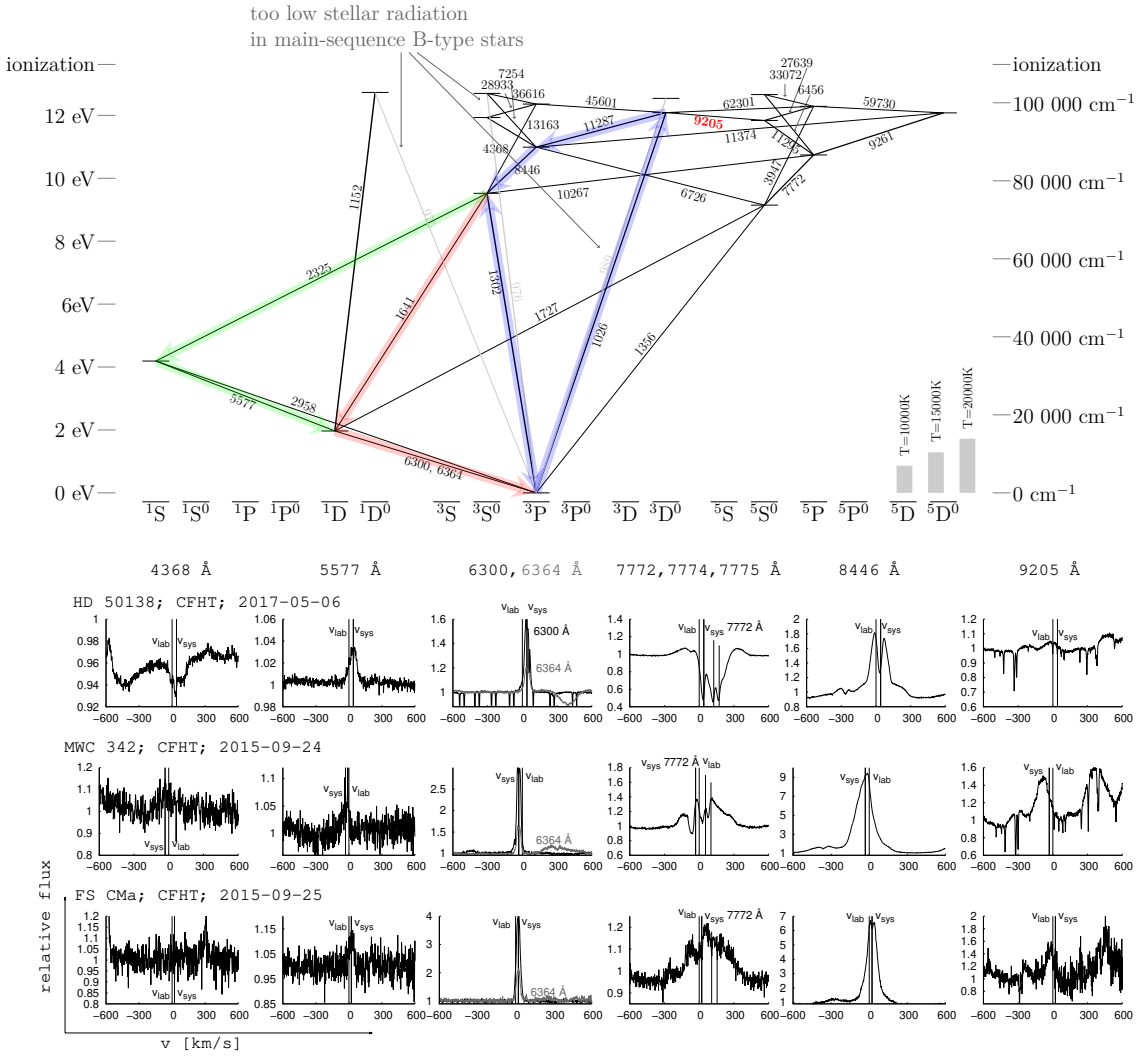

Figure 2.6: Grotrian diagram of O I (it follows Shore & Wahlgren 2010). The line thickness corresponds to the logarithm of the transition probability and the wavelength of transitions is written in Å. The grey rectangles in the right corner denote the kinetic energy of electrons for the temperatures 10 000, 15 000, and 20 000 K. Thick transparent arrows denote the different excitation cycles caused by UV radiation, which we would like to stress here. Especially, we point to the transition 9 205 Å, which connects the triplets and singlets to quadruplets. Depending on the strength of this line, the other oxygen lines show similar profile in different stars. We identified three typical oxygen spectra, which we plotted under the diagram.

an important role in the spectrum formation of FS CMa stars, because some of them show signs of UV excess (Korčáková et al. 2022; Bergner et al. 1990).

2.5.1 Variability of the Oxygen Lines

Forbidden oxygen lines show only slight changes, which can be revealed in long-term monitoring studies (e.g. Polster et al. 2012; Kučerová et al. 2013; Jeřábková et al. 2016). The dependence of the strength of [O I] $\lambda\lambda$ 6 300, 6 364 Å on the strength of the Hα line in the spectrum of HD 50138 is visible in Jeřábková et al. (2016).

The lines from the permitted transitions, 7 772, 8 446 Å, are variable in both strength and shape, especially the triplet 7 772 Å. The variability is best described for HD 50138 (Jaschek et al. 1992; Jaschek & Andrillat 1998; Borges Fernandes et al. 2009). The observations of Marchiano et al. (2012) show the changes of the line profile shape depending on the orbital phase of GG Car.

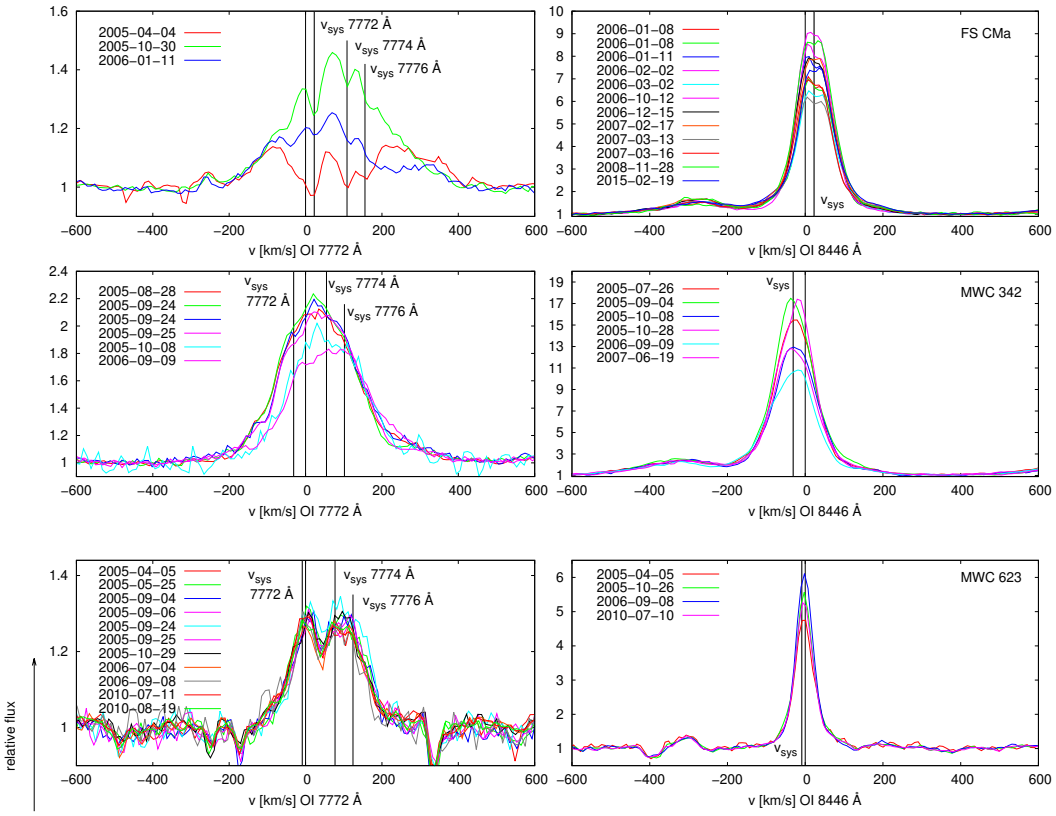

Figure 2.7: O I 7 772 Å and 8 446 Å long-term variability. Spectra are taken at the Ondřejov Observatory (see Tab. A.1). Near the line O I 8 446 Å, the Pa 18 is visible at $\sim$ -300 km s^{-1}.

In the Fig. 2.7 we plot the profiles of $\lambda\lambda$ 7 772, 8 446 Å lines of FS CMa, MWC 342, and MWC 623 taken at the Ondřejov Observatory (R$\sim$ 12 500). All four lines (O I triplet 7 772, 7 774, 7 776 Å, and O I 8 446 Å) are placed exactly at the system velocity defined by the forbidden oxygen lines for all stars. The most stable is the O I triplet 7 772 Å in MWC 623 which does not show changes during

a period of five years. However, another O I line at 8 446 Å does. This indicates that the conditions in the envelope of this star allow the separation of triplets and quadruplets. Indeed, the lines 6 726 and 9 205 Å (Fig. 2.6) are not present in the spectrum of this star (Table A.1, *sp 5*). O I 7 772 Å triplet of MWC 342 is purely in emission (see Fig. 2.7). However, the variations only during one year (from August 2005 to September 2006) are plotted. The line itself shows more extreme changes, which are visible in the Fig. 2.6 where the spectrum from September 2015 is shown.

2.6 Silicon Lines

Permitted lines of singly ionised silicon are very strong in FS CMa objects, especially the $\lambda\lambda$ 6 347, 6 371 Å doublet. Silicon lines in emission are seen in the spectra of FS CMa, AS 160, AS 225, AS 319, MWC 137, MWC 657, SS 170, MWC 342, and MWC 623 [1]. Absorption was detected in IRAS 17449+2320(*sp 1*, and Korčáková et al. 2022) and HD 50138 (Jeřábková et al. 2016). When in absorption, the lines are very variable, showing night-to-night changes and a similar behaviour to the He I lines – pure absorption, pure emission, absorption with emission wings, P Cygni profile, as well as inverse P Cygni profile. This doublet can be used for diagnostics (Sect. 3.2).

The Si II triplet $\lambda\lambda$ 3 854, 3 856, and 3 863 Å lines are also very intence, with the exception of the 3 854 Å line. The lines $\lambda\lambda$ 4 130 and 4 128 Å are usually very weak except for HD 50138 (Table A.1 *sp 2*) and IRAS 17449+2320 (Table A.1 *sp 1*). These two stars also have very strong triplet.

The Si II doublet $\lambda\lambda$ 6347, 6371 Å is magnetically sensitive. The Zeeman split is about 0.27 Å in IRAS 17449+2320 (Table A.1, *sp 2*). Because the magnetic field was discovered only recently (Korčáková et al. 2022), this effect has not been taken in the analysis previously and may affect e.g. radial velocity measurements.

2.7 Resonance Lines

The UV radiation of FS CMa is significant above 1 000 Å, which is sufficient for ionisation of only several neutral metals, the most important of which are C, Si, S, and Fe. Therefore the resonance lines which could be investigated are Na I D1 (5 895.92 Å) and D2 (5 889.95 Å) in the visible region and Ca II H (3 968.47 Å) and K (3 933.66 Å) in the near UV. However, the Ca I H line is blended with Heϵ which limits its usage for simple diagnostics. All resonance lines are affected by very strong interstellar extinction. Below we describe their line profiles without taking the latter into account.

The spectra of FS CMa stars used in this study (Table A.1) and described in the literature almost always show ***symmetric emission*** in the Na I D1 and D2 lines, whose wings reach from $\pm$100 km s^{-1} to $\pm$ 200 km s^{-1}. The Ca II K has the same profile. However, different profile shapes have been detected as

[1] FS CMa (long-term Ondřejov campaign and spectra in the Table A.1), AS 160 (*sp 1*, *sp 2*), AS 225 (*sp 1*, *sp 2*), AS 319 (*sp 1*, *sp 2*), MWC 137 (*sp 1*, *sp 2*, *sp 3*, *sp 4*), MWC 657 (*sp 1*), SS 170 (*sp 1*, *sp 2*), MWC 342 (*sp 4*, long-term campaign Kučerová et al. (2013)), and MWC 623 (*sp 3*), reference with respect to the Table A.1.

well. ***Asymmetric emission*** is very rare. We found it only in one spectrum of AS 160 (Table A.1, *sp 1*). An evidence of expansion of the circumstellar region is seen in the ***P Cygni profile*** of MWC 922 (Table A.1, *sp 1*). Cidale et al. (2012) claim to detect such a profile in the spectrum of CPD−52°9243.

Inverse P Cygni profiles, which are signs of the matter infall, have been observed in the spectra of IRAS 07080+0605 (Table A.1, *sp 1*) and V669 Cep (for a description of the variability of the absorption part, Miroshnichenko et al. 2002a).

Pure absorption is also not a common phenomenon. We found it in MWC 623 (Table A.1, *sp 1- sp 5*) and MWC 728 (Table A.1, *sp 1*). Pure absorption was previously described only in two other stars, MWC 657 (Miroshnichenko et al. 2000a) and HDE 327083 (Miroshnichenko et al. 2003b). ***The absence of the stellar resonance lines*** was found in Hen 3-140 (Miroshnichenko et al. 2001; Ca II K,), MWC 17 (Zickgraf 2003; Na I D1, D2), MWC 728 (Miroshnichenko et al. 2015), and CD−24°5721 (Zickgraf 2003; Na I D1, D2).

Broad absorption wings with central emission, which are seen only in IRAS 00470+6429 (Miroshnichenko et al. 2009), are very unusual.

The Na I D1 and D2 line profiles were found ***different from one another only once*** (Hen 3-140, Miroshnichenko et al. 2001).

Emission in the Na I D1, D2 and Ca II K lines is stable on a time scale of weeks (Pogodin 1997, de Winter & van den Ancker 1997, Miroshnichenko et al. 2002a, Marchiano et al. 2012), but it does change on a longer time scale of years (Fig. 2.8). However, the absorption parts, if detected, are very variable. It is either P Cygni, inverse P Cygni, or discrete components (see next Section 2.7.1).

2.7.1 Discrete Absorption Components of the Resonance Lines

We found satellite absorption components of the resonance lines Na I D1, D2, and Ca II K in the spectra of MWC 342, AS 225, AS 174, HD 328990, and HD 50138 (Fig. 2.9). The presence of such a component of Ca II K line reported for the first time Babcock (1958) in the spectra of FS CMa. The evolution of these features of Na I D1, D2 lines is visible well in Pogodin (1997) in the spectra taken with the CES spectrograph ($R = 40\,000$) on March 15 – 18, 1994. The night-to-night evolution of these absorptions together with the line profile changes of He I 5 876 Å is clearly visible there. Pogodin (1997) noticed that the weak absorptions in the Hα line are located at the same velocity as those of the absorption components of the resonance lines. Similar time series of the Na I D1, D2 satellite absorption in the spectrum of FS CMa were caught by de Winter & van den Ancker (1997) on October 9–14, 1993 taken with a Boller and Chivens spectrograph ($R = 55\,000$). Changes of the satellite absorptions of Na I D1, D2 with the orbital phase of GG Car system were presented by Marchiano et al. (2012).

The satellite absorptions of Na I D1, D2, and Ca II K lines are usually blue-shifted with a displacement between 100 km s^{-1}and 200 km s^{-1}. However, in the spectrum of AS 174 (Table A.1, *sp 1*) there are observed at a radial velocity of ~ -400 km s^{-1}.

We were able to trace two of these events in the Ondřejov spectra. The profile changes of the Si II $\lambda\lambda$ 6 347, 6 371 Å, He I 6 678 Å, and Hα lines before and after

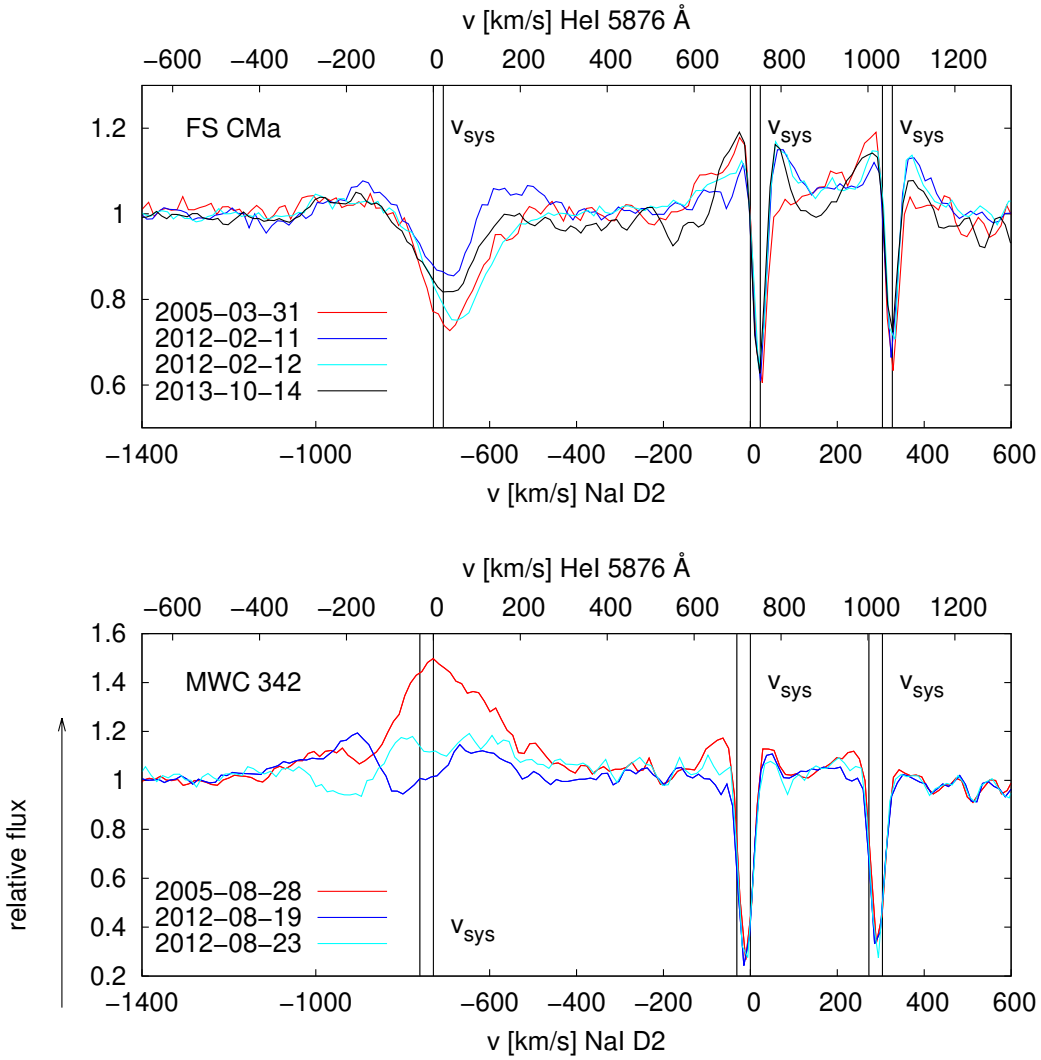

Figure 2.8: Long-term variability of the Na I D1 and D2 lines. Spectra are taken at the Ondřejov Observatory.

the appearance of the satellite absorption components in the resonance Na I D1, D2, and Ca II K lines are shown in the Fig. 2.10 for HD 50138 and in Fig. B.1 for MWC 342. Moreover, the Hβ line is plotted for HD 50138 and O I 8 446 Å for MWC 342. Together with the Ondřejov spectra, the corresponding high resolution spectra (Fig. 2.9) convolved to the Ondřejov resolution are plotted by a thick black line. As expected, the forbidden emission line [O I] 6 364 Å remains unaffected. The red part of the Hα line shows only smooth long-term changes, even in HD 50138, where the resonance absorption appears at +100 km s^{-1}. On the other hand, a weak absorption is present in the blue peak of the Hα line at a radial velocity of ~ -60 km s^{-1}except for the two last spectra, where the Hα line has a smooth shape.

An important behaviour is caught in the Si II $\lambda\lambda$ 6 347, 6 371 Å lines of HD 50138. The black line, representing a high resolution spectrum, shows the same discrete absorption as the resonance lines. Almost the same line profile was

detected six days earlier (thin pink line, Fig. 2.10). However, five days earlier (the thick red line, Fig. 2.10), the absorption at this velocity is negligible. A series of spectra taken during a few subsequent days by Pogodin (1997) does not show such a rapid variability. It is more likely that we have detected two separate events.

The appearance of the satellite absorption components is common in classical Be stars, especially in the UV resonance lines. The first notes were published by Doazan et al. (1980) and interpreted as mass ejection events. The UV spectra show clear discrete absorption components of C IV and N V in the IUE spectra of 59 Cyg. Comparing with the observations in the visible range, they found that the star was also active in the UV during the quiescent phase in the visible. The profiles of the resonance Mg II $\lambda\lambda$ 2795.523, 2802.698 Å lines in 64 classical Be stars were analysed by Lyratzi et al. (2007). They described the discrete absorption components by a kinematical model of multiple rotating regions.

2.8 Forbidden Lines

The strongest forbidden lines, which are always present in the spectra of FS CMa stars, are those of neutral oxygen, [O I] $\lambda\lambda$ 6 300, 6 364 Å. The [S II] $\lambda\lambda$ 6 716, 6 731 Å lines are usually observed, and the [N II] $\lambda\lambda$ 6 548, 6 583 Å lines are occasionally detected. The forbidden lines of S II and N II may be used for the nebular diagnostics (see Sec. 3.2).

Forbidden lines are very narrow with FWHM reaching $\sim$ 50 km s^{-1}. They are symmetric, sometimes double-peaked and are relatively stable with observed variations on timescales of months and years (Polster et al. 2012; Kučerová et al. 2013; Miroshnichenko et al. 2015; Jeřábková et al. 2016).

Forbidden lines are used as tracers of the conditions in the outer parts. However, one has to be careful with the interpretation, especially the lines of [O I] (see Sec. 3.1).

2.9 Spectro-astrometry

The spectro-astrometry may be a very effective method for detection of the binarity. However, it has its limitations. It works well only in a certain interval of angular separation of the components and the presence of the material around the star may also affect the shift at the CCD chip.

Baines et al. (2006) took observations of 28 Herbig Ae/Be stars. Luckily, they included several FS CMa stars into the list of observed stars. They report a new discovery of binarity in FS CMa, HD 50138, and HD 85567. MWC 790 also "infiltrated" the list of Herbig Ae/Be stars of Wheelwright et al. (2010b). However, the observations did not prove, that the star is binary, even if some spectro-astrometric signal was detected.

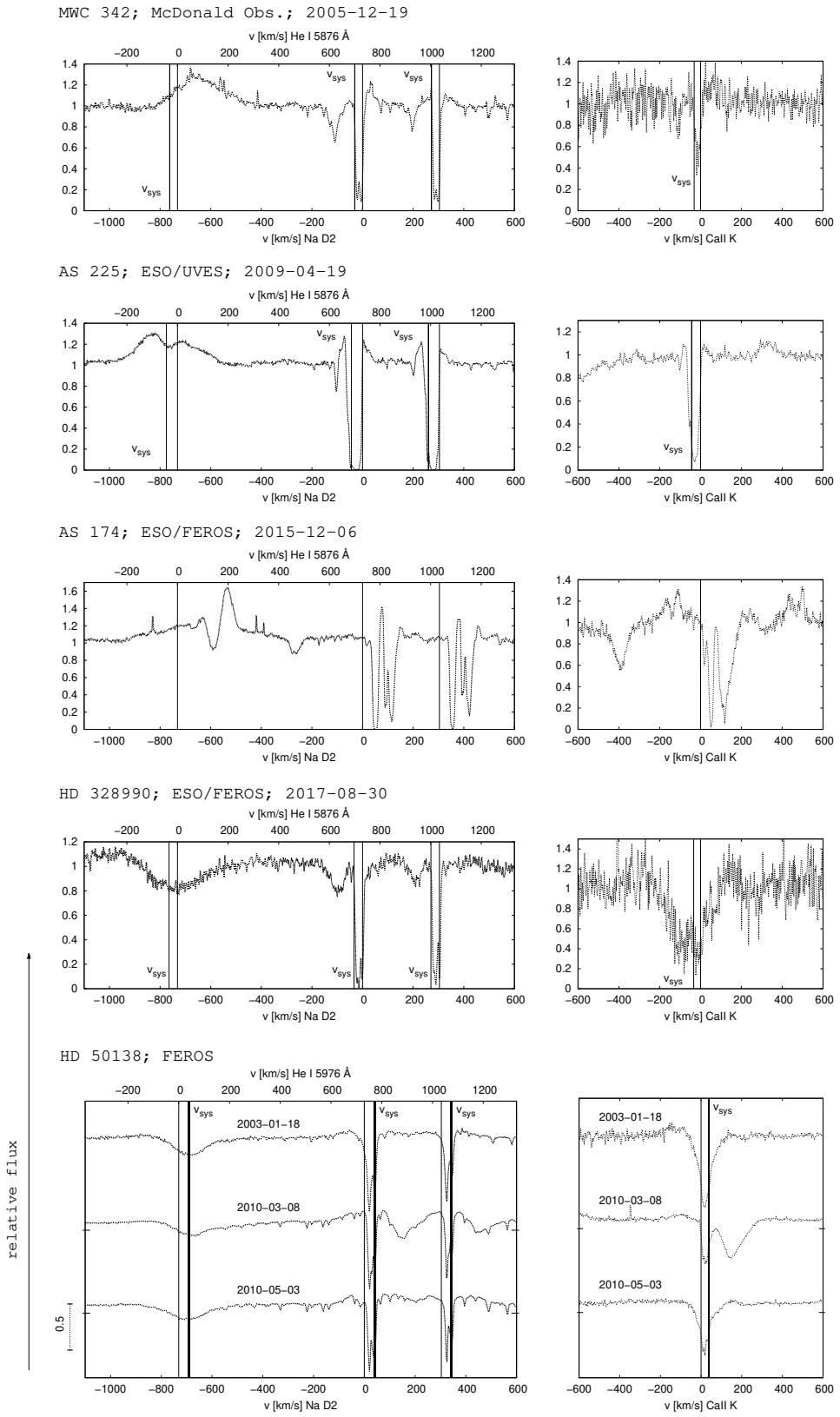

Figure 2.9: The detection of a discrete absorption component in resonance lines. Details of the spectra are shown in Table A.1.

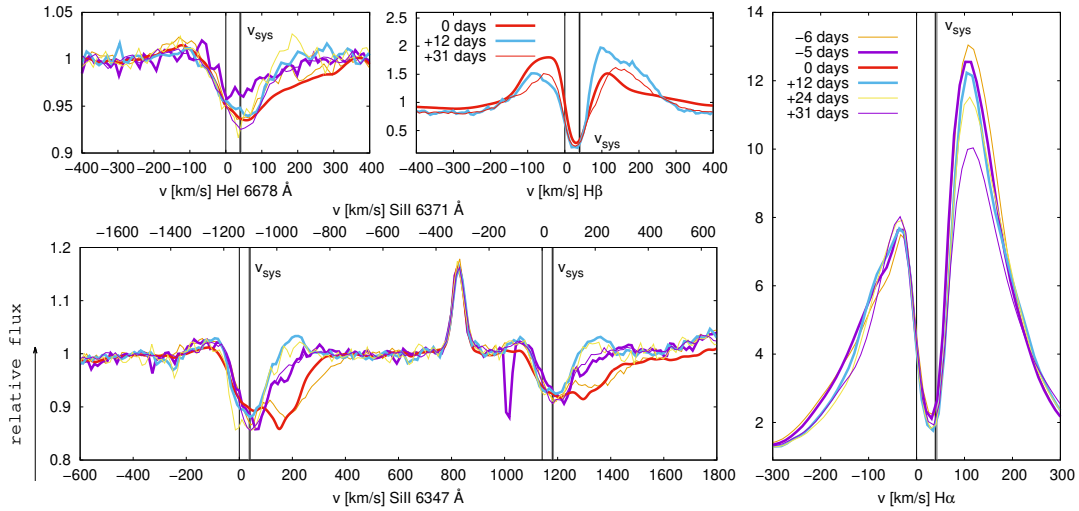

Figure 2.10: The line profiles of selected lines of HD 50138 before (warm colors) and after (cold colors) the detection of the discrete absorption component in resonance lines on 2010-03-08 in a FEROS spectrum (Fig. 2.9). This FEROS spectrum is plotted here by the thick black line. The thick blue and red lines indicate the closest in time spectra to that taken with FEROS. The plotted spectra were taken during the Ondřejov campaign (see Table A.1), namely, on 2010-03-01, 2010-03-02, 2010-03-19, 2010-03-31 in the Hα region, and on 2010-03-19 and 2010-04-07 in the Hβ region. The FEROS spectrum is convolved to the Ondřejov resolution. The Hα line from the FEROS spectrum is not shown here because of the uncertain continuum normalisation in the corresponding èchelle order.

2.10 Polarimetry

Polarimetry is a powerful tool to discover and study the geometry of different regions of the cirucmstellar matter. It may reveal the disk or structure of the outflow, symmetric wind, jets, or geometrically more open cones. It is able to distinguish between the disk, or symmetric wind in the case of geometrically small source, when the line profiles are very similar. It can also determine the disk inclination, as well as the disk opening angle. The latter value may point to the process of the disk formation. Polarimetry is a useful method not only for the determination of the geometrical properties of the circumstellar matter, but also for the conditions and physical processes that take place there. Base on it, it is possible to decide whether the electron scattering, or scattering on the dust particles plays a role there. The wavelength dependence of the scattered radiation allows the determination of the size of the dust particles, as well as their possible orientation in the presence of the magnetic field. The benefit for the study of the FS CMa stars is also the location of the different line-forming regions and the detection of the possible magnetic field.

The first extended polarimetric study of FS CMa stars (although not called that at that time) was done by Zickgraf & Schulte-Ladbeck (1989). Using the 1.23 m telescope at Calar Alto they found the intrinsic polarization in MWC 342, MWC 349, MWC 623, MWC 645, and MWC 939 in U, B, V, I, and Hα filters.

MWC 1055 did not show an intrinsic polarisation signal. The wavelength dependence of the polarization of MWC 645 and MWC 939 is similar to the one observed in classical Be stars. This points to Thomson scattering. However, the polarisation of MWC 645 is stronger than that in classical Be stars. The analysis of the polarimetric measurements of these two stars gives a very large opening angle, ~ 30 deg, which supports the two-component wind model. On the other hand, Mie scattering takes place in two other stars, MWC 342 and MWC 623. The radius of the scattered particles must be larger than $0.05 \ldots 0.07$ μ m and the particles with radii from 0.08 to 0.1 μ m are the most responsible for the scattering.

Not only the polarimetric signal, but also its variability studied Yudin & Evans (1998) at the South African Astronomical Observatory (SAAO). They obtained the measurements for several FS CMa stars, namely, MWC 137, HD 85567, AS 119, HD 50138, AS 160, 3 Pup, and HD 87643. They found rapid variability on the time-scale of minutes in AS 160 ($\sim$10 min) and 3 Pup ($\sim$ 30 min). Both stars also show changes in days. In several days, HD 87643 also changes. HD 85567 shows the night-to-night variability. The variations are also detectable in AS 119.

Oudmaijer & Drew (1999) studied the polarization across the Hα line. They noticed that the scattered radiation from FS CMa comes from two separated regions. The electron scattering take place in the bipolar outflow, while the Mie scattering from the disk. Moreover, the disk can not be homogeneuos, but clumpy. Two distinct line-forming regions are also around HD 50138. There must be the disk close to the star and more extended region. Oudmaijer & Drew (1999) also obseved MWC 137, AS 116, and HD 87643.

This field dealing with FS CMa stars sometimes profits from the wrong classification of these stars, whose properties are similar to the pre-main sequence stars, as well as post-AGB objects. Many of the FS CMa stars were included into the list of Herbig Ae/Be stars, which appeared to be a huge benefit, especially in the polarimetry. Harrington & Kuhn (2007) observed Herbig Ae/Be stars in the Hα line. HD 50138 was hidden in his list. Ababakr et al. (2016) studied polarization not only in Balmer lines, but also in He I lines and forbidden lines of O I. They obtained the polarization measurements for HD 85667 and CPD-48 5215. Later (Ababakr et al. 2017), they extended the number of observed stars to 56 among them were FS CMa, HD 50138, MWC 342, MWC 623, MWC 137, HD 87643, AS 116, and CPD-48 5215.

Several objects were studied in more detail. Luckily, FS CMa belongs to them. Coyne & Vrba (1976) observed FS CMa over four years, which allowed them to study the valiability of the polarization parameters. While the intrinsic polarization changed during the individual epochs, the polarisation angle changed between epochs, but not on shorter time-scale. They found that Thomson as well as Mie scattering play a role there. Combining the polarimetric data, derived exctinction curves and spectroscopy, they determined the $\dot{M}$=$7 \times 10^{-8} \mathrm{M}_{\odot}/\mathrm{yr}$, the inner radius of the dust ring (45 au), the height of the disk ($\sim$ 15 au), the mean density ($5 \times 10^{-7} \mathrm{cm}^3$), and the radius of scattered particles (0.5μm). They also found that the gas-to-dust ratio is an order of magnitude smaller than it is observed in ISM. The first UV and optical spectropolarimetry of FS CMa obtained Schulte-Ladbeck et al. (1992). For UV, they used the Wisconsin Ultraviolet

Photo-Polarimetr (WUPPE) placed at Astro-I space shuttle. The observations revealed two distinguished regions, the dusty disk and polar lobes. The disk is very optically thick composed of large grains, as revealed by Mie scattering. It must be located relatively far from the star, because the point-source approximation of the central star fits the observations well. On the other hand, polar lobes are optically thin and composed of small grain, allowing the Rayleigh regime of the scattering. Based on the observations at 4.2m William Herschel Telescope (WHT) at La Palma and previously published, Patel et al. (2006) found the correlation between the photometrical and polarimetrical changes and concluded that binarity is not likely responsible for the variability. The observations also point to the aspherical ionized region around the star. The polarimetric variability of FS CMa also studied Lee et al. (2018). They noticed that there was an episode of dust formation around 1990. The newly created disk has a different elongation from the main disk. They derived the limit for the grains that must be larger than 1 μm. The first polarimetric diferential images of FS CMa constructed Laws et al. (2020). The images reveal a disk and bipolar outflow, resembling an hourglass.

Another well studies star is HD 50138. The first UV spectropolarimetry obtained Bjorkman et al. (1998) using the Wisconsin Ultraviolet Photo-Polarimeter Experiment (WUPPE) mounted on Astro-2 mission. They complemented the UV observations by optical spectropolarimetry with the polarimeter HPOL ($3190 - 6050$ and $5960 - 10410$ Å) at the 0.9m telescope of the Wisconsin's Pine Bluff Observatory. The intrinsic polarization in the UV region is very similar to the one observed in classical Be stars. The electron scattering dominates there, as well as in the optical region. The observations may be explained by the geometrically thin equatorial disk. As dust scattering contributes only marginally, the dust component is not very significant or is composed of large particles, larger than 1 μm. In that case, the particles shield the light and do not scatter. Lee et al. (2018) also studied HD 50138 in their work. They noticed that in 1995 the dust formation must occur. Small grains were created in the inner edge of the disk and rapidly grew.

Bergner et al. (1990) found the correlations of the polarimetry and photometry in MWC 342. On the other hand, the photometrical changes do not correlate with the polarimetry in MWC 349A as show measurements of Meyer et al. (2002). Because the photometry as well as line emission changed on shorter time-scale than the polarimetry, it is probable that the optically thick clouds shield the emission region. They found that MWC 349A is surrounded by the dusty disk, which is perpendicular to the bipolar outflow, however; the electron scattering plays a more imporant role than Mie scattering. Elvius (1974) also mentioned the presence of dust clouds around MWC 349A. The spectropolarimetry of MWC 349A in the range from 8 to 13 μm provided Aitken et al. (1990). They found a peak at 11μm for which silicate grains are responsible. The grains are located in the dense rotating disk. The position angle points to the presence of a magnetic field normal to the disk plane. The rotating disk was also discovered in GG Car (Pereyra et al. 2009). Oudmaijer et al. (1998) combined spectroastrometry with spectroscopy and broad- and narrow-band imaging to study HD 87643. The observations reveal the fast polar wind ($\sim$ 1 000 km s^{-1}) and the slowly rotating expanding disk. The radiatively driven wind originates not only from the star, but also from the disk.

2.11 Imaging and Interferomety

An extensive survey of the presence of a nebula around B[e] stars was done by Marston & McCollum (2008). Using the Hα narrow band filter at the 60-inch telescope at Mt. Palomar they found an extensive nebula with the presence of a central ring around MWC 137, a thin shell around MWC 349, a faint shell surrounding MWC 342 and MWC 657, and lobes around MWC 819. They also took pictures of IRAS 18316-0028, however, they detected no nebula. MWC 137 was further observed by Kraus et al. (2017) in the Hα filter and with VLT/MUSE instrument by Mehner et al. (2016). The nebula of HD 87643 was studied by Surdej et al. (1981) and Surdej & Swings (1983). Results of a more extensive work can be found in Oudmaijer et al. (1998). They obtained images in V, R, Hα, and Si II lines. B, V, and R images of HD 87643 taken by ESO/WFI camera reveal extended nebula with a very complex structure (Millour et al. 2009).

The bipolar outflow of FS CMa was found on IR images obtained by Laws et al. (2020). They also studied HD 87643 where they detected not only the nebula, but also the companion. An extensive nebula of MWC 819 was studied on the IR images taken by WISE W2 (4.6μm),W3 (12μm), and W4 (22μm) (Arias et al. 2018). A nebula around IRAS 13068-6255 revealed SPITZER images (Gvaramadze et al. 2010). Later, Gvaramadze & Menten (2012) found a bipolar nebula around MWC 349A on SPITZER images.

MWC 349A is the brightest radio continuum star at the centimeter wavelengths and therefore its nebular structure is currently the best studied one among FS CMa stars. The first images from the Very Large Array (VLA) revealed the massive interacting binary (Cohen et al. 1985). A more detailed study of White & Becker (1985) at 2 cm at VLA showed that we are looking at the edge-on bipolar nebula, where the dust is forming in the equatorial plane. Tafoya et al. (2004) mapped the wind-wind interaction region at wavelengths from 7 mm to 90 cm at VLA. Moreover, they found the variability of MWC 349A. The images in H30α recombination line using the Submillimeter Array (SMA) constructed Weintroub et al. (2008). A complex view on the structure of all the surrounding region and wind-wind interaction region brought Strelnitski et al. (2013). They present images from Spitzer, Herschel, CO map, and Hα filters.

The inner parts of MWC 349A nebula, the disk structure, is better observable using IR or visible interferometry. The observations of Sallum et al. (2017) performed at Large Binocular Telescope Interferometer (LBTI) reached the best resolution. Quirrenbach & Albrecht (2010) noticed from the observations taken at VLTI/MIDI that the forbidden emission region is larger than the dusty ring. The inner disk also revealed the segment-tilting experiment at the KECK telescope (Monnier et al. 2009). One of the first observations using the technique speckle interferometry was done by Hofmann et al. (2002) at Russian 6 m telescope in J, H, and K bands.

In the observing program of Monnier et al. (2009), FS CMa, HD 50138, and MWC 342 have been included and resolved. The brightest star in the visible of these three stars is HD 50138, which was observed after that several times. Borges Fernandes et al. (2011) used not only the segment-tilting experiment at the KECK telescope, but also VLTI/MIDI and VLTI/AMBER. They were able to determine the size and orientation of the disk on the sky. Ellerbroek et al.

(2015) used VLTI/AMBER not only in the continuum, but also in Brγ, which allowed the construction of the maps in several velocity bands. Kluska et al. (2016) were able to detect structural changes of the nebula between 2010 and 2013 using the VLTI/PIONIER instrument. Moreover, they showed that this object is not likely the binary. They were not able to reproduce the observations by the secondary; however, the data fit well with the disk model. Koutoulaki et al. (2018) extended the VLTI/AMBER observations to the Pfund series. They found that the hydrogen emission comes from the wind region, which has a radial size of about 0.4 au and forms a disk-like structure with a very large opening angle. Varga et al. (2019) were able to determine the mineralogical composition of the dust (see Sect. 3.3). The variations of the visibility functions, i.e. changes of the structure, studied Kobus et al. (2020).

Another typical representative of the FS CMa group is MWC 342. IOTA infrared interferometer revealed elongated emission and a ring diameter about 3.1 ± 0.3 au. An enormous amount of work was done by instruments MIDI and AMBER at VLTI. Both were used for the study of CPD-57 2874 by Domiciano de Souza et al. (2007). They found that the emission of the hot dust has a disk-like structure. Its size at 2.2 μm is about 4.5×8.5 au and at 12 μm about 30×38 au. MIDI observation of the brightest FS CMa star, namely 3 Pup, revealed two dusty rings (Meilland et al. 2010). Domiciano de Souza et al. (2011) also used MIDI for CPD-57 2874. They determined the inner radius of the dusty disk of 12.7 au or 14.4, depending on the distance (1.7 kpc and 2.5 kpc, respectively). They also measured the dust temperature at the inner radius ($\sim$ 1 500 K) and found its linear decrease with the radius. MIDI also resolved the dusty ring around CPD-52 9243 (Cidale et al. 2012) determining the upper limit for the inner edge to be $\sim$ 28 au. AMBER, operating at shorter wavelengths, discovered a circum-binary disk around MWC 873, whose radius is $\sim$ 5.1 au ($\sim 40.5\,\mathrm{R}_\star$) and width $\sim$ 2.1 au ($\sim 23\,\mathrm{R}_\star$) (Wheelwright et al. 2012). This instrument was used twice for the study of HD 85567. Wheelwright et al. (2013) found that the symmetric gaseous disk is surrounded by the dusty disk. They found no sign of binarity. Vural et al. (2014) analysis showed that the model of the disk with halo fits the observation very well. MIDI and AMBER detected secondary at a distance of about 51 au around HD 87643 (a candidate object, Millour et al. 2009). Another candidate object, MWC 137, was studied by the Fabry-Perot interferometr placed at Russian 6 m telescope. The velocity maps of the [Si II] lines revealed an extended emission out of the main nebula.

2.12 Photometry

The photometrical studies are mostly based on individual observational campaigns, and large databases are not currently fully used. The American Association of Variable Star Observers (AAVSO) database[2] contains extensive data on FS CMa, MWC 349, HD 50138, V669 Cep, MWC 17, MWC 939, CPD-57 2874, HD 85567, HD 87643, GG Car, and CI Cam. The All Sky Automated Survey (ASAS) Pojmanski (1997)[3] was used for the studies of 3 Pup, MWC 137,

[2]https://www.aavso.org/

[3]http://www.astrouw.edu.pl/asas/

CPD-57 2874, CPD-52 9243, HD 87643, GG Car (Maravelias et al. 2018), and IRAS 07080+0605 (Arias et al. 2018). All Sky Automated Survey for Supernovae (ASAS-SN[4]) used Porter et al. (2021a) for the study of GG Car. The most precise photometrical data from the TESS satellite (Transiting Exoplanet Survey Satellite[5]) offer new possibilities for research. Recently Mikulášek et al. (2020) found the light curve variations of an Ap star caused by the occultations of the matter trapped above the atmosphere in the magnetic field loops. The first work based on TESS data in the field of FS CMa stars is done by Kraus et al. (2021) for MWC 137.

The light curves of FS CMa stars are very complicated. A short review can be found in Korčáková et al. (2017a). The light curves may be affected by the occasional events of dust formation (Miroshnichenko & Corporon 1999a, MWC 342), the variable emission of the gaseous envelope, and an eclipse of the dusty regions (Chkhikvadze et al. 2002, MWC 342). Therefore, it is not surprising that FS CMa stars usually show multiperiodic behaviour (see Table A.5). In most objects, it is better to talk about some scale of the variability rather than about the regular periodicity. This topic is discussed in detail in Section 3.4. Let us now focus on other photometrical properties.

The (U-B) vs. (B-V) diagram plotted by Bergner et al. (1990) shows that MWC 342 is a large outlier compared to color indexes of normal stars. A more detailed study of the color indexes of all types of stars showing the B[e] phenomenon is presented in Chen et al. (2021). Based on the data from IRAS, WISE, and 2MASS satellites, they compare the photometirical properties, e.g. color-color diagrams, of the individual groups of the B[e] stars with each other, but also with the classical Be stars. There have been found correlations and anticorrelations between color indexes (MWC 342, Bergner et al. 1990; CI Cam, Miroshnichenko 1995; AS 78 and MWC 657 Miroshnichenko et al. 2000a). Miroshnichenko et al. (2000a) noticed that when $U-B$ and $B-V$ decreased, $V-R$ and $V-I$ increased. Moreover, the temporal variations of $U-B$ and $B-V$ color indexes show a positive correlation, which indicates that we have a "clear" view of the star, not through the most dense parts of the disk. Such variations of the color indexes are observed in the classical Be stars during the formation of a new shell Harmanec (1983).

2.13 Molecules

The group of FS CMa stars was defined based on the presence of hot dust. In some objects, e.g. MWC 349 (White & Becker 1985), the dust is just being formed. Therefore, in at least several objects, the molecular component must be present. To create a molecule, a sufficient density of matter in a sufficiently cold region must be available. This can be reached by, e.g. wind-wind interaction, which is observed in the above-mentioned star (White & Becker 1985). However, these are not the only conditions. Molecules are very sensitive to the UV radiation. They are quickly dissociated under its influence. B-type stars have relatively strong UV radiation. It definitely prevents the presence of molecules around an

[4]https://www.astronomy.ohio-state.edu/asassn/
[5]https://tess.mit.edu/

ordinary B-type star. Therefore, the shielding effect must be very effective to detect molecules around such hot objects. The most frequent molecule, which is observed, is CO. It is natural because of its very strong bound. The presence of CO molecule is very beneficial for us. The ratio of $^{12}C/^{13}C$ isotopes is an indicator of the age of the object (Kraus 2009). This is crucial for FS CMa stars, because their spectra and photometrical properties may be interpreted as both, pre- and post-main sequence stars. Higher abundance of ^{13}CO was detected in GG Car (Kraus 2009; Kraus et al. 2013), CPD-57 2874 (Kraus 2009), MWC 873 (Wheelwright et al. 2012), and MWC 137 Muratore et al. (2015) proving the evolved phase.

Other molecules were detected very rarely, especially TiO and H_3^+ (see Table A.4). Polycyclic aromatic hydrocarbons (PAHs) were found by analysing the FUV extinction function in FS CMa (Brown et al. 1995). If the observations of an individual object prove the presence of the Keplerian disk where the molecules are present, the molecular emission may be used to determine the conditions in the individual parts of the disk (Maravelias et al. 2018).

2.14 Spectral Energy Distribution

The shape of the spectral energy distribution (SED) is one of the features that defines the FS CMa group. Strong IR excess due to the hot dust must be present there. This additional emission creates a peak between 10 and 30 μm, which decreases sharply at longer wavelengths (Miroshnichenko 2007).

As one of the signs defining the group, the SED is discussed in many papers. The SED is usually used for the determination of the dust temperature by fitting the Planck function, or multiple Planck functions. At this point, I would like to mention extensive works in which the IR properties of several objects are discussed and compared. Such a comparison of MWC 819, MWC 645 with η Car was done by Swings & Allen (1973). Allen (1973) measured the brightness of 248 emission-line stars in H (1.6 μm), K (2.2 μm), and L (3.5 μm) filters. He discussed the effect of the dust emission and free-free emission for stars with different $H-K$ and $K-L$ indexes and showed the SED of FS CMa, HD 50138, MWC 342, and CI Cam (later called FS CMa stars) and Herbig Ae/Be stars (HD 31648, HD 190073, MWC 297), and MWC 300, which has been later identified as a supergiant, the nearest supergiant in the Milky Way. A year later, Allen (1974) published a similar study focused on planetary nebula. He also included several emission-line stars. He compared the SED of 3 Pup, MWC 349, MWC 623, MWC 17, MWC 790, and MWC 1055, with another emission-line star MWC 778 and planetary nebulae Hen 2-442, MWC 922 (Red Square Nebula), M 2-56, and Hb 12. Malfait et al. (1998) studied the Herbig Ae/Be stars, however, HD 50138 and HD 85567 infiltrated their list. Gauba et al. (2003) focused his work on post-AGB candidates. Among the stars, for which he showed the SED is MWC 939. The SED of twelve FS CMa stars is shown in Miroshnichenko et al. (2007). The properties of HD 85567, Hen 3-140, and Hen 3-1398 discussed Miroshnichenko et al. (2001). For a more detailed analysis of the SED, I refer to the Sect. 3.3.

2.15 Magnetic Field

The detection of the magnetic field in FS CMa stars is a difficult task due to the dynamical circumstellar matter. The line deformation by the velocity suppresses the Zeeman split. The first who mentioned the mag. field was Babcock (1958) in FS CMa, however, it was a false discovery. He used for the measurements [S II] doublet $\lambda\lambda$ 4 068, 4 076 Å, which is split by the expansion of the envelope and not by the mag. field.

The discovery of the mag. field in FS CMa stars was reported only recently by Korčáková et al. (2022). They found the Zeeman split of metallic lines of C I, N I, O I, Mg I, Ti II, Fe I, and Fe II in IRAS 17449+2320 based on which they determined the mean magnetic field modulus to 6.2 ± 0.2 kG. This value is comparable with Ap stars with the strongest mag. field. The doublets, triplets, as well as quadruplets gave consistent results proving that the line split is caused by the mag. field and not by the expansion of the envelope. The number of high resolution and high S/N data is not sufficient to show if there is a dependence of the mean mag. field modulus on the energy of the lower level (Korčáková et al. 2022, Fig. A.3), which may be used as the "scan" of the mag. field through the photosphere, and its temporal dependence (Fig. 2.11). Note, to study the mag. field variability, one has to compare the measured values only for the same line because the different lines are formed in different depths, but especially because some ions drift according to the mag. field creating spots on the surface.

The measurement of the mag. field in FS CMa stars has a little less accuracy than in magnetic Ap stars nowadays. Most of the lines used for the measurement in Ap stars have very well determined Landé factors. This is not the case of FS CMa stars, which have higher temperature, therefore other lines are possible to use. Only recently, the observation technique allowed the investigation of mag. field in B-type stars, therefore the accurate data for all important lines has not been determined yet.

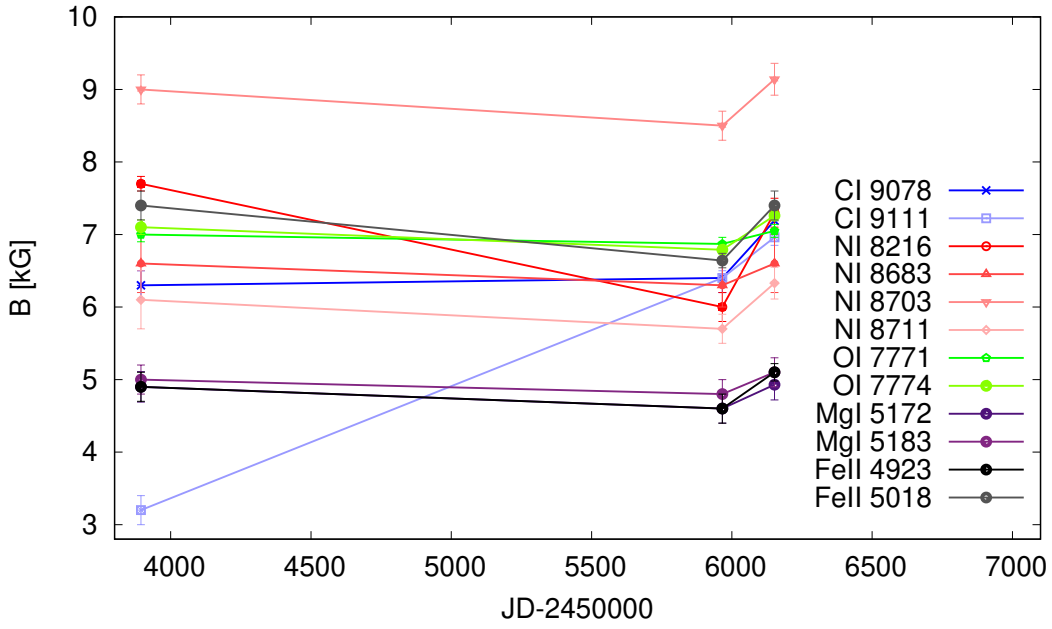

Figure 2.11: The temporal dependence of the mean mag. field modulus of the individual lines in IRAS 17449+2320. The data are adopted from Korčáková et al. (2022).

Chapter 3

Results of Analysis and Modelling

A colleague of mine once said that novae are a textbook of the radiative transfer. If so, then FS CMa stars are something like the final exam.

Before we start to discuss the most important results of the analysis, let us point to some observational aspects, which have important consequences for the analysis. The large amount of circumstellar matter complicates the analysis. Standard approaches are usually not possible to be used without some improvements, even something as simple as the measurement of the equivalent width (EW). Therefore, it is not surprising that, e.g., the spectra disentangling gives strange results and the interpretation must be carefully done. The velocity gradient deforms the line profiles, however, its value is not large enough to separate individual regions and, e.g., Sobolev approximation (Sobolev 1946) can not be used.

The mag. field may affect, among others, the radial velocity measurements. Especially, the most frequently used doublet Si II $\lambda\lambda$ 6 347, 6 371 Å is magnetically very sensitive. To determine the stellar parameters, mag. null lines should be used. However, no commonly used mag. null lines are sufficiently strong in these stars.

To see the complexity of the problem, let us first mention non-LTE effects playing an important role in the circumstellar environment of FS CMa stars.

3.1 non-LTE

Extended, low-density circumstellar matter itself offers perfect conditions for non-LTE effects. Taking into account that UV radiation is sufficiently strong to excite resonance levels, the multiple scattering plays an important role. The gradient of the velocity is large enough to link the nearby resonance lines, but small enough to separate the region into parts which can not directly communicate. Watching only one line, it is hard to distinguish if the line is changed because of the non-LTE effects, or because of the temperature and density changes.

The best example is the coincidence of the Lβ and O I 1 026 Å resonance lines. The cascades from the upper O I levels affect optical lines, including the forbidden lines (see Sec. 2.5 and Fig. 2.6). This effect limits the usage of [O I] lines as the tracers of the outer parts, which is very frequently done. The Hα and [O I] $\lambda\lambda$ 6 300, 6 364 Å lines may even show the same variability, as it is observed in HD 50138 (Jeřábková et al. 2016). How strong the optical pumping

is, it is possible to see also on the Hα polarisation measurements of Harrington & Kuhn (2007) in HD 50138 or on the profiles of Paschen and Balmer lines, which are almost mirror images (Fig. 2.5).

The density around some stars is sufficiently low to see some effects observed in nebulae. One of these is that triplet lines are systematically stronger than singlet lines in very low density medium. This is due to the lower energy of triplet levels, which are more populated when collisions are not sufficiently frequent. The effect is visible best on He lines. The Fig. 3.1 shows He I line profiles of FS CMa, however, this effect is even better visible in the spectra of IRAS 17449+2320 (Korčáková et al. 2022, Fig. A4).

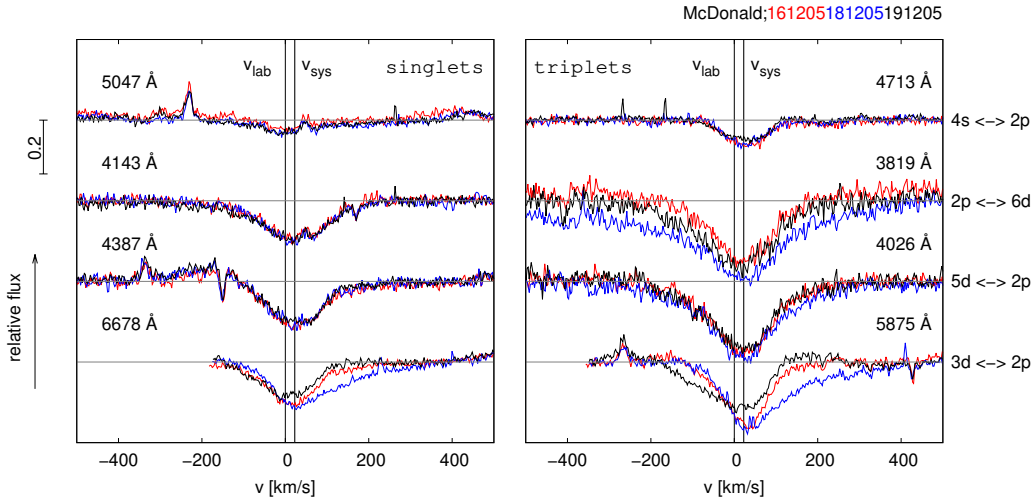

Figure 3.1: Singlet vs. triplet transitions of He I on the example of FS CMa spectra taken at McDonald Observatory. Note, the line 6 678 Å shows a night-to-night variability in Ondřejov spectra.

3.2 Nebular Diagnostics

The low density in the outer parts allows the usage of standard methods for nebulae. The [O I] $\lambda\lambda$ 6 300, 6 364 Å lines only provide information about the optical depth. Even worse, only their intensity ratio 3:1 can be used for justification of the usage of the optically thin approximation in the line forming region, because these lines have a common upper level.

The opposite situation, a common lower level, is the case of singly ionized sulfur and nitrogen. [S II] $\lambda\lambda$ 6716, 6731 Å are usually present in the spectrum and can be used for estimating the electron density in their formation region. [N II] $\lambda\lambda$ 6716, 6731 Å provide the same information, however, their presence in the spectra of FS CMa stars is very rare.

3.2.1 BPT Diagrams

BPT (**B**aldwin, **P**hillips, & **T**erlevich, Baldwin et al. 1981) diagrams are plots of different emission line intensity ratios. Since these ratios depend on the temperature of the ionisation source, one can easily distinguish different types of objects,

e.g., supernova remnants, planetary nebulae, HII regions, or symbiotic stars. This diagnostic is very useful for external galaxies, where the angular resolution is too small for an accurate classification of individual sources.

Such kind of diagnostics may be very useful for FS CMa stars, since the list of members and candidate objects is contaminated with some proto-planetary nebulae or symbiotic stars. Unfortunately, the ionisation source of FS CMa stars typically has too low temperature to use all BPT diagrams, most of which are based on the ratios of the [O II], [O III], or [N II] lines. Instead of that, FS CMa stars have [S II] and [N I] lines in the spectra, which limits the usage of the classical BPT diagrams only for those related with the Hα line.

Another complication arises due to deformation of the emission lines by expansion. Double-peaked profiles were frequently detected. Therefore, the EWs instead of the line intensity is necessary to use. This is valid for optically thin forbidden lines, however, the Hα line is affected by the absorption, which can slightly change the source position in the diagrams. I show here two BPT diagrams, Figs. 3.2.1, 3.2.1, and two others in appendix (B.0.1). The position of FS CMa stars is clearly separated from those of planetary nebulae, and even more from HII regions or supernova remnants. This is expected, because the temperatures of the B-type stars in FS CMa objects are at least an order of magnitude lower. On the other hand, it is possible to use BPT diagrams to distinguish proto-planetary nebulae from FS CMa stars. In every figure, we plotted MWC 939 (black triangle), which has been included in the list of FS CMa stars, but it belongs to proto-planetary nebulae.

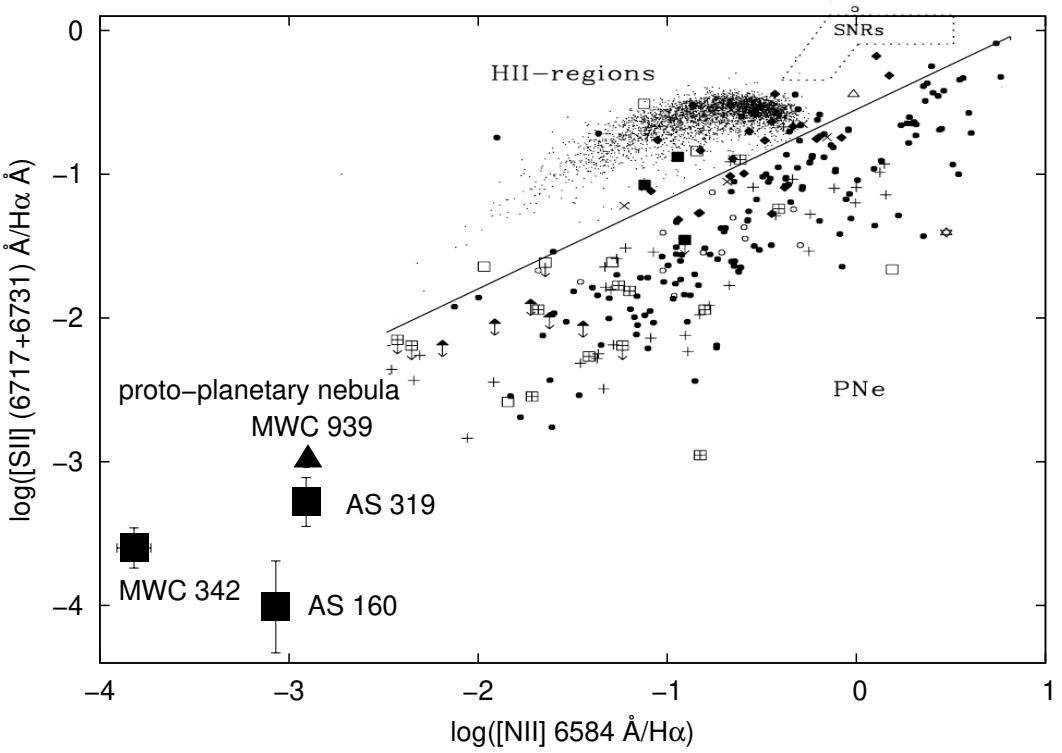

Figure 3.2: BPT diagram based on Kniazev et al. (2008), Fig. 4, upper panel. The added values for FS CMa stars are based on the EW measurements.

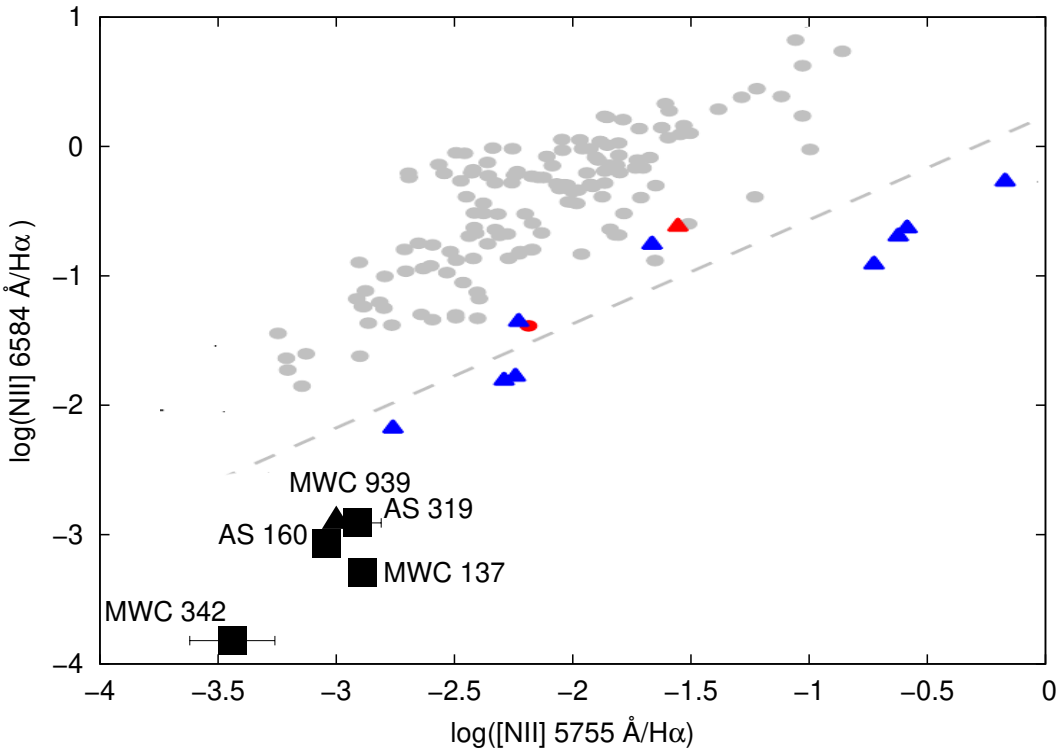

Figure 3.3: BPT diagram of Iłkiewicz & Mikołajewska (2017), Fig. 3 a). MWC 939 (black triangle) is a B[e] protoplanetary nebula. Gray circles denote planetary nebulae. Blue colour separates symbiotic stars of different types; S-type are marked by rings, D'-type circles, and D-type with triangles. Red symbols are symbiotic stars with the presence of [OIII] lines. Similar to the previous picture, the added values for FS CMa stars are based on the measurements of EWs.

3.3 Dust

The lack of sharp spectral features in the dust radiation prevents the applicability of the methods used for the analysis of atomic or molecular spectra. For the determination of the dust composition and grain size, the shape of the extinction curve is used. However, the circumstellar extinction may be even more complicated than that of the diffuse interstellar medium (ISM). Therefore, the applicability of normal extinction curves is limited (Sitko et al. 1994). The main reason is the geometry of the dusty shell. If the dust around the star creates the disk, or ring, and we see the disk edge-on, the scattered photons toward the "polar" directions are lost and not replaced as it is in homogeneous medium. The small grains may be removed by the radiative force of the central star. Such a lack of small-sized grains makes the extinction curve smoother. However, the same shape of the extinction curve can create the optically thick clumps of dust. Moreover, these clumps may orbit the star, which was observed in, e.g., FS CMa (de Winter & van den Ancker 1997).

Most of FS CMa stars show the presence of warm and cold dust. Miroshnichenko (2010) found a weak silicate emission at 10 and 18 μm in most FS CMa stars observed with Spitzer. The silicate emission at 12 μm detected Gauba et al.

(2003) around MWC 939, moreover, they also found the emission features at 8.2, 8.6, and 11.3 μm for which polycyclic aromatic hydrocarbons are responsible. Their modelling of the SED showed that the hot dust component, close to the star, is composed from graphite grains, while silicate grains are in outer, colder, disk. The VLTI/MIDI observations of Varga et al. (2019) revealed the stratification of the dusty disk around HD 50138. They found that the inner parts of the disk are composed of forsterite grains. In the farther regions, both forsterite and enstatite are present, while in the outermost parts are amorphous silicate grains.

The SED allows the determination of the inner and outer radius of the dusty ring/rings. For example, Malfait et al. (1998) tabulated the parameters for HD 50138 and HD 85567. Unfortunately, complex modelling of the gaseous and dusty region including cooling and heating by radiation and the detailed radiative transfer was done for only one star, IRAS 00470+6429 (Carciofi et al. 2010).

The episodes of the dust formation have been observed in some objects, e.g., FS CMa (Swings & Allen 1971; de Winter & van den Ancker 1997), MWC 349 (Josselin et al. 1998), or MWC 342 Miroshnichenko & Corporon (1999a). Dust absorbs and scatters the radiation, which caused the additional observed variability. The optically thick clumps may be created, leading to even more complicated photometric behaviour.

3.4 Periodicity

Finding the regular periodicity in FS CMa stars is a little tricky. The photometry as well as spectrum are affected by pulsations, continuous outflow, rotating gas structures in the disk, occulting by dusty regions, occasional events of the material infall, as well as occasional events of the formation of a new shell. The possible secondary enters into the game, and not only by a simple radial velocity changes or eclipse. It may, e.g., generate pulsations of the primary (Porter et al. 2021a). Therefore not sufficient data coverage may show changes that mimic the periodicity and have been misinterpreted as the regular periodicity. The found short-term period may change from season to season, as has been observed in some objects, e.g. MWC 342 (Mel'Nikov 1997).

Depending on the line-formation region, the spectral line varies on many timescales. Helium and metal absorption lines show nigh-to-night variability. The line-profile shape may change from pure absorption, P Cygni profile, inverse P Cygni profile, pure emission, as well as absorption with the emission wings. The emission lines of metal and Balmer lines do change on the timescale of weeks and moths. The forbidden emission lines show variations in the order of months and years. This behaviour is visible well in Kučerová et al. (2013) (MWC 342), Jeřábková et al. (2016) (HD 50138), Korčáková et al. (2022) (IRAS 17449+2320), and photometry in de Winter & van den Ancker (1997) (GG Car) and Šimon et al. (2007) (CI Cam). The effort in the period analysis reflects the Table A.5.

pulsations

Goranskij & Barsukova (2009) found at CI Cam two pulsation periods 0.41521 ± 0.00004 and 0.26647 ± 0.00002 d that are close to the 3:2 ratio and may cause the beating phenomenon. Even more complicated are the pulsations of GG Car. Porter et al. (2021a) noticed that the tidal forces of the secondary component

generate $l = 2$ f-mode with the period of 1.583156 ± 0.0002 d. The amplitude of this pulsation mode depends on the orbital phase being the largest at the periastron.

orbital period

Several objects among FS CMa stars have been proven to be binaries. The most famous one is CI Cam that is the Be/X-ray binary. Barsukova et al. (2006a) found an orbital period of 19.41 ± 0.02 d. The brightest star of this group is 3 Pup, where the orbital period was measured to be 137.4 ± 0.1 d (Miroshnichenko et al. 2020a). The above mentioned interacting binary GG Car has the orbital period 31.01 ± 0.01 (Porter et al. 2021b). Very large semiamplitude (52 ± 3 km s^{-1}) was found by Khokhlov et al. (2018) at AS 386. Their orbital solution shows the period of 131.27 ± 0.09 d and gives the lower limit of the secondary to 7 $M_\odot$. Because there are no spectral lines of the secondary component in the visual region the companion is most likely a black hole.

multiperiodicity, a chaotic behaviour

Other FS CMa stars show more complicated behaviour. The best example is FS CMa itself. de Winter & van den Ancker (1997) analysed the photometetric data over 25 years supplemented by spectroscopic data from 1923 to 1990. Around 1950, an episode of intensive dust generation occurred. Consequently, the star became fainter about more than 1.5 mag. Dust clouds, shock fronts, material infall, or dust destruction are probably responsible for the variability on time scales of a few years. Instability in an accretion flow produces a variation on the scale from hours to days. All these processes are accompanied by material outflow which reveals itself in the line profile of Hα, He I, and resonance Na I lines. Similar behaviour shows MWC 342 (Kučerová et al. 2013), however, no explanation has been given so far.

3.5 Velocity determination

The gradient of the velocity field in the line-forming region complicates the numerical description of the problem. On the other hand, it offers a great tool for diagnostics. Especially here, where only a small gradient and only in a narrow region close to the central object is set. The advantage is that such a small gradient does not significantly increase the escape probability, but the line profile maps it. As an example, the Hϵ line can be used for this purpose (Fig. 2.5). The line is still very strong, forms close to the central star, and is not affected by moving structures in the envelope. Moreover, the Paδ line can be used as a tracer of Hϵ. However, one has to be aware of a few problems. Transition probability of Balmer lines is high enough for multiple scattering to become important, which will smooth the information about the velocity gradient. The same effect has sphericity, if the line-forming region is located farther from the star.

Si II lines are very appropriate for this purpose in these objects, especially the $\lambda\lambda$ 6347, 6371 Å doublet. They have a common lower level and there is a small shift of the absorption part of the line (Jeřábková et al. 2016). Furthermore, the analysis can be extended using the Si II triplet $\lambda\lambda$ 3 854, 3 856, and 3 863 Å lines. However, there arises a complication of sufficient S/N in this spectral region.

Especially this is problematic for the 3 854 Å line.

3.6 Rotation Velocity

The question of whether FS CMa stars are fast rotators or slowly rotating stars is even more important for these objects than for other stellar types. Luminosity and UV flux of FS CMa stars are too low to run the stellar wind driven by the radiation. Therefore, another physical phenomenon must be behind the mass outflow. Such a mechanism may be rotation. The fast rotation, near the critical velocity, supported by the pulsations is responsible for the creation of the decretion disk of classical Be stars (e.g. Rivinius et al. 2013), i.e. stars of similar masses. On the other hand, if FS CMa stars are post-merger objects and the strong mag. field has been creating during the merger process, they slow down very quickly.

Table A.6 summarises the measured rotation velocities of FS CMa stars. The determination of the stellar rotation velocity is affected by a large error, because only $v \sin i$ value is possible to be measured. Moreover, one has to take into account motion in photospheric regions of FS CMa stars. Outflow, possible pulsations, occasional matter infall, and matter in upper layers change the line profile and cause the measurements even more inaccurate. Such an effect is visible well in e.g. MWC 657 (Fig. 7 Miroshnichenko et al. 2000b). A similar problem is connected also with the B[e] supergiants (Kraus et al. 2016). Despite this, it seems that FS CMa stars are rather slow rotators (Miroshnichenko 2007).

3.7 Mass-loss Rate

The mass-loss rate ($\dot{M}$) determination for FS CMa stars is not a trivial task. Strong non-LTE effects require the inclusion of many transitions from different elements to be used in solving the statistical equilibrium equations. The shielding effect has to be described correctly in 3D geometry. The geometry of the model can not be simplified also for a realistic description of the matter distribution. However, this problem can be even more complicated, which will become clearer after summarising the current state of knowledge.

The $\dot{M}$ has been derived only for three FS CMa type objects: HD 87643 (de Freitas Pacheco et al. 1982), AS 78 (Miroshnichenko et al. 2000a), and IRAS 00470+6429 (Carciofi et al. 2010). de Freitas Pacheco et al. (1982) found $\dot{M}$ of HD 87643 by comparing the observed EWs of the Fe II multiplet 42 lines with the calculated values. These authors have used a three-level model of the iron atom to include UV excitation and following fluorescence responsible for creating emission lines in the visible region. Their model is based on the Sobolev approximation, spherical geometry, and nebular approximation. They used a slightly different description of the velocity of the flow from the classical β law. de Freitas Pacheco et al. (1982) reached the best fit with the observations for an $\dot{M}$ of $7{\cdot}10^{-7}\mathrm{M}_{\odot}{\cdot}\mathrm{yr}^{-1}$.

Spherical geometry was also used by (Miroshnichenko et al. 2000a) for the determination of $\dot{M}$ of AS 78. To calculate the radiative transfer, they adopted the code of Pogodin (1986). The best fit of the Hβ line was found for a model with $\dot{M}{=}1.5 \cdot 10^{-6}\mathrm{M}_{\odot} \cdot \mathrm{yr}^{-1}$. Miroshnichenko et al. (2000a) showed that this

value is in agreement with a raw guess based on the properties of P Cygni and HDE 316285. However, their model was not able to reproduce the Hβ, Hγ, and Hδ profiles simultaneously.

The best physical model of a FS CMa star was presented by Carciofi et al. (2010) for IRAS 00470+6429. They used a non-LTE Monte Carlo radiative transfer code `HDUST` (Carciofi & Bjorkman 2006, 2008). Since this code is 3D, they were able to include the latitudinal dependence of the circumstellar matter properties. Moreover, they solved consistently the temperature structure of the wind and were able to determine the dust creation radius. They found that $\dot{M}$ is in the range $(2.5-2.9)\cdot 10^{-7}\mathrm{M}_{\odot}\cdot\mathrm{yr}^{-1}$. Despite `HDUST` includes dust properties, only hydrogen gas was used in modelling.

These studies derived values of $\dot{M}$ for FS CMa stars in a range from $2.5\cdot 10^{-7}$ to $1.5\cdot 10^{-6}\mathrm{M}_{\odot}\cdot\mathrm{yr}^{-1}$. This is at least an order of magnitude lower than the lowest value determined for the B[e] supergiants ($M_{\odot}\geq 1\cdot 10^{-5}$, Zickgraf 2006) and at least two orders of magnitude higher than those of classical Be stars ($10^{-10}-10^{-8}\mathrm{M}_{\odot}\cdot\mathrm{yr}^{-1}$, Snow & Marlborough 1976; Gathier et al. 1981). de Freitas Pacheco et al. (1982) noticed that their value of $\dot{M}$ leads to the situation when the mechanical momentum carried out is larger than the momentum given by the photons to the matter in the single scattering limit. This suggests that another mechanism than the radiation pressure has to be involved.

All three models use smoothly accelerated prescription for the velocity of the stellar wind, i.e., the β law or a similar one. It assumes that the outflow starts at a low speed at the photosphere and smoothly accelerates approaching the terminal velocity in infinity, i.e., the circumstellar matter continues to freely expand into the interstellar matter (ISM). However, this is not the case for most of the FS CMa stars. The observations (e.g. Kučerová et al. 2013; Jeřábková et al. 2016) show that the decelerating layers as well as the material infall are present. If the circumstellar matter cannot freely escape into the ISM and at least a small portion of the material is accumulated around the star, the $\dot{M}$ derived from the fitting of the lines that form in the envelope could be orders of magnitude overestimated.

The last note is needed to be said about the sample of stars for which the estimate of the $\dot{M}$ exists. All three stars are different from the main representatives of this group, such as FS CMa, MWC 342, and HD 50138. HD 87643, AS 78, and IRAS 00470+6429 show classical P Cygni profiles of the Balmer lines, including the Hα line. Moreover, HD 87643 has P Cygni profiles also for Fe II lines. Derived expansion velocities are about 1 200 km s^{-1}, which is almost an order of magnitude larger than what the main representatives show. Taking into account the presented results and problems, the question how large is the mass loss in FS CMa stars remains fully opened.

3.8 Empirical Model

The obtained observations finally allow the construction of the empirical model of FS CMa stars. In the Fig. 3.8 is the possible model of the main representatives. This model can not be applied for questionable objects, such as CI Cam.

The slowly rotating central star is surrounded by a geometrically and optically thick disk, which is disturbed by the mag. field. The disk is surrounded by the

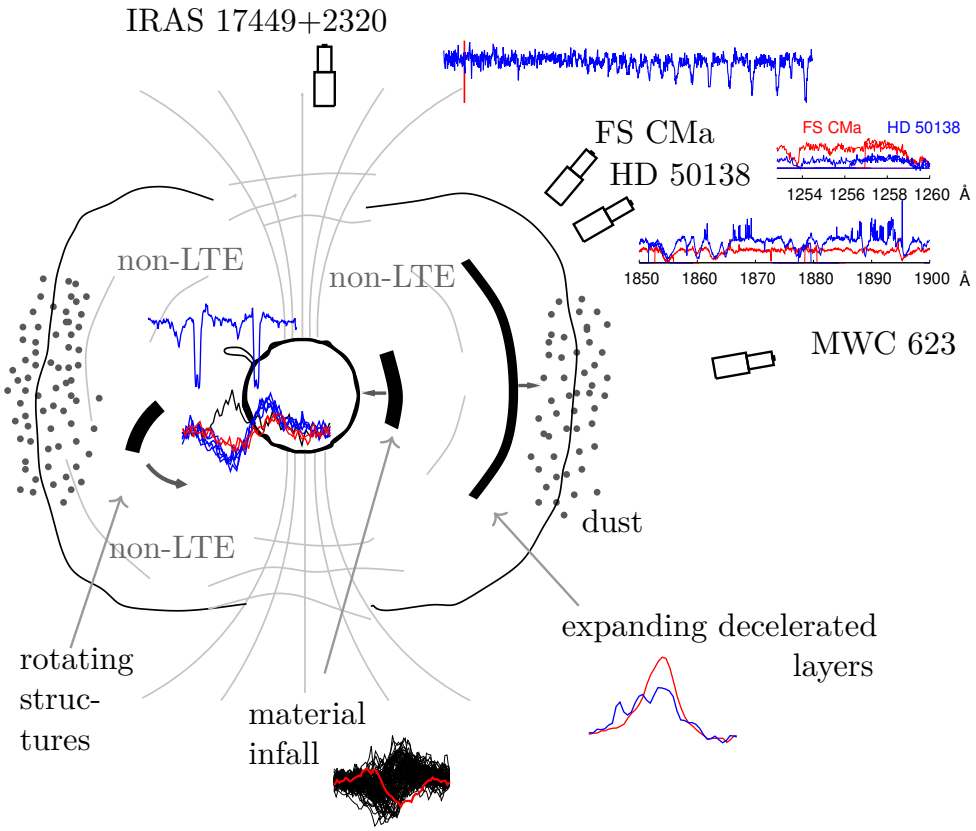

Figure 3.4: Empirical model of FS CMa stars (the improved figure from Korčáková et al. 2019).

dusty ring. The disk is far from being homogeneous. Expanding layers are present that can even slow down. A part of the material may from time to time fall back to the central star. This occasion is rare, similar to B[e] supergiants. On the other hand, small-scale rotating inhomogenities are observed frequently. They are probably caused by the material ejecta from the central star. There are some signatures that the central star is a pulsator and the beating phenomenon may play an important role there.

The speed of moving structures usually does not exceed ~ 200 km s^{-1}, which significantly deforms the line profiles and the velocity field must be included in the calculations of the synthetic spectra. Moreover, the velocity gradient connects some of the lines which links the spectral lines and their variability of different species, e.g., Lβ and O I resonance line 1 026 Å and following cascades. Unfortunately, the velocity gradient is too low to separate the individual parts of the object to simplify the numerical procedure. While the inner parts are very dynamical, the outer parts are stable, the turbulent velocity does not exceed 40 km s^{-1}. The low density and strong UV radiation are perfect conditions for non-LTE effects. In some objects, the overpopulation of triplet states compared to singlet states is detected, which points to the conditions close to the nebular case. Multiple scattering must also be included into account in the future modelling.

The observed spectrum of such an object is very different depending on the angle of view. The radiation penetrating through the disk changes very much. If

we see the disk from the edge, the strong iron curtain appears, or the spectral lines corresponding to an object of lower temperature may be formed, e.g., K-type spectrum of MWC 623 or lithium resonance lines. On the other hand, seeing the disk from the pole, the UV excess may be observed.

Chapter 4

Nature of FS CMa Stars

FS CMa stars are, maybe, the last stellar objects whose nature and evolution status has not yet been determined. The widely accepted explanation, which is sometimes presented as the only one, is the binarity. However, going carefully through the arguments in favour and against, one can see that the current binarity does not have such an observational support and other explanations, at least for some of FS CMa stars, are more realistic. One of these possibilities is the merger scenario for which only recently a strong evidence has been observed.

4.1 Current Binarity

The binarity is the most favourite scenario because of:

i) **large amount of circumstellar material**

The determined $\dot{M}$ (de Freitas Pacheco et al. 1982, Carciofi et al. 2010, Miroshnichenko et al. 2000a) is between $2.5 \cdot 10^{-7}$ and $1.5 \cdot 10^{-6} M_{\odot} \cdot \mathrm{yr}^{-1}$. de Freitas Pacheco et al. (1982) noticed that these values can not be reached by the radiatively driven wind of the central star. The single main-sequence star is not able to produce such amount of material, but it can be easily supplied to the circumstellar region by the mass transfer from the companion. This is taken as the strongest argument for the binarity.

Up to now, there are only three calculations of the $\dot{M}$ for FS CMa stars done for HD 87643 (de Freitas Pacheco et al. 1982), AS 78 (Miroshnichenko et al. 2000a), and IRAS 00470+6429 (Carciofi et al. 2010). All three stars are among the most massive FS CMa stars. However, the more serious problem is hidden in the approximations of the models. They use a smoothly accelerated velocity law, the β-law, or a similar one. It was the best approximation according to the knowledge of that time, but later, the expanding decelerated layers were observed (Kučerová et al. 2013). In such the case, the matter is more accumulated around the star and $\dot{M}$ is highly overestimated.

ii) **dust**

$\dot{M}$ value sufficient for dust creation is not possible to reach for a single B-type star during the life on the main-sequence. However, the dust is easily created during the merging process.

iii) **binarity is the natural phenomenon for hot stars**

The fraction of binaries in late B-type stars is about 30% (see review Vanbeveren & Mennekens 2017). Even higher fraction of binaries is observed in higher temperatures. The search done by Villaseñor et al. 2021 for early B-type binaries showed it may be also 95%. This is taken as one of the strongest arguments for the binarity. But, FS CMa stars are rather late B-type stars, where the fraction of binaries has not been found to be so high. Moreover, even if there are extensive studies of radial velocities of B-type stars (Chini et al. 2012, Villaseñor et al. 2021), especially early B-type stars are affected by stellar wind, or pulsations, which causes the line-profile changes and may strongly affect the result.

iv) **companion**

To find the companion around stars which are surrounded by such a large amount of circumstellar material is sometimes very tricky. The line profiles are affected by inhomogenities of the surrounding material, which affects the radial velocity measurements. Moreover, one has to be careful what exactly describes the individual parts of the line profile and what is therefore measured. Despite this, the companion of several objects has been found. The most evident is the companion of **CI Cam**, which is a compact object. Based on photometric and spectroscopic data, Barsukova et al. (2006b) found the orbital period of a white dwarf to be (19.41 ± 0.02) d. However, it may be under the debate whether to include this star in FS CMa stars, because it undergoes X-ray outbursts and therefore was classified as a high mass X-ray binary (Hynes et al. 2002, Robinson et al. 2002). CI Cam is also frequently named among the B[e] supergiants (e.g. Bartlett et al. 2019).

The regular periodicity was also found in **MWC 728** (Miroshnichenko et al. 2015). The period about 27.5 d was determined based on the radial velocities of forty-four spectra between 2004 and 2015, which were obtained in short observational runs always during the full moon. Moreover, the radial velocity curve (Miroshnichenko et al. 2015, Fig. 7) shows significant deviations indicating another companion or another physical process. The cross-correlation of twenty-seven spectra of **AS 386** obtained between 2009 and 2017 points to the period of 131.27 ± 0.09 d (Khokhlov et al. 2018). The orbital parameters set the lower mass limit for the secondary to 7 $M_\odot$. The large RV semiamplitude ($\sim$52 km s^{-1}) and the lack of the spectral lines of the secondary lead the authors to conclude that the secondary is most likely a black hole. Based on an extensive set of spectra (148), Miroshnichenko et al. (2020a) found the regular period of **3 Pup** to be 137.4 ± 0.1 d and determined the masses of the components to 8.8 ± 0.5 $M_\odot$ and 0.75 ± 0.25 $M_\odot$.

Spectroastrometric observations on the Hα line of Baines et al. (2006) point to the binarity of three out of five measured FS CMa stars, **FS CMa** itself, **HD 50138**, and **HD 85567**. However, the shift of the Hα position is small for FS CMa and HD 50138. Later, HD 50138 was studied interferometricaly by Kluska et al. (2016). They were not able to fit the observed data by the presence of the secondary component. The image reconstruction showed the variable disk structure with a moving bright spot and probably constant disk orientation around 60°. Such geometry may affect the spectroastrometric observations. Baines et al. (2006) discussed the accuracy and limits of the spectroastrometry only for the case of two stars and double-peaked or P Cygni profile. In their later work (Mendigutía et al. 2018) they also modelled the effect of the disk and the

disk with the secondary, which changed the position of the line.

vi) **composed spectrum**

The spectrum of **MWC 623** is composed by two stellar spectra, B4III and K2II-Ib (Zickgraf 2001). This would be the definitive proof of the binarity if there was not such a lot of material around the star. The spectrum passing through the disk has to be significantly changed, showing the absorption features corresponding to the low temperature and low rotation as well as turbulent velocity, which is observed. The observations of Polster et al. (2012) show a small amplitude of the radial velocities ($\sim$ 4 km s^{-1}) and a possible correlation of the radial velocities of the K-component and Hα emission wings. The variability of the Hα bisectors was not possible to model by the secondary component (Polster et al. 2018). The polarimetric observations of Zickgraf & Schulte-Ladbeck (1989) support the idea of the line formation in the pseudoatmosphere of the disk. Their measurements show the presence of the dusty disk. Based on similar spectra with MWC 623 at some wavelength interval, Miroshnichenko et al. (2002a) designated also **V669 Cep** as the binary.

v) **presence of Li i lines**

Li I lines can not be found in B-type stars because of the low ionisation potential ($\sim$ 5.4 eV). However, Li I resonance doublet 6 708 Å is detectable in about half of FS CMa stars (Korčáková et al. 2020). This is taken as one of the strongest arguments in favor of the binarity. On the other hand, the Li I lines, as a cold spectrum of the K component mentioned above, may be formed through the optically thick disk. This possibility supports the observations of MWC 623, which has the strongest Li I resonance doublet 6 708 Å, and the study of Korčáková et al. (2020) showed that stars with Li I lines have sharp central absorption of He I 5 876 Å line.

vi) **regular periodicity**

The regular variability of the RVs caused by the orbital motion was found in CI Cam (Barsukova et al. 2006a), 3 Pup (Johnson & Neubauer 1946; Plets et al. 1995), GG Car (Porter et al. 2021b), and AS 386 (Khokhlov et al. 2018). MWC 728 (Miroshnichenko et al. 2015) is probably also binary, however several questions remain with this star and more data are necessary to confirm the companion and its properties. Because circumstellar matter affects the line profiles, it is a little bit tricky to find the periods hidden in the data and even more difficult to interpret the results correctly. The Table A.5 shows these problems well. For details, see the Sect. 3.4.

viii) **central quasi-emission peak**

A small emission peak is sometimes observed near the centre of the Hα depression (HD 50138, Jeřábková et al. 2016; MWC 728, Miroshnichenko et al. 2015, and FS CMa, Table A.1 *sp 1*). It is supposed that it originates near the Lagrangian point L1 (A. Miroshnichenko, private communication). Indeed, MWC 728 has been found to be a binary (Miroshnichenko et al. 2015). On the other hand, there are other explanations. *a)* It may just be an accidental observation of a hump moving close to the center of the Hα depression. Moving structures are a common phenomenon in FS CMa stars (de Winter & van den Ancker 1997, Pogodin 1997, Kučerová et al. 2013, Miroshnichenko et al. 2015, Jeřábková et al. 2016, and Miroshnichenko et al. 2020a.) *b)* It may just be a radiative transfer effect

(Hanuschik 1995), when the scattered light comes from the upper parts of the outer regions of the disk. A detailed discussion of this phenomenon can be found in Rivinius (2005).

ix) **hot source**

The indications for the additional source at higher temperature than the visible star were found for MWC 342 (from the photometry, Miroshnichenko & Corporon 1999b) and IRAS 17449+2320 (from the spectral fitting and line-intensity changes, Korčáková et al. 2022). This additional hot source, which does not have detectable spectral lines in the visible and IR regions, is easily explained by IRAS 17449+2320 because of its very strong mag. field (6.2 ± 0.2 kG). The hot compact companion was proven for CI Cam.

I describe this part in detail to see the complexity of the problem. Other extensive overviews dealing with the binary nature of FS CMa stars may be found in Miroshnichenko et al. (2013), Miroshnichenko & Zharikov (2015), Polster et al. (2018), Miroshnichenko (2018), and Miroshnichenko et al. (2020b).

4.2 Merger Origin

From the list above, it is possible to see that only one compelling argument for the binarity is the presence of warm dust. The binarity of some objects, e.g., CI Cam, cannot be refuted. However, the number of such unambiguously proven binaries is extremely small. It indicates that the nature of FS CMa stars may be different. One of the most serious possibilities is that these objects, or at least some of them, are mergers. The merger scenario naturally explains the observed phenomena:

i) **large amount of gas and dust**

The matter is ejected before the merger process, through the Lagrange point L2, during, and also after the merger process. The newly created star rotates at critical velocity, which allows the formation of the decretion disk. Moreover, the Eddington limit may be crossed in some cases.

ii) **geometrically thick disk, extended area of the line formation, hot continuum source, slow stellar rotation, FS CMa stars vs. classical Be stars**

During the merger process, the strong mag. field is generated (Schneider et al. 2020). As stronger the mag. field is as faster the star is slowing down. This is the reason why FS CMa stars are slow rotators, while classical Be stars, which occupy a similar part of the HRD and also have emission-line spectra, rotate at the critical velocity allowing the formation of the decretion disk.

The mag. field is also responsible for the destruction of the equatorial disk and the geometrically thick disk linked with a "corona" is observed (Fig. 3.8) instead of the theoretical α disk. The line formation regions are more extended and more diverse than in, e.g., the mentioned classical Be stars. The mag. field naturally explains the presence of a hot continuum source in IRAS 17449+2320 (Korčáková et al. 2022) and MWC 342 Miroshnichenko & Corporon 1999b.

iii) **slow wind, material infall, outflow, material ejecta, quasi-periodicity, scarcely detection of the regular periodicity**

All these phenomena are natural for post-merger systems. Especially, let us mention the quasi-periodicity observed in MWC 342 (Kučerová et al. 2013), HD 50138 (Jeřábková et al. 2016), the stars for which the longest temporal description is available. The found regular periodicities in some cases suffer from wrong data sampling, the phase curve shows the extreme deviations, or the temporal coverage is too short for the result to be considered a stable period (for details see Sec. 3.4).

vi) **lack of proven secondaries**

The Table A.5 summaries all the detected period found in FS CMa stars. Not all of them may be considered to be orbital periods. For details see Sects. 3.4 and 4.1.

The merger scenario explains all currently observed phenomena. The question is only whether there are enough such events. The latest observations and simulations show that the merger process must be taken into account. The detailed discussion is presented in Korčáková et al. (2022). Moreover, Vanbeveren & Mennekens (2017) show that about 20% of B-type stars have merger origin.

4.3 Post-AGB Stars

The presence of a warm dust, emission line spectra, and location out of the star-forming regions indicate that FS CMa stars may be post-AGB stars. Moreover, among the B[e] stars, compact planetary nebulae are identified as one of four main groups (Lamers et al. 1998). Indeed, several FS CMa stars have been included in the lists of post-AGB stars, or their candidates.

Hen3-938 has a spectrum very similar to OY Gem, already known protoplanetary nebula (Miroshnichenko et al. 1999). CPD-48 5215 (Hen3-847) is included in Torun catalog of post-AGB and related objects (Szczerba et al. 2007) as a post-AGB object. Gauba & Parthasarathy (2004) studied the chemical composition of the dust around this star in detail and supported the idea of a post-AGB star. Similar dust properties as CPD-48 5215 has MWC 939 (Gauba et al. 2003).

Certainly, there must be hidden post-AGB objects among FS CMa stars, but this is not the nature of all of them. Not all the spectral properties of post-AGB stars fit the FS CMa group. Massive post-AGB stars have an IR peak at $\lambda \geq 3\mu$m. Low-mass post-AGB stars do not have strong emission lines in the spectrum and evolve very slowly, whereas FS CMa objects are very dynamical (Miroshnichenko 2018).

Concluding Remarks and Future Perspectives

The recent discovery of a very strong magnetic field in IRAS 17449+2320 (Korčáková et al. 2022) supports the idea of the merger origin for at least some FS CMa stars. To find the nature of these stars, the last stellar objects whose origin and evolutionary status have not been determined, the need of the detailed review has arisen. Therefore this thesis has such a form.

To help the committee, let me summarise my main contributions to the field. The details are described at p. 80 and the full list of the papers in the field of FS CMa stars can be found at p. 76.

- discovery of the strong magnetic field in IRAS 17449+2320 (Korčáková et al. 2022) and a post-marger origin of this star
- finding of the iron curtain in FS CMa stars and the discussion of its consequences for the spectral-line formation (Korčáková et al. 2019)
- first detailed description of the long-term spectral behaviour of a FS CMa object (Polster et al. 2012)
- first detection of an expanding decelerating layer in FS CMa stars (Kučerová et al. 2013) and its consequence for the determination of the $\dot{M}$ (Korčáková et al. 2022, this thesis)
- first detection of the material infall in FS CMa stars (Kučerová et al. 2013), previously known in the B[e] supergiants and similar objects
- periodicity (Polster et al. 2012, Kučerová et al. 2013, Jeřábková et al. 2016), Korčáková et al. 2022)
- spectral variability (Polster et al. 2012, Kučerová et al. 2013, Jeřábková et al. 2016), Kříček et al. 2017, Korčáková et al. 2022)
- modelling of the variability of the Hα bisectors (Polster et al. 2018)
- possibility of the usage of Li I resonance doublet as a tracer of the primordial lithium (Korčáková et al. 2020, successfull ESO/UVES proposal)
- first BPT diagrams of FS CMa stars (this thesis)

The field has made significant progress in last ten years. Finally, there is sufficient information to start with the realistic modelling of the processes taking place in the individual objects. However, we still face many problems and questions. The most pressing question is "Is FS CMa group a homogeneous sample of stars?" FS CMa stars were just a renaming of the group the B[e] stars with

warm dust (B[e]WD). Therefore the stars were included into this group according to the shape of the IR excess indicating relatively warm dust. This has led to the situation where Be/X-ray binaries with a compact companion are included, as well as late B-/early A-type stars whose properties fit well to the merger systems. Among these stars, some proto-planetary nebulae are probably hidden. Careful analysis of the individual objects of spectroscopic and photometric data from UV to IR is needed to identify the merger systems. After that, it is possible that we will see the evolution sequence of the merging process.

We still have possibilities to extend the current analysis. For example, BPT diagrams are not used even if they have the potential to identify proto-planetary nebulae and possible hidden symbiotic stars. The UV radiation is completely overlooked, although it is largely responsible for the formation of the visible and IR spectra and its variability. The dynamical processes in the envelopes may be monitored instead of the Hϵ line by the Paδ line, which is easily observable. A lot of photometrical data are hidden in the databases of several observatories not being analysed. New possibilities offers TESS satellite. The precision of which reaches so good values that the magnetic field may be indirectly found (Mikulášek et al. 2020). Obtaining more high resolution and high S/N spectra of FS CMa stars with the magnetic field will allow to study the temporal variability of the magnetic field, as well as its changes through the photosphere.

The method of Doppler imaging may be used to reconstruct the map of individual elements on the surface (at least for IRAS 17449+2320). The potential of the Li I lines is also overlooked. It will probably not lead to the solution of the primordial lithium problem, but it may bring new insights into the life cycle of this element. Identifying the merger sequence may change our view on the evolution of the first stars and early galaxies. The dust and heavy elements produced during the merger processes definitely affected the formation of the first stars. The only question is how large this influence is.

The FS CMa stars may contribute to our deeper understanding of the universe and therefore certainly deserve more attention. They are excellent teachers of the radiative transfer and hydrodynamics. These are the reasons why I plan to stay in this field and involve students at different levels, from simple projects for first-year bachelor students to the postdoctoral fellowship.

Acknowledgements

I thank to A. Miroshnichenko, N. Manset, V. Votruba, S. V. Zharikov, P. Zasche, M. Wolf, M. Šlechta, J. Polster, B. Kučerová, M. Dovčiak, P. Corporon, J. Kubát, M. Kraus, P. Berardi, and P. Škoda for some spectra. Data were obtained at Perek 2 m telescope, Ondřejov, Czech Republic and at the Canada-France-Hawaii Telescope (CFHT) which is operated by the National Research Council of Canada, the Institut National des Sciences de l'Univers of the Centre National de la Recherche Scientique of France, and the University of Hawaii. The observations at the Canada-France-Hawaii Telescope were performed with care and respect from the summit of Maunakea which is a significant cultural and historic site. This work has made use of data from the European Space Agency (ESA) mission *Gaia* (`https://www.cosmos.esa.int/gaia`), processed by the *Gaia* Data Processing and Analysis Consortium (DPAC, `https://www.cosmos.esa.int/web/gaia/dpac/consortium`). Funding for the DPAC has been provided by national institutions, in particular the institutions participating in the *Gaia* Multilateral Agreement. This work uses NIST database (Kramida et al. 2018) [1], and van Hoof (2018) line list and database. This research has made use of NASA's Astrophysics Data System.

The research of DK was supported by grant GA 17-00871S of the Czech Science Foundation.

[1]NIST Atomic Spectra Database (ver. 5.6.1), [Online]. Available: https://physics.nist.gov/asd [2019, May 25]. National Institute of Standards and Technology, Gaithersburg, MD. DOI: https://doi.org/10.18434/T4W30F

Bibliography

Ababakr, K. M., Oudmaijer, R. D., & Vink, J. S. 2016, MNRAS, 461, 3089

Ababakr, K. M., Oudmaijer, R. D., & Vink, J. S. 2017, MNRAS, 472, 854

Aitken, D. K., Smith, C. H., Roche, P. F., & Wright, C. M. 1990, MNRAS, 247, 466

Allen, D. A. 1973, MNRAS, 161, 145

Allen, D. A. 1974, MNRAS, 168, 1

Allen, D. A. & Swings, J. P. 1972, Astrophys. Lett., 10, 83

Allen, D. A. & Swings, J. P. 1976, A&A, 47, 293

Arias, M. L., Cidale, L. S., Kraus, M., et al. 2018, PASP, 130, 114201

Babcock, H. W. 1958, ApJS, 3, 141

Baines, D., Oudmaijer, R. D., Porter, J. M., & Pozzo, M. 2006, MNRAS, 367, 737

Baldwin, J. A., Phillips, M. M., & Terlevich, R. 1981, PASP, 93, 5

Barsukova, E. A., Borisov, N. V., Burenkov, A. N., et al. 2006a, Astronomy Reports, 50, 664

Barsukova, E. A., Borisov, N. V., Burenkov, A. N., et al. 2006b, in Astronomical Society of the Pacific Conference Series, Vol. 355, Stars with the B[e] Phenomenon, ed. M. Kraus & A. S. Miroshnichenko, 305

Barsukova, E. A., Borisov, N. V., Burenkov, A. N., et al. 2006c, in Astronomical Society of the Pacific Conference Series, Vol. 355, Stars with the B[e] Phenomenon, ed. M. Kraus & A. S. Miroshnichenko, 305

Barsukova, E. A., Borisov, N. V., Fabrika, S. N., Goranskij, V. P., & Metlova, N. V. 2002a, in Astronomical Society of the Pacific Conference Series, Vol. 261, The Physics of Cataclysmic Variables and Related Objects, ed. B. T. Gänsicke, K. Beuermann, & K. Reinsch, 463

Barsukova, E. A., Borisov, N. V., Goranskii, V. P., Lyutyi, V. M., & Metlova, N. V. 2002b, Astronomy Reports, 46, 275

Bartlett, E. S., Clark, J. S., & Negueruela, I. 2019, A&A, 622, A93

Bergner, Y. K., Miroshnichenko, A. S., Sudnik, I. S., et al. 1990, Astrofizika, 32, 203

Bjorkman, K. S., Miroshnichenko, A. S., Bjorkman, J. E., et al. 1998, ApJ, 509, 904

Borges Fernandes, M., Kraus, M., Chesneau, O., et al. 2009, A&A, 508, 309

Borges Fernandes, M., Meilland, A., Bendjoya, P., et al. 2011, A&A, 528, A20

Boubert, D. & Evans, N. W. 2018, MNRAS, 477, 5261

Bowen, I. S. 1927a, PASP, 39, 295

Bowen, I. S. 1927b, Nature, 120, 473

Brown, T. M., Buss, Richard, J., Grady, C., & Bjorkman, K. 1995, ApJ, 440, 865

Carciofi, A. C. & Bjorkman, J. E. 2006, ApJ, 639, 1081

Carciofi, A. C. & Bjorkman, J. E. 2008, ApJ, 684, 1374
Carciofi, A. C., Miroshnichenko, A. S., & Bjorkman, J. E. 2010, ApJ, 721, 1079
Cardelli, J. A., Clayton, G. C., & Mathis, J. S. 1989, ApJ, 345, 245
Chen, P.-S., Liu, J.-Y., & Shan, H.-G. 2021, PASJ, 73, 837
Chini, R., Hoffmeister, V. H., Nasseri, A., Stahl, O., & Zinnecker, H. 2012, MNRAS, 424, 1925
Chkhikvadze, J. N., Kakhiani, V. O., & Djaniashvili, E. B. 2002, Astrophysics, 45, 8
Ciatti, F., D'Odorico, S., & Mammano, A. 1974, A&A, 34, 181
Cidale, L. S., Borges Fernandes, M., Andruchow, I., et al. 2012, A&A, 548, A72
Cohen, M., Bieging, J. H., Dreher, J. W., & Welch, W. J. 1985, ApJ, 292, 249
Condori, C. A. H., Borges Fernandes, M., Kraus, M., Panoglou, D., & Guerrero, C. A. 2019, MNRAS, 488, 1090
Coyne, G. V. & Vrba, F. J. 1976, ApJ, 207, 790
de Freitas Pacheco, J. A., Gilra, D. P., & Pottasch, S. R. 1982, A&A, 108, 111
de la Fuente, D., Najarro, F., Trombley, C., Davies, B., & Figer, D. F. 2015, A&A, 575, A10
de Winter, D. & van den Ancker, M. E. 1997, A&AS, 121, 275
Doazan, V., Kuhi, L. V., & Thomas, R. N. 1980, ApJ, 235, L17
Domiciano de Souza, A., Bendjoya, P., Niccolini, G., et al. 2011, A&A, 525, A22
Domiciano de Souza, A., Driebe, T., Chesneau, O., et al. 2007, A&A, 464, 81
Ellerbroek, L. E., Benisty, M., Kraus, S., et al. 2015, A&A, 573, A77
Elvius, A. 1974, A&A, 34, 371
Gaia Collaboration, Brown, A. G. A., Vallenari, A., et al. 2018, A&A, 616, A1
Gaia Collaboration, Prusti, T., de Bruijne, J. H. J., et al. 2016, A&A, 595, A1
Gaposchkin, S. 1953, Annals of Harvard College Observatory, 113, 67
Gathier, R., Lamers, H. J. G. L. M., & Snow, T. P. 1981, ApJ, 247, 173
Gauba, G. & Parthasarathy, M. 2004, A&A, 417, 201
Gauba, G., Parthasarathy, M., Kumar, B., Yadav, R. K. S., & Sagar, R. 2003, A&A, 404, 305
Geballe, T. R. & Persson, S. E. 1987, ApJ, 312, 297
Geisel, S. L. 1970, ApJ, 161, L105
Gibb, E. L., Brittain, S. D., Rettig, T. W., et al. 2010, ApJ, 715, 757
Gill, David, S. 1901, MNRAS, 61
Goranskij, V. P. & Barsukova, E. A. 2009, Astrophysical Bulletin, 64, 50
Gosset, E., Surdej, J., & Swings, J. P. 1984, A&AS, 55, 411
Gottlieb, E. W. & Liller, W. 1978, ApJ, 225, 488
Green, G. M., Schlafly, E. F., Finkbeiner, D., et al. 2018, MNRAS, 478, 651
Gvaramadze, V. V., Kniazev, A. Y., & Fabrika, S. 2010, MNRAS, 405, 1047
Gvaramadze, V. V. & Menten, K. M. 2012, A&A, 541, A7
Hanuschik, R. W. 1995, A&A, 295, 423
Harmanec, P. 1983, Hvar Observatory Bulletin, 7, 55
Harrington, D. M. & Kuhn, J. R. 2007, ApJ, 667, L89
Hillier, D. J. 2006, in Astronomical Society of the Pacific Conference Series, Vol. 355, Stars with the B[e] Phenomenon, ed. M. Kraus & A. S. Miroshnichenko, 39
Hoffleit, D. & Jaschek, C. 1982, The Bright Star Catalogue. Fourth revised edition. (Containing data compiled through 1979).

Hofmann, K. H., Balega, Y., Ikhsanov, N. R., Miroshnichenko, A. S., & Weigelt, G. 2002, A&A, 395, 891
Hynes, R. I., Clark, J. S., Barsukova, E. A., et al. 2002, A&A, 392, 991
Iłkiewicz, K. & Mikołajewska, J. 2017, A&A, 606, A110
Inglis, D. R. & Teller, E. 1939, ApJ, 90, 439
Israelian, G., Friedjung, M., Graham, J., et al. 1996, A&A, 311, 643
Jaschek, C. & Andrillat, Y. 1998, A&AS, 128, 475
Jaschek, M., Jaschek, C., Andrillat, Y., & Houziaux, L. 1992, MNRAS, 254, 413
Jeřábková, T., Korčáková, D., Miroshnichenko, A., et al. 2016, A&A, 586, A116
Johnson, H. L. & Neubauer, F. J. 1946, PASP, 58, 248
Jorgenson, R. A., Kogan, L. R., & Strelnitski, V. 2000, AJ, 119, 3060
Josselin, E., Loup, C., Omont, A., et al. 1998, A&AS, 129, 45
Khokhlov, S. A., Miroshnichenko, A. S., Mennickent, R., et al. 2017, ApJ, 835, 53
Khokhlov, S. A., Miroshnichenko, A. S., Zharikov, S. V., et al. 2018, ApJ, 856, 158
Kluska, J., Benisty, M., Soulez, F., et al. 2016, A&A, 591, A82
Kniazev, A. Y., Pustilnik, S. A., & Zucker, D. B. 2008, MNRAS, 384, 1045
Kobus, J., Wolf, S., Ratzka, T., & Brunngräber, R. 2020, A&A, 642, A104
Korčáková, D., Sestito, F., Manset, N., et al. 2022, A&A, in print
Korčáková, D., Miroshnichenko, A., & Shore, S. N. 2017a, Open European Journal on Variable Stars, 180, 59
Korčáková, D., Miroshnichenko, A. S., Sestito, F., et al. 2021, in OBA Stars: Variability and Magnetic Fields. On-line conference, 6
Korčáková, D., Miroshnichenko, A. S., Zharikov, S. V., et al. 2020, Mem. Soc. Astron. Italiana, 91, 118
Korčáková, D., Polster, J., Jeřábková, T., et al. 2017b, in Astronomical Society of the Pacific Conference Series, Vol. 508, The B[e] Phenomenon: Forty Years of Studies, ed. A. Miroshnichenko, S. Zharikov, D. Korčáková, & M. Wolf, 301
Korčáková, D., Shore, S. N., Miroshnichenko, A., et al. 2019, in Astronomical Society of the Pacific Conference Series, Vol. 519, Radiative Signatures from the Cosmos, ed. K. Werner, C. Stehle, T. Rauch, & T. Lanz, 155
Koutoulaki, M., Garcia Lopez, R., Natta, A., et al. 2018, A&A, 614, A90
Kramida, A., Yu. Ralchenko, Reader, J., & and NIST ASD Team. 2018, NIST Atomic Spectra Database (ver. 5.6.1), [Online]. Available: `https://physics.nist.gov/asd` [2019, May 14]. National Institute of Standards and Technology, Gaithersburg, MD.
Kraus, M. 2009, A&A, 494, 253
Kraus, M., Arias, M. L., Cidale, L. S., & Torres, A. F. 2020, MNRAS, 493, 4308
Kraus, M., Cidale, L. S., Arias, M. L., et al. 2016, A&A, 593, A112
Kraus, M., Krügel, E., Thum, C., & Geballe, T. R. 2000, A&A, 362, 158
Kraus, M., Liimets, T., Cappa, C. E., et al. 2017, AJ, 154, 186
Kraus, M., Liimets, T., Moiseev, A., et al. 2021, AJ, 162, 150
Kraus, M., Oksala, M. E., Cidale, L. S., et al. 2015, ApJ, 800, L20
Kraus, M., Oksala, M. E., Nickeler, D. H., et al. 2013, A&A, 549, A28
Kruytbosch, W. E. 1930, Bull. Astron. Inst. Netherlands, 6, 11
Kučerová, B., Korčáková, D., Polster, J., et al. 2013, A&A, 554, A143
Kříček, R. 2013, Master thesis, Charles University in Prague, Czech Republic

Kříček, R., Korčáková, D., Jeřábková, T., et al. 2017, in Astronomical Society of the Pacific Conference Series, Vol. 508, The B[e] Phenomenon: Forty Years of Studies, ed. A. Miroshnichenko, S. Zharikov, D. Korčáková, & M. Wolf, 411–412
Lamers, H. J. G. L. M., Zickgraf, F.-J., de Winter, D., Houziaux, L., & Zorec, J. 1998, A&A, 340, 117
Laws, A. S. E., Harries, T. J., Setterholm, B. R., et al. 2020, ApJ, 888, 7
Lee, C.-D., Chen, W.-P., & Liu, S.-Y. 2016, A&A, 592, A130
Lee, C. D., Eswaraiah, C., Chen, W. P., & Pandey, A. K. 2018, AJ, 156, 115
Liermann, A., Schnurr, O., Kraus, M., et al. 2014, MNRAS, 443, 947
Lyratzi, E., Danezis, E., Popovic, L. C., et al. 2007, PASJ, 59, 357
Malfait, K., Bogaert, E., & Waelkens, C. 1998, A&A, 331, 211
Maravelias, G., Kraus, M., Cidale, L. S., et al. 2018, MNRAS, 480, 320
Marchiano, P., Brandi, E., Muratore, M. F., et al. 2012, A&A, 540, A91
Marston, A. P. & McCollum, B. 2008, A&A, 477, 193
Martin-Pintado, J., Neri, R., Thum, C., Planesas, P., & Bachiller, R. 1994, A&A, 286, 890
McGregor, P. J., Hyland, A. R., & Hillier, D. J. 1988, ApJ, 324, 1071
Mehner, A., de Wit, W. J., Groh, J. H., et al. 2016, A&A, 585, A81
Meilland, A., Kanaan, S., Borges Fernandes, M., et al. 2010, A&A, 512, A73
Mel'Nikov, S. Y. 1997, Astronomy Letters, 23, 799
Mendigutía, I., Oudmaijer, R. D., Schneider, P. C., et al. 2018, A&A, 618, L9
Merrill, P. W. 1924, PASP, 36, 225
Merrill, P. W. 1928, ApJ, 67, 405
Merrill, P. W. 1931, ApJ, 73, 348
Meyer, J. M., Nordsieck, K. H., & Hoffman, J. L. 2002, AJ, 123, 1639
Mikulášek, Z., Krtička, J., Shultz, M. E., et al. 2020, in Stellar Magnetism: A Workshop in Honour of the Career and Contributions of John D. Landstreet, ed. G. Wade, E. Alecian, D. Bohlender, & A. Sigut, Vol. 11, 46–53
Millour, F., Chesneau, O., Borges Fernandes, M., et al. 2009, A&A, 507, 317
Miroshnichenko, A. & Corporon, P. 1999a, A&A, 349, 126
Miroshnichenko, A. & Corporon, P. 1999b, A&A, 349, 126
Miroshnichenko, A., Zharikov, S. V., Manset N., J., & Raj, A. 2021a, in preparation
Miroshnichenko, A. S. 1995, Astronomical and Astrophysical Transactions, 6, 251
Miroshnichenko, A. S. 2006, in Astronomical Society of the Pacific Conference Series, Vol. 355, Stars with the B[e] Phenomenon, ed. M. Kraus & A. S. Miroshnichenko, 13
Miroshnichenko, A. S. 2007, ApJ, 667, 497
Miroshnichenko, A. S. 2010, in Revista Mexicana de Astronomia y Astrofisica Conference Series, Vol. 38, Revista Mexicana de Astronomia y Astrofisica Conference Series, 100–101
Miroshnichenko, A. S. 2018, Communications of the Byurakan Astrophysical Observatory, 65, 184
Miroshnichenko, A. S., Alimgazinova, N. S., Naurzbayeva, A. Z., et al. 2021b, in OBA Stars: Variability and Magnetic Fields. On-line conference, 4
Miroshnichenko, A. S., Bernabei, S., Bjorkman, K. S., et al. 2006, in Astronomical Society of the Pacific Conference Series, Vol. 355, Stars with the B[e]

Phenomenon, ed. M. Kraus & A. S. Miroshnichenko, 315
Miroshnichenko, A. S., Bjorkman, K. S., Chentsov, E. L., et al. 2002a, A&A, 388, 563
Miroshnichenko, A. S., Bjorkman, K. S., Chentsov, E. L., et al. 2002b, A&A, 388, 563
Miroshnichenko, A. S., Bjorkman, K. S., Grosso, M., et al. 2005, A&A, 436, 653
Miroshnichenko, A. S., Bjorkman, K. S., Klochkova, V. G., & Chentsov, E. L. 2002c, in Astronomical Society of the Pacific Conference Series, Vol. 279, Exotic Stars as Challenges to Evolution, ed. C. A. Tout & W. van Hamme, 303
Miroshnichenko, A. S., Chentsov, E. L., Klochkova, V. G., et al. 2000a, A&AS, 147, 5
Miroshnichenko, A. S., Chentsov, E. L., Klochkova, V. G., et al. 2000b, A&AS, 147, 5
Miroshnichenko, A. S., Chentsov, E. L., Klochkova, V. G., et al. 2009, ApJ, 700, 209
Miroshnichenko, A. S., Danford, S., Zharikov, S. V., et al. 2020a, ApJ, 897, 48
Miroshnichenko, A. S., Gray, R. O., Vieira, S. L. A., Kuratov, K. S., & Bergner, Y. K. 1999, A&A, 347, 137
Miroshnichenko, A. S., Klochkova, V. G., & Bjorkman, K. S. 2003a, Astronomy Letters, 29, 336
Miroshnichenko, A. S., Levato, H., Bjorkman, K. S., & Grosso, M. 2001, A&A, 371, 600
Miroshnichenko, A. S., Levato, H., Bjorkman, K. S., & Grosso, M. 2003b, A&A, 406, 673
Miroshnichenko, A. S., Levato, H., Bjorkman, K. S., & Grosso, M. 2003c, A&A, 406, 673
Miroshnichenko, A. S., Manset, N., Kusakin, A. V., et al. 2007, ApJ, 671, 828
Miroshnichenko, A. S., Manset, N., Polcaro, F., Rossi, C., & Zharikov, S. 2011, in Active OB Stars: Structure, Evolution, Mass Loss, and Critical Limits, ed. C. Neiner, G. Wade, G. Meynet, & G. Peters, Vol. 272, 260–264
Miroshnichenko, A. S., Polcaro, V. F., Rossi, C., et al. 2017, in Astronomical Society of the Pacific Conference Series, Vol. 508, The B[e] Phenomenon: Forty Years of Studies, ed. A. Miroshnichenko, S. Zharikov, D. Korčáková, & M. Wolf, 387
Miroshnichenko, A. S. & Zharikov, S. V. 2015, in EAS Publications Series, Vol. 71-72, EAS Publications Series, 181–186
Miroshnichenko, A. S., Zharikov, S. V., Danford, S., et al. 2015, ApJ, 809, 129
Miroshnichenko, A. S., Zharikov, S. V., Korčaková, D., et al. 2020b, Contributions of the Astronomical Observatory Skalnate Pleso, 50, 513
Miroshnichenko, A. S., Zharikov, S. V., Manset, N., Rossi, C., & Polcaro, V. F. 2013, Central European Astrophysical Bulletin, 37, 57
Monnier, J. D., Tuthill, P. G., Ireland, M., et al. 2009, ApJ, 700, 491
Morris, P. W., Eenens, P. R. J., Hanson, M. M., Conti, P. S., & Blum, R. D. 1996, ApJ, 470, 597
Muratore, M. F., Kraus, M., Oksala, M. E., et al. 2015, AJ, 149, 13
Nissen, W. 1954, Zeitschrift fur Physik, 139, 638
Nyman, L. A., Booth, R. S., Carlstrom, U., et al. 1992, A&AS, 93, 121
Osterbrock, D. E. & Ferland, G. J. 2006, Astrophysics of gaseous nebulae and

active galactic nuclei
Oudmaijer, R. D. & Drew, J. E. 1999, MNRAS, 305, 166
Oudmaijer, R. D. & Miroshnichenko, A. S. 2017, in Astronomical Society of the Pacific Conference Series, Vol. 508, The B[e] Phenomenon: Forty Years of Studies, ed. A. Miroshnichenko, S. Zharikov, D. Korčáková, & M. Wolf, 3
Oudmaijer, R. D., Proga, D., Drew, J. E., & de Winter, D. 1998, MNRAS, 300
Patel, M., Oudmaijer, R. D., Vink, J. S., Mottram, J. C., & Davies, B. 2006, MNRAS, 373, 1641
Pereyra, A., de Araújo, F. X., Magalhães, A. M., Borges Fernandes, M., & Domiciano de Souza, A. 2009, A&A, 508, 1337
Pickering, E. C. 1898, Harvard College Observatory Circular, 32, 1
Plets, H., Waelkens, C., & Trams, N. R. 1995, A&A, 293, 363
Pogodin, M. A. 1986, Astrofizika, 24, 491
Pogodin, M. A. 1997, A&A, 317, 185
Pojmanski, G. 1997, Acta Astron., 47, 467
Polster, J., Korčáková, D., & Manset, N. 2018, A&A, 617, A79
Polster, J., Korčáková, D., Votruba, V., et al. 2012, A&A, 542, A57
Porter, A., Blundell, K., Podsiadlowski, P., & Lee, S. 2021a, MNRAS, 503, 4802
Porter, A., Grant, D., Blundell, K., & Lee, S. 2021b, MNRAS, 501, 5554
Quirrenbach, A. & Albrecht, S. 2010, in Revista Mexicana de Astronomia y Astrofisica Conference Series, Vol. 38, Revista Mexicana de Astronomia y Astrofisica Conference Series, 74–76
Rivinius, T. 2005, Habilitationsschrift, Ruprecht-Karls-Universiät, Heidelberg
Rivinius, T., Carciofi, A. C., & Martayan, C. 2013, A&A Rev., 21, 69
Robinson, E. L., Ivans, I. I., & Welsh, W. F. 2002, ApJ, 565, 1169
Sallum, S., Eisner, J. A., Hinz, P. M., et al. 2017, ApJ, 844, 22
Schneider, F. R. N., Ohlmann, S. T., Podsiadlowski, P., et al. 2020, MNRAS, 495, 2796
Schulte-Ladbeck, R. E., Shepherd, D. S., Nordsieck, K. H., et al. 1992, ApJ, 401, L105
Sheikina, T. A., Miroshnichenko, A. S., & Corporon, P. 2000, in Astronomical Society of the Pacific Conference Series, Vol. 214, IAU Colloq. 175: The Be Phenomenon in Early-Type Stars, ed. M. A. Smith, H. F. Henrichs, & J. Fabregat, 494
Shevchenko, V. S., Grankin, K. N., Ibragimov, M. A., Mel'Nikov, S. Y., & Yakubov, S. D. 1993, Ap&SS, 202, 121
Shore, S. N. & Wahlgren, G. M. 2010, A&A, 515, A108
Sitko, M. L., Halbedel, E. M., Lawrence, G. F., Smith, J. A., & Yanow, K. 1994, ApJ, 432, 753
Snow, Jr., T. P. & Marlborough, J. M. 1976, ApJ, 203, L87
Sobolev, V. V. 1946, Dvizhushchiesia obolochki zvedz, Leningr. Gos. Univ., Leningrad
Strelnitski, V., Bieging, J. H., Hora, J., et al. 2013, ApJ, 777, 89
Strohmeier, W., Ott, H., & Schoffel, E. 1968, Information Bulletin on Variable Stars, 261, 1
Surdej, A., Surdej, J., Swings, J. P., & Wamsteker, W. 1981, A&A, 93, 285
Surdej, J. & Swings, J. P. 1983, A&A, 117, 359
Swings, J. P. 2006, in Astronomical Society of the Pacific Conference Series, Vol.

355, Stars with the B[e] Phenomenon, ed. M. Kraus & A. S. Miroshnichenko, 3
Swings, J. P. & Allen, D. A. 1971, ApJ, 167, L41
Swings, J. P. & Allen, D. A. 1973, Astrophys. Lett., 14, 65
Szczerba, R., Siódmiak, N., Stasińska, G., & Borkowski, J. 2007, A&A, 469, 799
Tafoya, D., Gómez, Y., & Rodríguez, L. F. 2004, ApJ, 610, 827
van Hoof, P. A. M. 2018, Galaxies, 6, 63
Vanbeveren, D. & Mennekens, N. 2017, in Astronomical Society of the Pacific Conference Series, Vol. 508, The B[e] Phenomenon: Forty Years of Studies, ed. A. Miroshnichenko, S. Zharikov, D. Korčáková, & M. Wolf, 121
Varga, J., Gerják, T., Ábrahám, P., et al. 2019, MNRAS, 485, 3112
Viironen, K., Mampaso, A., Corradi, R. L. M., et al. 2009, A&A, 502, 113
Villaseñor, J. I., Taylor, W. D., Evans, C. J., et al. 2021, MNRAS
Šimon, V., Bartolini, C., Guarnieri, A., Piccioni, A., & Hanžl, D. 2007, New A, 12, 578
Vural, J., Kraus, S., Kreplin, A., et al. 2014, A&A, 569, A25
Wackerling, L. R. 1970, MmRAS, 73, 153
Weintroub, J., Moran, J. M., Wilner, D. J., et al. 2008, ApJ, 677, 1140
Wheelwright, H. E., de Wit, W. J., Oudmaijer, R. D., & Vink, J. S. 2012, A&A, 538, A6
Wheelwright, H. E., Oudmaijer, R. D., de Wit, W. J., et al. 2010a, MNRAS, 408, 1840
Wheelwright, H. E., Oudmaijer, R. D., & Goodwin, S. P. 2010b, MNRAS, 401, 1199
Wheelwright, H. E., Weigelt, G., Caratti o Garatti, A., & Garcia Lopez, R. 2013, A&A, 558, A116
White, R. L. & Becker, R. H. 1985, in Bulletin of the American Astronomical Society, Vol. 17, 753
Yudin, R. V. & Evans, A. 1998, A&AS, 131, 401
Zickgraf, F. 2000, in Astronomical Society of the Pacific Conference Series, Vol. 214, IAU Colloq. 175: The Be Phenomenon in Early-Type Stars, ed. M. A. Smith, H. F. Henrichs, & J. Fabregat, 26
Zickgraf, F. J. 1998, Current Definition of B[e] Stars, ed. A. M. Hubert & C. Jaschek, Vol. 233, 1
Zickgraf, F. J. 2001, A&A, 375, 122
Zickgraf, F.-J. 2003, A&A, 408, 257
Zickgraf, F.-J. 2006, in Astronomical Society of the Pacific Conference Series, Vol. 355, Stars with the B[e] Phenomenon, ed. M. Kraus & A. S. Miroshnichenko, 135
Zickgraf, F. J. & Schulte-Ladbeck, R. E. 1989, A&A, 214, 274
Zickgraf, F. J., Wolf, B., Stahl, O., Leitherer, C., & Klare, G. 1985, A&A, 143, 421

Appendix A

Additional Tables

Table A.1: List of observations.

IRAS ID	other ID	date	time [UT]	telescope/spectrograph	R	exp. [s]	S/N	wavelength interval [Å]	observer/cataloque/ program ID	paper ID
No ID	FBS0022-021									
00470+6429										
01441+6026	MWC 17									
02103+7621		T Tauri star[1)]								
03421+2935	MWC 728	2013-10-27	10:39	SPM/2.21m	18 000	1 200	75	3835 – 7114		*sp 1*
03549+5602	AS 78									
04156+5552	CI Cam									
06070-0938	AS 119									
06071+2925										
06259-1301	FS CMa	2005-03-31	19:09	Ondřejov	11 200	1 200	75	5475 – 5988	Škoda	
		2005-04-04	18:43	Ondřejov	14 800	1 200	160	7520 – 8030	Škoda	
		2005-10-30	02:51	Ondřejov	14 800	5 400	200	7525 – 8036	Korčáková	
		2005-12-17	08:21	McDonald/cs23-e2	60 000	300	130	3582 – 10140	Miroshnichenko	*sp 1*
		2005-12-19	07:14	McDonald/cs23-e2	60 000	240	180	3582 – 10140	Miroshnichenko	*sp 2*
		2005-12-20	08:31	McDonald/cs23-e2	60 000	180	170	3582 – 10140	Miroshnichenko	*sp 3*
		2006-01-08	22:30	Ondřejov	16 100	3 600	40	8202 – 8710	Korčáková	
		2006-01-11	21:56	Ondřejov	14 800	3 600	150	7523 – 8034	Korčáková	
		2006-01-08	23:34	Ondřejov	16 100	3 600	30	8202 – 8710	Korčáková	
		2006-01-11	20:14	Ondřejov	16 100	5 400	100	8202 – 8710	Korčáková	
		2006-02-02	20:04	Ondřejov	16 100	2 908	40	8199 – 8707	Kučerová	
		2006-03-02	19:17	Ondřejov	16 100	2 234	50	8199 – 8707	Kučerová	

Table A.1: continued.

IRAS ID	other ID	date	time [UT]	telescope/spectrograph	R	exp. [s]	S/N	wavelength interval [Å]	observer/cataloque/ program ID	paper ID
		2006-10-12	03:49	Ondřejov	16 100	1 200	45	8197 – 8706	Kubát	
		2006-12-15	23:46	Ondřejov	16 100	1 200	55	8197 – 8706	Kubát	
		2007-02-17	20:08	Ondřejov	16 100	2 000	50	8199 – 8707	Kubát	
		2007-03-13	19:44	Ondřejov	16 100	2 400	70	8199 – 8708	Korčáková	
		2007-03-16	19:04	Ondřejov	16 100	1 200	65	8200 – 8708	Kubát	
		2008-11-28	00:37	Ondřejov	16 100	1 800	50	8188 – 8697	Kubát	
		2012-02-11	20:09	Ondřejov	11 200	3 600	100	5429 – 5942	Korčáková	
		2012-02-12	20:44	Ondřejov	11 200	3 600	120	5429 – 5942	Korčáková	
		2013-10-14	01:20	Ondřejov	11 200	3 145	130	5440 – 5913	Nemravová	
		2015-02-19	22:14	Ondřejov	16 100	2 000	70	8197 – 8666	Korčáková	
		2015-09-19	15:32	CFHT/Espadons	68 000	180	150	3694 – 10482	Manset/15BC07	
		2015-09-25		CFHT/Espadons	68 000		35	3695 – 1048		
		2015-10-30	13:43	CFHT/Espadons	68 000	175	140	3696 – 10481	Manset/15BC07	*sp 4*
		2016-01-22	11:40	CFHT/Espadons	68 000	180	150	3692 – 10481	Manset/15BC07	
		2016-01-28	12:05	CFHT/Espadons	68 000	175	130	3696 – 10481	Manset/15BC07	
06341+0159										
06491-0654	HD 50138	1978-12-21	12:39	IUE/SWP	8 000	4 800		1097 – 2085	NH051	*sp 1*
		2003-01-18	04:20	MPG/ESO-2.2/FEROS	48 000	110	110	3706 – 9223	ESO/70.D-0110(A)	
		2005-12-20	07:53	McDonald/cs23-e2	60 000	240	150	3582 – 10179	Miroshnichenko	*sp 2*
		2010-03-01	18:10	Ondřejov	12 500	1 200	200	6253 – 6765	Kraus	
		2010-03-02	18:16	Ondřejov	12 500	1 613	140	6254 – 6766	Kraus	

Table A.1: continued.

IRAS ID	other ID	date	time [UT]	telescope/spectrograph	R	exp. [s]	S/N	wavelength interval [Å]	observer/cataloque/ program ID	paper ID
		2010-03-08	03:47	MPG/ESO-2.2/FEROS	48 000	820	140	3708 – 9220	ESO/084.A-9016(A)	
		2010-03-19	21:01	Ondřejov	12 500	900	180	6257 – 6769	Škoda	
		2010-03-19	21:30	Ondřejov	18 500	2 600	35	4753 – 5005	Škoda	
		2010-03-31	20:46	Ondřejov	12 500	900	120	6257 – 6769	Škoda	
		2010-04-07	18:42	Ondřejov	12 500	1 200	270	6257 – 6769	Škoda	
		2010-04-07	19:10	Ondřejov	18 500	3 600	80	4753 – 5005	Škoda	
		2010-05-03	23:16	MPG/ESO-2.2/FEROS	48 000	450	180	3707 – 9185	ESO/085.D-0185(A)	
		2017-05-06	05:19	CFHT/Espadons	68 000	900	380	3668 – 10481	Manset/17AD88	*sp 3*
07080+0605		2004-12-21		CFHT/Espadons			60	3701 – 10482		*sp 1*
07370-2438	AS 160	2009-02-13	04:52	UT2/UVES	42 000	900	200	5655 – 9464	ESO/082.C-0831(A)	*sp 1*
		2009-02-13	04:59	UT2/UVES	41 000	900	160	3758 – 4985	ESO/082.C-0831(A)	*sp 2*
07377-2523										
07418-2850	3 Pup									
07455-3143	AS 174	2015-12-06	07:30	MPG/ESO-2.2/FEROS	48 000	1 200	100	3528 – 9217	ESO/096.A-9030(A)	*sp 1*
08128-5000	Hen3-140									
08307-3748	FX Vel	2015-10-13	8:00	MPG/ESO-2.2/FEROS	48 000	400	60	3528 – 9217	ESO/096.A-9039	
09350-5314	Hen3-298									
09369-5406	Hen3-303									
09489-6044	HD 85567									
10136-5736	CPD-57 2874									
No ID	GG Car									

Table A.1: continued.

IRAS ID	other ID	date	time [UT]	telescope/spectrograph	R	exp. [s]	S/N	wavelength interval [Å]	observer/cataloque/ program ID	paper ID
12584-4837	Hen3-847									
16031-5255	CPD-52 9243									
	HD 328990	2017-08-30	03:00	MPG/ESO-2.2/FEROS	48 000	1 000	35	3527 – 9215	ESO/099.A-9039(C)	
17108-3855	AS 222									
17117-4016	HDE 327083									
17175-3757	AS 225	2009-04-19	08:57	UT2/UVES	42 000	1800	160	5680 – 9460	ESO/083.C-0676(A)	*sp 1*
		2009-04-19	08:57	UT2/UVES	41 000	1800	50	3760 – 4985	ESO/083.C-0676(A)	*sp 2*
17213-3841	Hen3-1398									
17449+2320	StHa 145	2012-02-09	15:08	CFHT/Espadons	68 000	600	100	3697 – 10480	Manset/12AC12	*sp 1*
		2012-02-13	14:24	CFHT/Espadons	68 000	600	100	3696 – 10481	Manset/12AC12	
		2012-08-13		CFHT/Espadons	68 000					*sp 2*
		2016-09-22	05:04	CFHT/Espadons	68 000	1 067	100	3696 – 10481	Manset/16BD94	
18267-0606	MWC 300	B[e] supergiant								
18316-0028	SS 170	2009-08-08	04:50	UT2/UVES	42 000	786	40	9460 – 9460	ESO/083.C-0676(A)	*sp 1*
		2009-08-08	04:53	UT2/UVES	41 000	782	10	3758 – 4986	ESO/083.C-0676(A)	*sp 2*
18406-0508	AS 319	2009-08-27	03:02	UT2/UVES	42 000	600	80	5695 – 9460	ESO/083.C-0676(A)	*sp 1*
		2009-08-27	02:13	UT2/UVES	41 000	600	10	3760 – 4985	ESO/083.C-0676(A)	*sp 2*
19545+3058	MWC 623	1994-11-20	17:57	ELODIE	37 000	3 602	60	4000 – 6800	Bouvier	*sp 1*
		1995-08-11	22:45	ELODIE	37 000	5 400	60	4000 – 6800	Corporon	*sp 2*
		1995-08-23	00:11	ELODIE	37 000	5 400	50	4000 – 6800	Corporon	*sp 3*
		1996-07-28	22:33	ELODIE	37 000	5 400	55	4000 – 6800	Corporon	*sp 4*

Table A.1: continued.

IRAS ID	other ID	date	time [UT]	telescope/spectrograph	R	exp. [s]	S/N	wavelength interval [Å]	observer/cataloque/ program ID	paper ID
		2005-04-05	02:15	Ondřejov	14 800	3 400	30	7521 – 8031	Škoda	
		2005-04-05	03:18	Ondřejov	16 100	585	20	8198 – 8707	Škoda	
		2005-05-25	00:55	Ondřejov	14 800	3 600	50	7702 – 8212	Kubát	
		2005-09-04	23:54	Ondřejov	14 800	3 600	55	7710 – 8220	Korčáková	
		2005-09-06	22:56	Ondřejov	14 800	7 200	90	7710 – 8220	Korčáková	
		2005-09-24	23:43	Ondřejov	14 800	1 800	30	7510 – 8021	Votruba	
		2005-09-25	22:58	Ondřejov	14 800	1 800	40	7511 – 8021	Votruba	
		2005-10-26	17:31	Ondřejov	16 100	1 800	30	8202 – 8711	Kubát	
		2005-10-29	19:48	Ondřejov	14 800	5 400	40	7525 – 8035	Korčáková	
		2005-12-21	01:23	McDonald/cs23-e2	60 000	900	60	3583 – 10179	Miroshnichenko	*sp 5*
		2006-07-04	23:04	Ondřejov	14 800	3 600	50	7515 – 8025	Votruba	
		2006-09-08	20:48	Ondřejov	16 100	3 600	30	8197 – 8705	Kučerová	
		2006-09-08	22:09	Ondřejov	14 800	3 600	40	7506 – 8016	Kučerová	
		2010-07-10	23:08	Ondřejov	16 100	3 600	35	8192 – 8700	Polster	
		2010-07-11	00:18	Ondřejov	14 800	3 900	70	7515 – 8025	Polster	
		2010-08-19	21:55	Ondřejov	14 800	4 500	70	7512 – 8022	Polster	
20047+3305	AS 381									
20212+3920	MWC 342	2005-07-26	22:11	Ondřejov	16 100	1 800	25	8199 – 8708	Kubát	
		2005-08-28	20:45	Ondřejov	14 800	1 200	70	7509 – 8019	Dovčiak	
		2005-08-28	21:58	Ondřejov	11 200	3 000	70	5476 – 5989	Dovčiak	
		2005-09-04	20:37	Ondřejov	16 100	5 400	35	8207 – 8716	Korčáková	

Table A.1: continued.

IRAS ID	other ID	date	time [UT]	telescope/spectrograph	R	exp. [s]	S/N	wavelength interval [Å]	observer/cataloque/ program ID	paper ID
		2005-09-24	23:39	Ondřejov	14 800	3 600	80	7510 – 8020	Votruba	
		2005-09-24	21:51	Ondřejov	14 800	1 800	65	7510 – 8020	Votruba	
		2005-09-25	20:31	Ondřejov	14 800	1 800	70	7511 – 8022	Votruba	
		2005-10-08	20:54	Ondřejov	16 100	2 280	15	8202 – 8711	Kubát	
		2005-10-08	21:37	Ondřejov	14 800	1 800	20	7511 – 8022	Kubát	
		2005-10-28	17:54	Ondřejov	12 500	1 800	80	6268 – 6780	Korčáková	*sp 1*
		2005-10-28	20:02	Ondřejov	16 100	3 600	40	8203 – 8712	Korčáková	*sp 2*
		2005-10-28	20:02	Ondřejov	16 100	3 600	40	8203 – 8711	Korčáková	*sp 2*
		2005-10-30	19:19	Ondřejov	12 500	5 400	50	6268 – 6780	Korčáková	*sp 3*
		2005-12-19	01:05	McDonald/cs23-e2	60 000	900	115	3591 – 10183	Miroshnichenko	*sp 5*
		2006-01-11	16:47	Ondřejov	12 500	2 670	10	6267 – 6780	Korčáková	*sp 6*
		2006-05-05	01:24	Ondřejov	12 500	3 600	80	6259 – 6772	Šlechta	*sp 7*
		2006-09-09	18:46	Ondřejov	16 100	5 400	60	8196 – 8705	Kučerová	
		2006-09-09	20:24	Ondřejov	14 800	3 600	80	7505 – 8016	Kučerová	
		2007-06-19	21:55	Ondřejov	16 100	3 600	50	8191 – 8699	Korčáková	
		2012-08-19	22:49	Ondřejov	11 200	3 600	70	5457 – 5970	Kraus	
		2012-08-23	20:48	Ondřejov	11 200	3 600	50	5457 – 5970	Kraus	
		2015-09-24	07:09	CFHT/Espadons	68 000	1 080	120	3695 – 10500	Manset/ 15BC07	
		2015-12-01	04:59	CFHT/Espadons	68 000	1 080	120	3693 – 10481	Manset/15BC07	*sp 4*
20310+4029	MWC 349									
21516+5245	MWC 645									

Table A.1: continued.

IRAS ID	other ID	date	time [UT]	telescope/spectrograph	R	exp. [s]	S/N	wavelength interval [Å]	observer/cataloque/ program ID	paper ID
22065+5358	MWC 1055									
22248+6058	V669 Cep									
22407+6008	MWC 657	1994-08-28	02:34	ELODIE		3 600	40	4000 – 6800	Corporon, P.	*sp 1*
candidate objects										
02110+6212	VES 723									
	MWC 485									
05598-1000	AS 116									
06041+3012	MWC 790									
06158+1517	MWC 137	2009-11-13	07:56	UT2/UVES	42 000	600	100	5698 – 9460	ESO/084.C-1002(A)	*sp 1*
		2009-11-13	08:08	UT2/UVES	42 000	600	105	5698 – 9460	ESO/084.C-1002(A)	*sp 2*
		2009-11-13	08:10	UT2/UVES	41 000	600	60	3758 – 4985	ESO/084.C-1002(A)	*sp 3*
		2009-11-13	08:21	UT2/UVES	41 000	600	50	3758 – 4985	ESO/084.C-1002(A)	*sp 4*
06420+0122	MWC 819									
10028-5825	HD 87643									
13068-6255	He2-91									
13491-6318	Hen3-938									
16212-4836	Pe2-9									
20090+3809	AS 386									
20493+4849	AS 446									
21095+4726	GGR 8									

Table A.1: continued.

IRAS ID	other ID	date	time [UT]	telescope/spectrograph	R	exp. [s]	S/N	wavelength interval [Å]	observer/cataloque/ program ID	paper ID
	AS 466									
21263+4927	GGR 25									
protoplanetary nebulae										
18184-1302	MWC 922	2009-08-27	00:30	UT2/UVES	42 000	1 200	70	5655 – 9464	ESO/083.C-0676(A)	*sp 1*
18313-1738	MWC 939	2009-08-27	02:35	UT2/UVES	41 000	1 200	70	3732 – 5000	ESO/083.C-0676(A)	
		2009-08-27	02:35	UT2/UVES	42 000	1 200	100	5655 – 9464	ESO/083.C-0676(A)	

Table A.2: IUE spectra of Be stars.

ID	date	time	exp. time	wavelength interval	program ID
		[UT]	[s]	[Å]	
o And	1981-11-16	10:49	209	1097 – 2085	BEDAS
17 Tau	1978-09-12	23:43	105	1097 – 2085	UK027
β Psc	1980-10-17	08:26	419	1097 – 2085	BECAS

Spectra were taken by SWP camera with high dispersion and small aperture. The resolution is 0.2 Å.

Table A.3: Radial velocity of systems used in the presented figures.

IRAS ID	other ID	v_{sys} [km s^{-1}]	defined by
06259-1301	FS CMa	22.7 ± 0.3	[O I] 6364 Å [2)]
06491-0654	HD 50138	40 ± 4	[O I] $\lambda\lambda$ 6300, 6364 Å [3)]
	HD 328990	-33.5	[O I] 6300 Å
17175-3757	AS 225	-44.0 ± 0.4	[O I] $\lambda\lambda$ 6300, 6364 Å
17449+2320	StHa 145	-16 ± 2	[O I] $\lambda\lambda$ 6300, 6364 Å [4)]
19545+3058	MWC 623	-8.66 ± 0.14	[O I] 6300 Å [5)]
20212+3920	MWC 342	31.1 ± 0.3	[O I] 6300 Å [6)]

References. [1)] Miroshnichenko et al. (2007) [2)] Kříček (2013); [3)] Jeřábková et al. (2016); [4)] Carciofi et al. (2010); [5)] based on data from Polster et al. (2012); [6)] based on data from Kučerová et al. (2013);

Table A.4: Detected molecules.

IRAS ID	other ID	references
CO molecule		
06158+1517	MWC 137^{C}	Muratore et al. (2015), Liermann et al. (2014)
07418-2850	3 Pup	Kraus et al. (2015)
09350-5314	Hen3-298	Miroshnichenko et al. (2005)
09489-6044	HD 85567	Wheelwright et al. (2013)
10136-5736	CPD-57 2874	McGregor et al. (1988), Kraus et al. (2015), (Kraus 2009)
	GG Car	McGregor et al. (1988), Morris et al. (1996), Kraus et al. (2013)
12584-4837	Hen3-847	Nyman et al. (1992)
16031-5255	CPD-52 9243	McGregor et al. (1988), Cidale et al. (2012), Kraus et al. (2015)
17117-4016	HD 327083 = MWC 873	McGregor et al. (1988), Wheelwright et al. (2010a), Wheelwright et al. (2012), Kraus et al. (2015)
19545+3058	MWC 623	Liermann et al. (2014)
20090+3809	AS 386^{C}	Khokhlov et al. (2018)
20310+4029	MWC 349A	Geballe & Persson (1987), Martin-Pintado et al. (1994), Kraus et al. (2000), Gibb et al. (2010), Strelnitski et al. (2013) (maps of ^{12}CO and ^{13}CO), Kraus et al. (2020)
20047+3305	AS 381	Liermann et al. (2014)
SiO molecule		
07418-2850	3 Pup	Kraus et al. (2015)
10136-5736	CPD-57 2874	Kraus et al. (2015)

Table A.4: continued

IRAS ID	other ID	references
16031-5255	CPD-52 9243	Kraus et al. (2015)
17117-4016	HD 327083 = MWC 873	Kraus et al. (2015)
18313-1738	MWC 939	Gauba et al. (2003)
TiO molecule		
13491-6318	Hen3-938	Allen & Swings (1976)
H_3^+ molecule		
20310+4029	MWC 349A	Gibb et al. (2010)
PAHs		
06259-1301	FS CMa	Brown et al. (1995)
18313-1738	MWC 939	Gauba et al. (2003)

Notes. The superscript C denotes the candidate objects.

Table A.5: Detected periodicity in FS CMa stars.

IRAS ID	other ID	period	method	notes
03421+2935	MWC 728	27.5 d	RV	Miroshnichenko et al. (2015)
04156+5552	CI Cam	0.2667, 0.4153 d	UBVR	Goranskij & Barsukova (2009) pulsations
		11.7 d	UBVRIJHK	Miroshnichenko (1995) anticorelation of V and K filter
		11.7 d 1100 ± 50 d	V UBVR, Balmer emission, Fe II emission	Barsukova et al. (2002b), & Barsukova et al. (2002a)
		19.41 ± 0.02 d	RV, V photometry	Barsukova et al. (2006a) Barsukova et al. (2006c)
06158+1517	MWC 137^C	1.93 d	TESS photometry	Kraus et al. (2021) multiperiodicity
		332.4 d	ASAS photometry	Maravelias et al. (2018)
06491-0654	HD 50138	300 ± 500 d 600 ± 50 d $1\,000 \pm 600$ d $3\,200 \pm 500$ d $5\,000 \pm 500$ d	Hα EW Hα V/R Hα RV Hα EW, RV; [O I] EW Hα EW, RV	Jeřábková et al. (2016)
07080+0605		265 d	ASAS photometry	Arias et al. (2018)
07370-2438	AS 160	~ 10 min	V band polarimetry	Yudin & Evans (1998)

Table A.5: continued

IRAS ID	other ID	period	method	notes
07418-2850	3 Pup	136.9, 162.0, 237.1, 276.6, 308.8, 349.4, 414.8 d	ASAS photometry	Maravelias et al. (2018)
		137.4 ± 0.1 d	RV	Miroshnichenko et al. (2020a)
		137.867 d	RV	Johnson & Neubauer (1946)
		138.5, **161.3** d	RV	Plets et al. (1995)
08307-3748	FX Vel	1.052565 d	photometry	Strohmeier et al. (1968)
		387.9 d	photometry	Condori et al. (2019)
10136-5736	CPD-57 2874	21.5 d	ASAS photometry	Maravelias et al. (2018)
10028-5825	HD 87643[C]	104.8, 117.1, 147.1, 172.7, 192.7 d	ASAS photometry	Maravelias et al. (2018)
	GG Car	31.043 ± 0.014 d	phot. plate	Kruytbosch (1930)
		62.086 d	phot. plate	Gaposchkin (1953)
		31.020, 62.039 d	photoelectric UBV, uvby	Gosset et al. (1984)
		31.033 d	RVs of He I lines	Marchiano et al. (2012)
		31.0, 33.8 d	ASAS photometry	Maravelias et al. (2018)
		31.01 ± 0.1 d	photometry, spectroscopy	Porter et al. (2021b) orbital period
		1.583156 ± 0.0002 d	photometry, spectroscopy	Porter et al. (2021a) oscilations affected by tidal forces

Table A.5: continued

IRAS ID	other ID	period	method	notes
16031-5255	CPD-52 9243	24.7, 66.3, 174.2 d	ASAS photometry	Maravelias et al. (2018)
17117-4016	HD 327083	20.0, 23.9, 53.8, 82.3, 93.4, 107.9, 118.4, 152.6, 171.6	ASAS photometry	Maravelias et al. (2018)
17449+2320	StHa 145	36.1 ± 0.2 d	position of the Hα emission wings	Miroshnichenko et al. (2021a) probably rotational P
		800 d	Hα V/R	Korčáková et al. (2022) not a regular period
20090+3809	AS 386	131.27 ± 0.09 d	RV absorption and emission lines	Khokhlov et al. (2018)
20212+3920	MWC 342	14 d	UBVRI	Shevchenko et al. (1993)
		$14 - 46$ d (Tab. 3) $70 - 120$ d 66 d	UBVR	Mel'Nikov (1997) variable from season to season 1/2 of Bergner et al. (1990) 66 d more realistic
		16, 40 d	ubvyβ	Chkhikvadze et al. (2002)
		132 d	UBVRIJHK, polarimetry	Bergner et al. (1990)
		$1\,558 \pm 41$ d	Hα RV	Kučerová et al. (2013)
20310+4029	MWC 349	9.1 ± 0.3 yr	phot. plates	Jorgenson et al. (2000)
21516+5245	MWC 645	23.6 years	Harward phot. plates	Gottlieb & Liller (1978)

Notes. The superscript C denotes the candidate objects.

Table A.6: Measured rotation velocities of the central stars of FS CMa stars.

IRAS ID	other ID	rot. velocity	method	notes
00470+6429		low rot. vel.	line width	Miroshnichenko et al. (2009)
03421+2935	MWC 728	$v \sin i \sim 110$ km s^{-1}	He I, Mg II lines	Miroshnichenko et al. (2015)
03549+5602	AS 78	$v \sin i \sim 70$ km s^{-1}	He I lines	Miroshnichenko et al. (2000a)
06158+1517	MWC 137^{C}	$v_{\rm eq.} < 10$ km s^{-1}	evolutionary models	Kraus et al. (2021)
06259-1301	FS CMa	$v_{\rm eq.} < 70$ km s^{-1}	line profiles	Israelian et al. (1996)
06491-0654	HD 50138	90 km s^{-1}		Lee et al. (2016)
07080+0605		$v \sin i = 65 \pm 2$ km s^{-1}	Fe II, Si II lines	Arias et al. (2018)
07370-2438	AS 160	$v \sin i \sim 200$ km s^{-1}	fit of He I 5876 Å	Miroshnichenko et al. (2003a)
07418-2850	3 Pup	$v \sin i = 73$ km s^{-1}		Hoffleit & Jaschek (1982)
		$v \sin i = 50 \pm 5$ km s^{-1}	line width	Plets et al. (1995)
		$v \sin i = 35 \pm 5$ km s^{-1}	Fourier transform	Miroshnichenko et al. (2020a)
08128-5000	Hen3-140	$v \sin i = 70$ km s^{-1}	comparison with SYNSPEC	Miroshnichenko et al. (2001)
09350-5314	Hen3-298	not rapid rotator	He I line width	Miroshnichenko et al. (2005)
09489-6044	HD 85567	$v \sin i = 50$ km s^{-1}	comparison with SYNSPEC	Miroshnichenko et al. (2001)
		$v \sin i = 73$ km s^{-1}	Fourier transform	Khokhlov et al. (2017)
16031-5255	CPD-52 9243	$v = 36 \pm 4$ km s^{-1}	line profiles & interferometry	Cidale et al. (2012)
17117-4016	HDE 327083	$v \sin i \sim 200$ km s^{-1}		Miroshnichenko et al. (2003c)
17213-3841	Hen3-1398	$v \sin i \sim 50$ km s^{-1}	comparison with SYNSPEC	Miroshnichenko et al. (2001)
20090+3809	AS 386	$v \sin i = 25 \pm 3$ km s^{-1}	Fourier transform	Khokhlov et al. (2018)

Table A.6: continued

IRAS ID	other ID	rot. velocity	method	notes
22248+6058	V669 Cep	$v \sin i \sim 50$ km s^{-1}	line profiles	Miroshnichenko et al. (2002b)
22407+6008	MWC 657	$v \sin i \sim 100$ km s^{-1}	line profiles	Miroshnichenko et al. (2000b)

Notes. The superscript C denotes the candidate objects.

Appendix B

Additional Figures

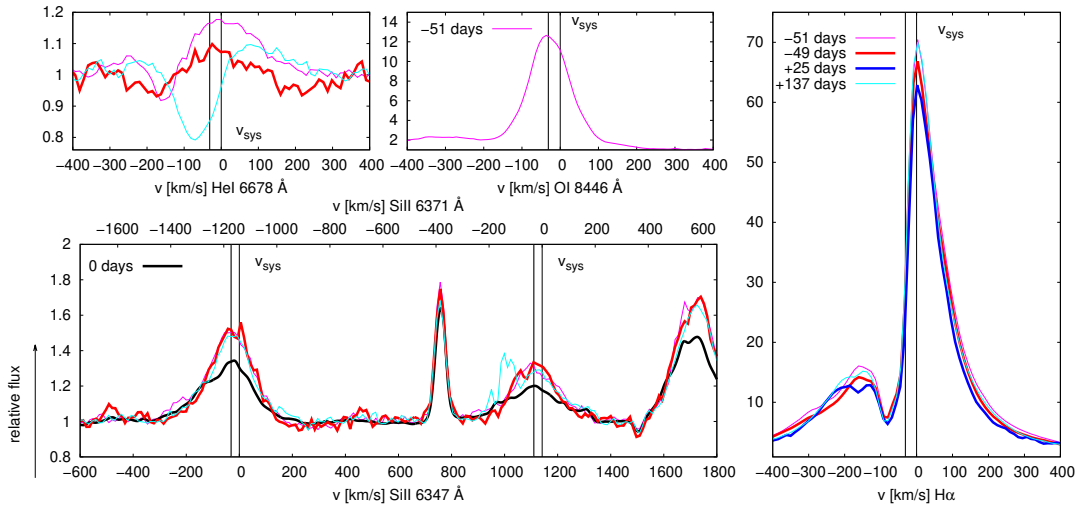

Figure B.1: The line profiles of selected lines of MWC 342 before (warm colors) and after (cold colors) the detection of the discrete absorption component in resonance lines on 2005-12-19 in McDonald's spectra (Fig. 2.9) plotted here by the black line in the Si II region. The thick red and blue lines indicate the closest spectrum to the McDonald's one. The potted spectra were taken during the observation campaign (Kučerová et al. 2013) at Ondřejov 2m telescope: 2005-10-28, 2005-10-30, 2006-01-11, and 2006-05-05 in the Hα region, and 2005-10-28 in the near IR region. The Ondřejov spectrum taken at 2006-01-11 (25 days after the McDonald one) is too noisy, that only the Hα line profile was achieve with the sufficient quality. McDonald's spectrum is convolved to the Ondřejov resolution. Due to angle of the grating setting, and normalization accuracy (for the Hα line), only Si II region is possible to straightly compare.

B.0.1 Additional BPT Plots.

The correction to the interstellar reddening is apllied only to the Fig. B.2. Measured values are corrected to the reddening using Cardelli et al. (1989) law with $R_V = 3.1$. $E(B-V)$ obtained from `Bayestar17`[1] Green et al. 2018, and their values are 3.9 for AS 160 and for 0.28 MWC 939. The distances are based on the GAIA DR2 Gaia Collaboration et al. (2016, 2018). The interstellar reddening is not necessary to be done for other presented diagrams, because every used line is from the short wavelength interval in the red region. The line ratios for FS CMa stars plotted in Figs. B.2 and B.3 are based on the measurements of EWs. For the justification of this approximation see Sec. 3.2.1.

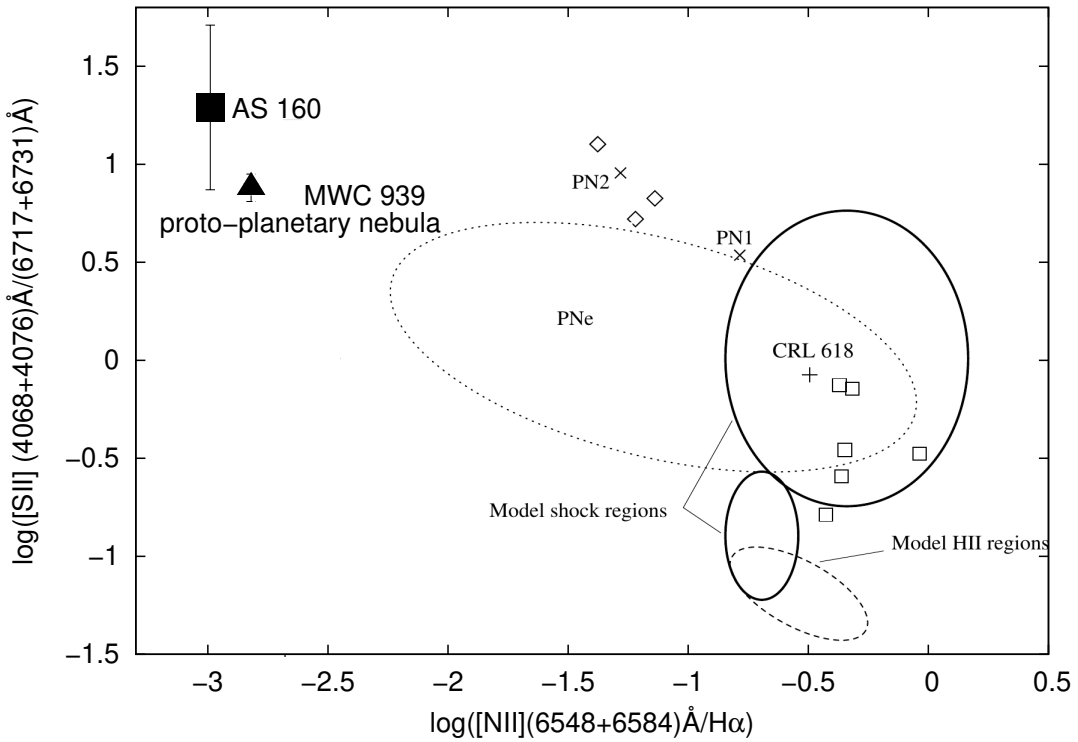

Figure B.2: The position of different ionisation sources Viironen et al. (2009), Fig. 13 with the comparison of the FS CMa star AS 160 and the proto-planetary nebula MWC 939.

[1] http://argonaut.skymaps.info

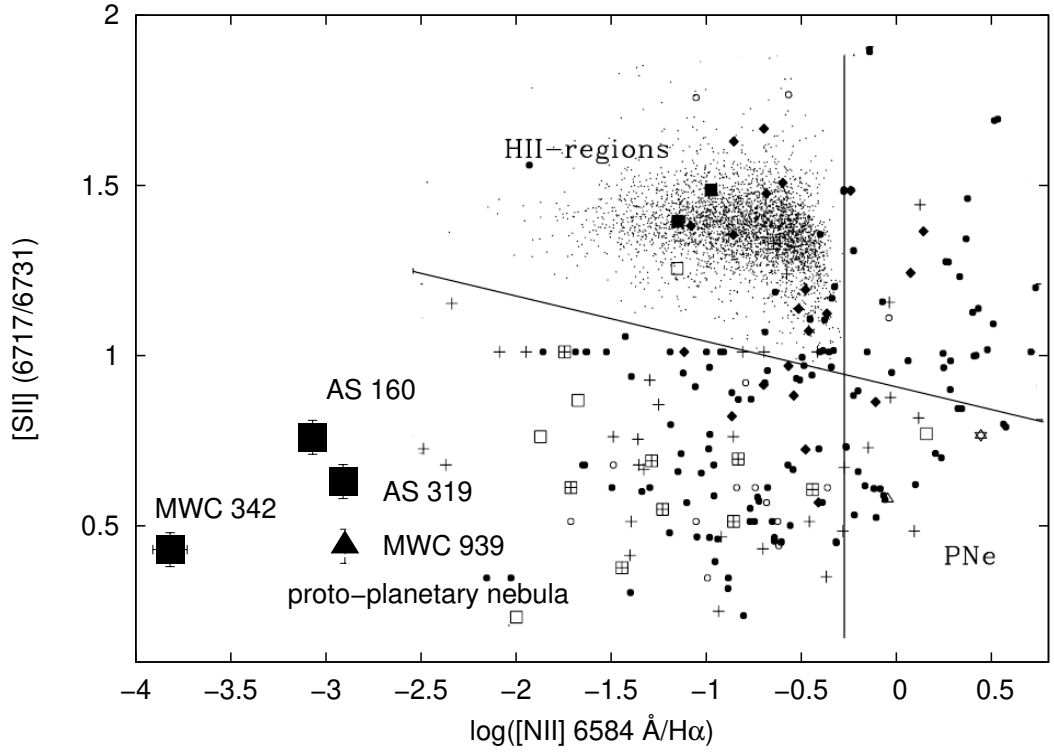

Figure B.3: Supplementary BPT diagram to Fig. 3.2.1, based on Fig. 4 (lower panel) from Kniazev et al. (2008).

Author Contribution to the Field of FS CMa Stars

Korčáková, D., ***Sestito***, F., Manset, N., Votruba, V., Šlechta, M., Danford , S., Kroupa, P., ***Dvořáková***, N., Raj, A., Chojnowski, S. D., and Singh, H. P. 2022, *"First detection of a magnetic field in low-luminosity B[e] stars. New scenarios for the nature and evolutionary stages of FS CMa stars "*, A&A, in print, doi:https://doi.org/10.1051/0004-6361/202141016

Korčáková, D., ***Polster***, J., ***Jeřábková***, T., ***Rutsch***, P., ***Kříček***, R., ***Kučerová***, B., Šlechta, M., Škoda, P., Votruba, V., Juryšek, J., and Kubát, J. 2017a, *"Long-Term Spectroscopic Monitoring of B[e] Stars at the Ondřejov Observatory"*, in Astronomical Society of the Pacific Conference Series, Vol. 508, The B[e] Phenomenon: Forty Years of Studies, ed. A. Miroshnichenko, S. Zharikov, D. **Korčáková**, & M. Wolf, 301

Korčáková, D., Miroshnichenko, A., and Shore, S. N. 2017b, *"B[e] Stars - Penetrating the Mystery of the Circumstellar Matter"*, Open European Journal on Variable Stars, 180, 59

Korčáková, D., Miroshnichenko, A. S., ***Sestito***, F., Zharikov, S. V., Manset, N., Votruba, V., Slechta, M., Danford, S., Kroupa, P., Raj, A., ***Dvořáková***, N., Khokhlov, S. A., Kusakin, A., Reva, I. V., Kokumbaeva, R. I., Omarov, C. T., Chojnowski, S. D., Alimgazinova, N. S., Naurzbayeva, A. Z., and Kuratova, A. K. 2021, *"The First Detection of a Strong Magnetic Field in a FS CMa Star"*, in OBA Stars: Variability and Magnetic Fields. On-line conference, 6, doi:10.5281/zenodo.4999795

Korčáková, D., Miroshnichenko, A. S., Zharikov, S. V., Manset, N., Danford, S., Votruba, V., and ***Dvořáková***, N. 2020, *"Mystery of lithium in FS CMa stars."*, Mem. Soc. Astron. Italiana, 91, 118

Korčáková, D., Shore, S. N., Miroshnichenko, A., Zharikov, S. V., ***Jeřábková***, T., ***Kříček***, R., ***Dvořáková***, N., Votruba, V., Manset, N., and Šlechta, M. 2019, *"Tracing Physical Processes Affecting Spectral Formation in the Low-luminosity B[e] Stars of the FS CMa Group"*, in Astronomical Society of the Pacific Conference Series, Vol. 519, Radiative Signatures from the Cosmos, ed. K. Werner, C. Stehle, T. Rauch, & T. Lanz, 155

Sestito, F., Shore, S. N., **Korčáková**, D., Miroshnichenko, A. S., and Zharikov, S. V. 2017, *"Spectroscopic Variations of the B[e] Star IRAS 17449+2320"*, in Astronomical Society of the Pacific Conference Series, Vol. 508, The B[e]

Phenomenon: Forty Years of Studies, ed. A. Miroshnichenko, S. Zharikov, D. **Korčáková**, & M. Wolf, 401

Jeřábková, T., **Korčáková**, D., Miroshnichenko, A. S., Danford, S., Zharikov, S. V., ***Kříček***, R., Zasche, P., Votruba, V., Šlechta, M., Škoda, P., and Janík, J. 2017, *"Time-Dependent Spectral Feature Variations of the FS CMa Star HD 50138"*, in Astronomical Society of the Pacific Conference Series, Vol. 508, The B[e] Phenomenon: Forty Years of Studies, ed. A. Miroshnichenko, S. Zharikov, D. **Korčáková**, & M. Wolf, 375

Kučerová, B., **Korčáková**, D., ***Polster***, J., Wolf, M., Votruba, V., Kubát, J., Škoda, P., Šlechta, M., and Křížek, M. 2013, *"Time-dependent spectral-feature variations of stars displaying the B[e] phenomenon. II. MWC 342"*, A&A, 554, A143, doi:10.1051/0004-6361/201117437

Kučerová, B., **Korčáková**, D., Kubát, J., Šlechta, M., Votruba, V., Škoda, P., and Hadrava, P. 2006, *"Observations of B[e] Stars with the Ondřejov 2m telescope"*, in Astronomical Society of the Pacific Conference Series, Vol. 355, Stars with the B[e] Phenomenon, ed. M. Kraus & A. S. Miroshnichenko, 355

Kříček, R., **Korčáková**, D., Jeřábková, T., Klement, R., Miroshnichenko, A. S., Danford, S., Kubát, J., ***Kučerová***, B., Škoda, P., and Šlechta, M. 2017, *"Spectral Variations and Simple Models of FS CMa"*, in Astronomical Society of the Pacific Conference Series, Vol. 508, The B[e] Phenomenon: Forty Years of Studies, ed. A. Miroshnichenko, S. Zharikov, D. **Korčáková**, & M. Wolf, 411–412

Polster, J., **Korčáková**, D., and Manset, N. 2018, *"Time-dependent spectral-feature variations of stars displaying the B[e] phenomenon. IV. V2028 Cygni: modelling of Hα bisector variability"*, A&A, 617, A79, doi:10.1051/0004-6361/201832772

Polster, J., **Korčáková**, D., Votruba, V., Škoda, P., Šlechta, M., and ***Kučerová***, B. 2011, *"Emission features in a B[e] binary system V2028 Cyg"*, in Active OB Stars: Structure, Evolution, Mass Loss, and Critical Limits, ed. C. Neiner, G. Wade, G. Meynet, & G. Peters, Vol. 272, 533–534, doi:10.1017/S1743921311011331

Polster, J., **Korčáková**, D., Votruba, V., Škoda, P., Šlechta, M., and ***Kučerová***, B. 2012a, *"Is the B[e] Star V2028 Cyg a Binary?"*, in From Interacting Binaries to Exoplanets: Essential Modeling Tools, ed. M. T. Richards & I. Hubeny, Vol. 282, 309–310, doi:10.1017/S1743921311027657

Polster, J., **Korčáková**, D., Votruba, V., Škoda, P., Šlechta, M., ***Kučerová***, B., and Kubát, J. 2012b, *"Time-dependent spectral-feature variations of stars displaying the B[e] phenomenon. I. V2028 Cygni"*, A&A, 542, A57, doi:10.1051/0004-6361/201117210

Jeřábková, T., **Korčáková**, D., Miroshnichenko, A., Danford, S., Zharikov, S. V., ***Kříček***, R., Zasche, P., Votruba, V., Šlechta, M., Škoda, P., and Janík, J. 2016, *"Time-dependent spectral-feature variations of stars displaying the B[e] phenomenon. III. HD 50138"*, A&A, 586, A116, doi:10.1051/0004-6361/201526290

Miroshnichenko, A. S., Zharikov, S. V., **Korčáková**, D., Manset, N., Mennickent, R., Khokhlov, S. A., Danford, S., Raj, A., and Zakhozhay, O. V. 2020, *"Binarity among objects with the Be and B[e] phenomena"*, Contributions of the Astronomical Observatory Skalnate Pleso, 50, 513, doi:10.31577/caosp.2020.50.2.513

Miroshnichenko, A. S., Zharikov, S. V., Danford, S., Manset, N., **Korčáková**, D., ***Kříček***, R., Šlechta, M., Omarov, C. T., Kusakin, A. V., Kuratov, K. S., and Grankin, K. N. 2015, *"Toward Understanding the B[e] Phenomenon. V. Nature and Spectral Variations of the MWC 728 Binary System."*, ApJ, 809, 129, doi:10.1088/0004-637X/809/2/129

Students of D. Korčáková are denoted by the bold italic font.

B.1 Key Publications

Korčáková, D., ***Sestito***, F., Manset, N., et al. 2022, *"First detection of a magnetic field in low-luminosity B[e] stars. New scenarios for the nature and evolutionary stages of FS CMa stars"*., A&A, in print

We discovered a very strong (6.2 ± 0.2 kG) magnetic field in IRAS 17449+2320. We found that this star has higher space velocities, especially the value toward the galactic pole is large. Both are evidence of the merger origin of this star. This discovery opens the possibility that, at least several objects among FS CMa stars, are post-merger systems.

Korčáková , D., Miroshnichenko, A. S., Zharikov, S. V., et al. 2020, *"Mystery of lithium in FS CMa stars."*, Mem. Soc. Astron. Italiana, 91, 118

We pointed to the possibility that lithium lines are formed in the pseudoatmoshere of the disk of FS CMa stars. In that case, Li I resonance lines may help to solve the cosmological problem of the primordial lithium.

Korčáková, D., Shore, S. N., Miroshnichenko, A., et al. 2019, *"Tracing Physical Processes Affecting Spectral Formation in the Low-luminosity B[e] Stars of the FS CMa Group*, in Astronomical Society of the Pacific Conference Series, Vol. 519, Radiative Signatures from the Cosmos, ed. K. Werner, C. Stehle, T. Rauch, & T. Lanz, 155

The review of the spectral properties of the whole FS CMa group is presented. We report the presence of the iron curtain in FS CMa stars.

Polster, J., **Korčáková**, D., & Manset, N. 2018, *"Time-dependent spectral-feature variations of stars displaying the B[e] phenomenon. IV. V2028 Cygni: modelling of Hα bisector variability"*, A&A, 617, A79

V2028 Cygni has a composed spectrum of a cold (K-type) and hot (B-type) star. This would be an unambiguous proof of the binarity in a standard star. However, FS CMa stars are surrounded by large amount of the circumstellar material and the interpretation is not straightforward in these objects. Our modelling of the Hα bisector variability showed that the absorption lines of the

K-type spectrum probably originates in the pseudoatmoshere of the disk which disputes the binary nature of V2028 Cygni.

Jeřábková, T., **Korčáková**, D., Miroshnichenko, A., et al. 2016, *"Time-dependent spectral-feature variations of stars displaying the B[e] phenomenon. III. HD 50138"*, A&A, 586, A116

The analysis of 130 spectra of HD 50138 over the twenty years allowed us to study the periodical behaviour of spectral features. We discovered the rotating structures in the disk and detected $V/R > 1$ for the first time in FS CMa stars. The important finding was the strong connection of the Hα line and [O I] doublet $\lambda\lambda$ 3600, 6364 Å. This points to the much stronger non-LTE effects and shifting of the[O I] line formation region as was previously thought.

Korčáková, D., ***Polster***, J., Jeřábková, T., et al. 2017, *"Long-Term Spectroscopic Monitoring of B[e] Stars at the Ondřejov Observatory"*, in Astronomical Society of the Pacific Conference Series, Vol. 508, The B[e] Phenomenon: Forty Years of Studies, ed. A. Miroshnichenko, S. Zharikov, D. **Korčáková**, & M. Wolf, 301 A&A, 586, A116

The observation campaign of FS CMa stars at the Ondřejov observatory was presented.

Kučerová, B., **Korčáková**, D., ***Polster***, J., et al. 2013, *"Time-dependent spectral-feature variations of stars displaying the B[e] phenomenon. II. MWC 342"*, A&A, 554, A143

Analysing of 102 spectra from the Ondřejov observatory between the years 2004-2010 we discovered expanding decelerating layers. Together with the constant outflow, the event of material infall was observed (similar situation as in more massive B[e] supergiants). The data allowed to describe the periodical behaviour of several lines on the different time scales. Such a complex study of the variability was presented for the first time.

Polster, J., **Korčáková**, D., Votruba, V., et al. 2012, *"Time-dependent spectral-feature variations of stars displaying the B[e] phenomenon. I. V2028 Cygni"*, A&A, 542, A57

The long-term spectroscopic observations were presented for the first time. The analysis allowed to specify and restricts the properties of future models.